

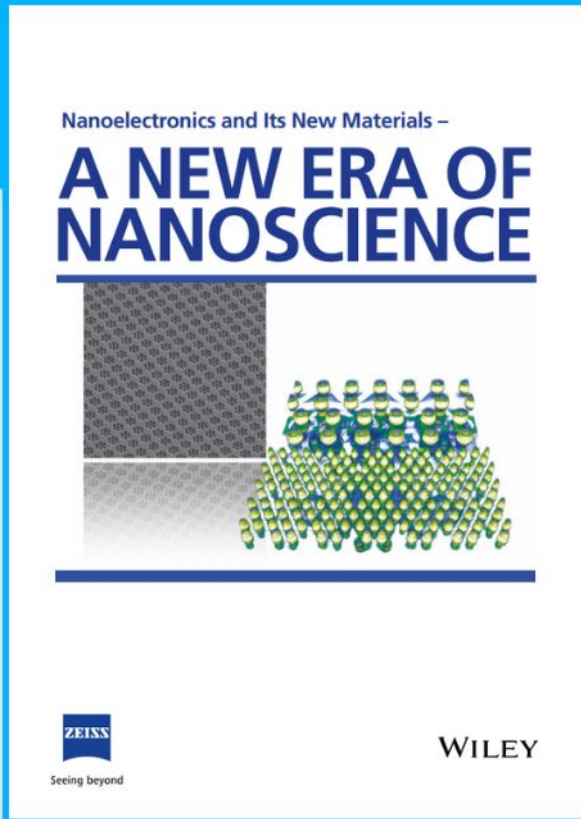


Nanoelectronics and Its New Materials – A NEW ERA OF NANOSCIENCE

Discover the recent advances in electronics research and fundamental nanoscience.

Nanotechnology has become the driving force behind breakthroughs in engineering, materials science, physics, chemistry, and biological sciences. In this compendium, we delve into a wide range of novel applications that highlight recent advances in electronics research and fundamental nanoscience. From surface analysis and defect detection to tailored optical functionality and transparent nanowire electrodes, this eBook covers key topics that will revolutionize the future of electronics.

To get your hands on this valuable resource and unleash the power of nanotechnology, simply download the eBook now. Stay ahead of the curve and embrace the future of electronics with nanoscience as your guide.



Seeing beyond

WILEY

Covalent–Organic Framework (COF)-Core–Shell Composites: Classification, Synthesis, Properties, and Applications

Teng Li, Yuan Pan, Binbin Shao, Xiansheng Zhang, Ting Wu, Qingyun He, Miao He, Lin Ge, Linfeng Zhou, Sheng Liu, Xuemei Zheng, Jie Ye, and Zhifeng Liu*

Core–shell structures, where the “guest” material is encapsulated within a protective shell, integrate the advantages of different materials to enhance the overall properties of the composite. Covalent–organic frameworks (COFs) are favorable candidates for composing core–shell structures due to their inherent porosity, good activity, excellent stability, and other advantages. In particular, COFs as shells to encapsulate other functional materials are becoming increasingly popular in the fields of environmental remediation and energy conversion. However, there is a lack of reviews on COF-based core–shell materials. In this context, this review provides a systematic summary of the current research on COF-based core–shell composites. First, a simple classification is made for COF-based core–shell composites. The second part of the review describes the main synthesis methods. The changes brought about by the COF shell and core–shell structures on the properties of the composites and their applications in photocatalysis, electrocatalysis, adsorption, sensing, and supercapacitors are then emphasized. Finally, new perspectives on the future development and challenges of composites are presented. The purpose of this study is to provide future insights into the design and application of COF-based core–shell composites.

to satisfy human needs, which leads to serious environmental pollution and energy scarcity.^[1–5] Therefore, developing renewable energy sources and solving environmental pollution are the two technological challenges of modern society in the 21st century.^[6–8] Currently, researchers have developed a variety of materials for sustainable techniques, such as graphitic carbon nitride (g-C₃N₄),^[9] metal–organic frameworks (MOFs),^[10] etc. Among all possible options, COFs are considered as one of the effective substances that can solve problems relating to energy conversion and environmental remediation.^[11–14]

Since Yaghi's group first reported on COFs in 2005, numerous researches have been performed on COFs and their derivatives (Figure 1a).^[15,16] COFs are an emerging family of organic porous crystalline polymers consisting of light elements (C, N, O) connected by covalent bonds, that possessing a 2D or 3D mesh structure.^[17] Due to their special structure, COFs have a number of unique properties including

superior stability, low density, topological structure diversity, large surface area, and high charge carrier mobility, which make them an ideal candidate in heterogeneous catalysis, optoelectronic devices, and energy storage.^[11–14,18–20] COFs clearly have contributed to new energy development and environmental protection, but there are some drawbacks that limit their practical application. For example, the photocatalytic efficiency of COFs is often unsatisfactory due to the low electron-hole mobility and rapid carrier recombination; moreover, the inherent insulating properties of COF materials lead to relatively low current density, which limits their application in electrochemistry. Some strategies have been developed to overcome these shortcomings. For instance, depositing some nanoparticles, such as CdS, on the surface of COFs to introduce more active sites or building heterostructures to accelerate the separation of photogenerated electrons and holes.^[21,22] While the poor conductivity of the COFs can be overcome by hybridization with other conductive materials or the introduction of transition metal active sites.^[23] Among these strategies, the cooperation of COFs with other specialty components to form core–shell structures has attracted the interest of researchers (Figure 1b,c) as it demonstrates a synergistic effect by

1. Introduction

Due to the development of human society and the expansion of industrialization, there is an increasing demand for energy

T. Li, Y. Pan, B. Shao, X. Zhang, T. Wu, Q. He, M. He, L. Ge, L. Zhou, S. Liu, X. Zheng, Z. Liu
College of Environmental Science and Engineering
Hunan University and Key Laboratory of Environmental Biology and Pollution Control (Hunan University)
Ministry of Education
Changsha 410082, P. R. China
E-mail: zhifengliu@hnu.edu.cn

J. Ye
Fujian Provincial Key Laboratory of Soil Environmental Health and Regulation
College of Resources and Environment
Fujian Agriculture and Forestry University
Fuzhou 350002, China

The ORCID identification number(s) for the author(s) of this article can be found under <https://doi.org/10.1002/adfm.202304990>

DOI: 10.1002/adfm.202304990

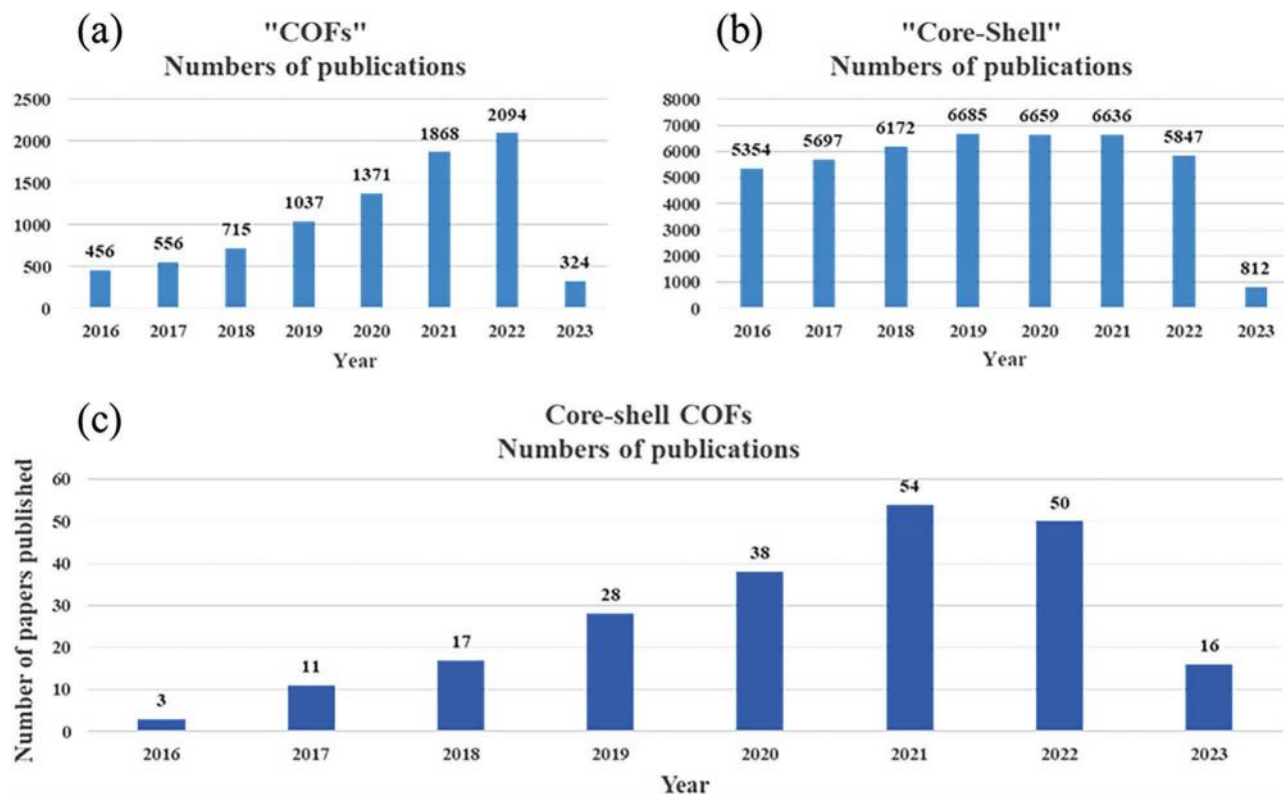


Figure 1. The number of publications on COFs and core-shell from 2016 to 2022. The data are taken from the “Web of Science.”

integrating the preeminent physicochemical properties of multi-components to demonstrate enhanced performance.

A core-shell structure is a composite nanomaterial composed of an inner layer of “guest” substance encapsulated in other materials, with the core-shell usually interconnected by chemical or physical interactions. In general, core-shell structure forms spontaneously when the specific surface energy of the components making up the shell is much lower than that of the nuclear particles in the medium. Based on the type and arrangement of components, they can be classified as inorganic@inorganic, inorganic@organic, organic@inorganic, and organic@organic, while the selection of core and shell materials usually depends on the design criterion and the utilization purpose.^[24–30] For example, there is a preference for synthesizing nanomaterials with excellent thermal and chemical stability, regular structural systems, abundant active sites, or excellent photoelectric conversion properties; and therefore, various COFs based on triazoles, imines, β -ketoenamine, and hydrazines are favored by researchers. Core-shell materials typically exhibit improved performance, which is primarily due to the composite and complementary of the heterogeneous materials, highlighted by the following: I) combinations of materials with different properties to form core-shell structures that not only combine the individually unique functions of the core and shell, but also have new properties resulting from their interactions; II) satisfactory physicochemical properties could be achieved by adjustment of the shape, size, or composition of the core and shell; III) the encapsulation of the shell reduces the toxicity of the nanoparticles, improves biocompatibility, and allows modifica-

tion with biomolecules; and IV) stability is an important criterion to measure whether the material can be practically applied. For substances that are not stable, especially those sensitive to oxidation and corrosion, the core-shell structure improves stability by separating the core directly from the external environment and avoiding direct contact.^[31,32] Based on these properties, the construction of the core-shell structures effectively expands the scope of applications of COFs, including photocatalysis,^[33–35] electrocatalysis,^[36,37] biomedical,^[38,39] energy storage and conversion,^[40,41] sensing,^[42,43] and adsorption.^[44–46] COF-based catalysts with core-shell structures usually have high photocatalytic or electrocatalytic activity, and the active sites may be located at the core, shell, or interface. TiO_2 @COF-3 is a typical example.^[47] Due to the enhanced photon adsorption capacity and covalent linkage between the core-shell composites, this enhances the photocatalytic activity, exhibiting the highest CO_2 photoconversion (92.5%) among all experimental groups, which is 10.1 and 12.9 times more than pure TiO_2 and COFs, respectively. For electrocatalysis, the introduction of conductive materials and the unique core-shell structure thus brought overcome the drawback of the poor conductivity of COFs and is conducive to offering a novel direction for the fabrication of COF-derived electrocatalysts.^[48]

Previously, many articles have reviewed different aspects of COF-based materials, including magnetic,^[49] heterogeneous catalysis,^[50] chirality,^[51] doping,^[52] etc. This review provides a comprehensive understanding of COF-based core-shell materials. There are two types of COF-based core-shell composites: one consisting of COFs as the shell and other materials as the core,

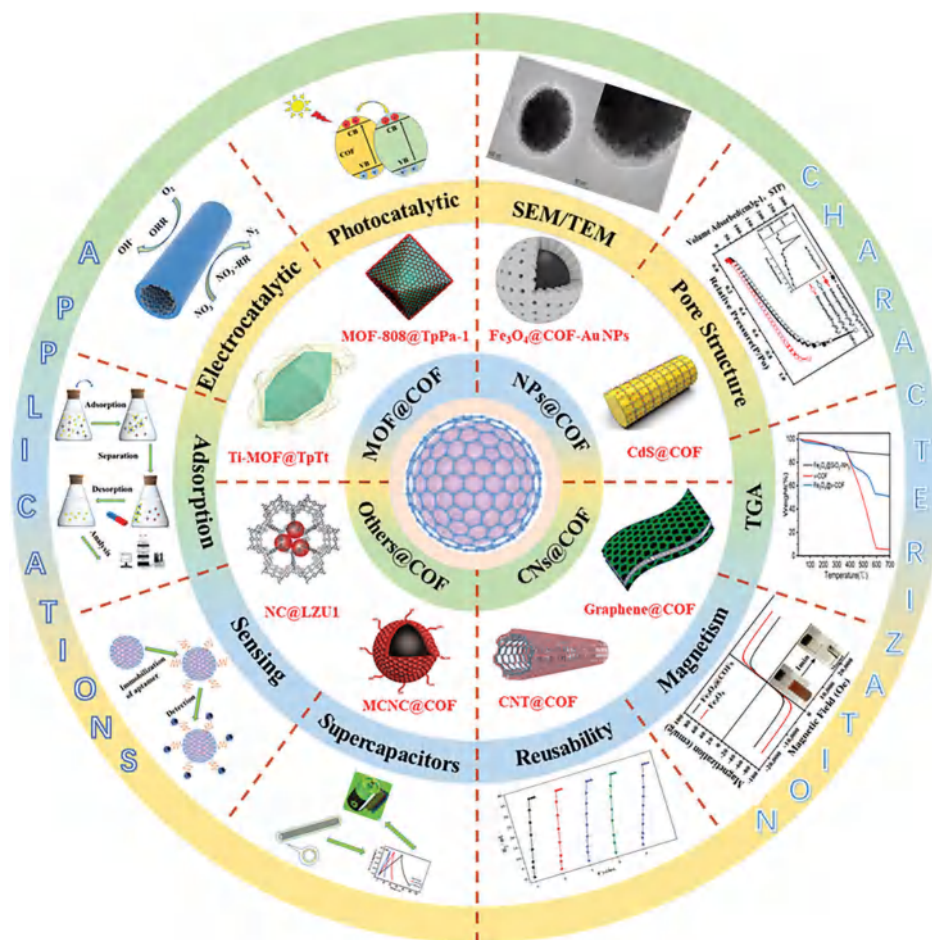


Figure 2. Classifications, characterization, and applications of COF-based core-shell hybrids. Reproduced with permission.^[44] Copyright 2019, Springer-Verlag GmbH Austria. Reproduced with permission.^[174] Copyright 2017, The Royal Society of Chemistry. Reproduced with permission.^[175] Copyright 2023, Elsevier. Reproduced with permission.^[176] Copyright 2023, American Chemical Society. Reproduced with permission.^[57] Copyright 2021, Wiley-VCH.

and the other being the complete opposite. At present, most of the studies focus on COFs as the shell, which is determined by the physical and chemical properties of COFs themselves. Therefore, we also focus the discussion on the former. Herein, we systematically present the classification, synthesis strategies, different applications, as well as the mechanisms of performance improvement of these composites (**Figure 2**) with particular reference to the following areas: I) the classification of COF-based core-shell materials; II) the design principles and methods for synthesizing COF-based core-shell materials; III) the detailed description of the enhancement mechanism of COF-based core-shell structures for various applications; and IV) the detailed applications and functions in environment and energy of COF-based core-shell materials. This work aims to provide a comprehensive review of COF-based core-shell materials and a deep understanding of their future development and application.

2. Classification

Thanks to the numerous substrates, various COF-based core-shell materials with controllable structures have been successfully fabricated, which has greatly enriched the diversity of com-

posites. In this chapter, a systematic summary discussion of the reported COF-based core-shell materials is presented from the aspects of different substrates. With the exception of a few examples of COF@MOF, most research has focused on the use of COFs as a shell for nuclear shell materials. The present COF-based core-shell composite materials can be classified into the following types of architectures: MOF/COF core-shell hybrids, carbon nanomaterials@COF, metal nanoparticles@COF, and other types.

2.1. MOF/COF Core-Shell Hybrids

Despite the fact that individual MOF and COF materials have been designed and applied in several fields, they are still unable to meet specific requirements due to inherent drawbacks.^[53,54] Consequently, some researchers have explored the possibility of achieving superior properties by combining MOFs and COFs. By growing TPA-COF shells on the surface of amino-functionalized rod-shaped NH₂-MIL-68 using a modified solvothermal method, Peng et al. firstly prepared a novel MOF@COF composite with outstanding structural properties as well as enhanced catalytic

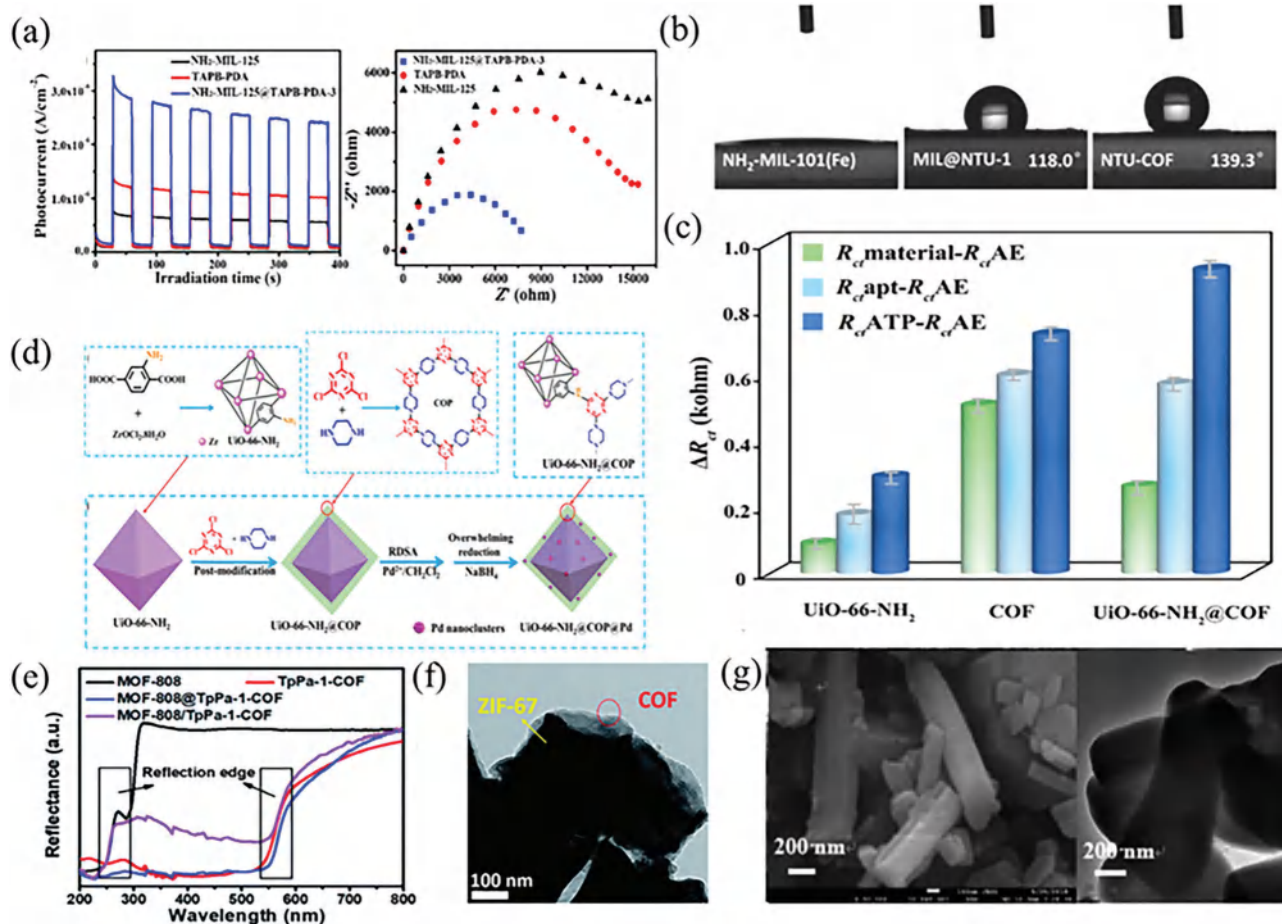


Figure 3. a) EIS Nyquist plots (left) and PL spectra (right) of several materials. Reproduced with permission.^[55] Copyright 2019, Elsevier B.V. and Science Press. b) Water contact angle of several materials. Reproduced with permission.^[58] Copyright 2019, Wiley-VCH. c) Electrochemical sensing properties of several aptasensors are measured by the ΔR_{ct} value. Reproduced with permission.^[36] Copyright 2021, Elsevier B.V. d) Schematic diagram of the synthesis of MOF, COF, and MOF@COF composites doped with Pd nanoclusters. Reproduced with permission.^[62] Copyright 2020, American Chemical Society. e) UV–visible DRS of several materials. Reproduced with permission.^[63] Copyright 2021, The Royal Society of Chemistry. f) TEM image of COF@ZIF. Reproduced with permission.^[65] Copyright 2022, The Royal Society of Chemistry. g) SEM and TEM images of Ce-MOF@MCA500 hybrids. Reproduced with permission.^[67] Copyright 2018, Elsevier B.V.

performance in 2018, indicating that the formation of core–shell hybrids opened a novel way for the cooperation between MOFs and COFs.^[33] Up to now, the formation of MOF@COF nanocomposite has relied mainly on forming an imine bond ($\text{C}=\text{N}$) between the retained NH_2 group of MOFs and the aldehyde presented on COFs by the Schiff base reaction.^[55] MIL-MOFs and UiO-MOFs are often used for fabricating MOF@COF core–shell heterostructures due to their excellent stability, good crystallinity, flexibility of synthesis methods, and versatile properties.^[56] We believe that combining COFs with MOFs to obtain efficient functional materials will remain a popular research area in the near future.

2.1.1. MIL-Based MOF@COF

As a branch of MOFs, materials from Institute Lavoisier (MIL) typically have better thermal stability, great light collection ability, and large specific surface area, especially MIL-MOF crys-

tals often present a functional amino group [such as $\text{NH}_2\text{-MIL-125(Ti)}$, $\text{NH}_2\text{-MIL-101(Fe)}$], which are often selected as the core of the MIL-MOF@COF hybrid materials forms covalent bonds with the carboxyl or aldehyde groups of COFs, resulting in the strong binding between MOFs and COFs.^[53] The development of a range of MIL-based MOF@COF hybrids can properly combine the favorable properties of the two to obtain composite materials with higher performance.^[57] For instance, Lu et al. developed a core–shell $\text{NH}_2\text{-MIL-125(Ti)}@\text{TAPB-PDA}$ compound.^[55] Compared with pure COFs and MOFs, the core–shell hybrids showed the smallest circular radius, the lowest charge transfer resistance, and the highest photocurrent density (Figure 3a), indicating the formation of strong covalent bonds between the core–shell interfaces, which can effectively broaden the absorption bandwidth and promote the separation of photogenerated electron–hole pairs. The bandgap of COF was 2.57 eV, which was narrower than that of MOF (2.81 eV). Thus, COFs were more likely to produce electron–hole pairs, while MOFs acted like powerful catalysts. Under visible light irradiation, the photogenerated

electrons on the conduction band (CB) of COFs were transferred to the CB of MOFs through covalent bonds and reacted with O_2 to form $\bullet O_2^-$, while the holes on the valence band (VB) of COFs combined with electrons in benzyl alcohol (BA) to form BA radicals, and finally the two reacted to obtain the final product benzaldehyde. The photocatalytic performance experiments showed that the photocatalytic oxidation efficiency of the prepared hybrids for alcohol was 94.7%, which was 2.5 and 15 times higher than that of pure MOFs and COFs, respectively. It is worth mentioning that an excessively thick COF shell will limit the ability of the reactants to migrate and diffuse or reduce the photoinduced electron transfer efficiency. In this study, the optimal thickness of the COF shell was 20 nm. In addition, the environmental wetability of the catalyst affects the catalytic performance, and the hydrophobic COF shell can be used to modify the hydrophilic-hydrophobic properties of the compounds. Recently, Cai's group prepared a novel NH_2 -MIL-101 (Fe)@NTU hybrid material by covalently attaching COF building blocks to the MOF core to form a COF shell.^[58] As shown in Figure 3b, the water contact angle of NH_2 -MIL-101(Fe)@NTU1 was 118.0° , which was slightly lower than that of NTU-COF at 139.3° , while the MOF was completely wetted. The aromatic backbone and nanostructure of the COF shell provided a good hydrophobic environment and cooperated with the MOF core to promote the mechanism of the free radical pathway; thus, its conversion capacity (32%) and selectivity (84%) for styrene oxidation are better than 24% and 26% of pure MOF. Some MIL-MOF@COF hybrids can also be used as precursors to synthesize composites with new physicochemical properties by pyrolysis. For example, Liu et al. prepared a TiO_2 @COF material, where the role of MOF@COF was as an intermediate of pyrolysis for selective functionalization. It was confirmed that the MOF@COF core-shell material was used as a precursor to effectively overcome the metal particles leaching that occurs with single MOF pyrolysis and the uncontrollable structure caused by COF pyrolysis.^[59] In particular, NH_2 -MIL-125 (Ti) was selected as the core to promote the growth of COF shells, and it can be converted to TiO_2 nanoparticles under specific conditions, providing abundant faradic active sites, while the selection of TP-DQ COF depends on excellent porosity and stability. It was confirmed that the salt adsorption capacity (SAC) of TiO_2 @COF was 33.66 mg g^{-1} , and it still had good stability after 40 cycles.

2.1.2. UiO-Based MOF@COF

UiO-type MOFs usually consist of oxidation group nodes and dicarboxylate linkers with excellent stability, tunability, and thus a series of UiO-based MOFs (including UiO-66, UiO-67, and UiO-68) can combine with COFs to form a core-shell construction, which improves their potential applications in numerous fields.^[53,60] He's group prepared NH_2 -UiO-66@TAPB-DMTP-COF composites and made them into electrochemical aptasensor for the sensitive detection of adenosine triphosphate (ATP) and chloramphenicol (CAP) in samples.^[36] As shown in Figure 3c, the MOF@COF-modified electrode possessed higher ΔR_{ct} (R_{ct} : charge transfer resistance) values during both immobilization and detection, indicating the stronger electrochemical performance and sensitivity of the composite, which was attributed to the positive synergistic effects of the core and shell, which en-

hanced the affinity and π - π stacking of the aptamer with the core and shell, respectively. As a result, the sensor showed excellent sensing performance in the detection range of 1.0×10^{-5} to 5.0 ng mL^{-1} . Fu's group prepared a unique MOF@COF adsorbent, in which the hexahedral cage structure of UiO-66 was selected as the core. The authors claimed that hydrogen bonds and π - π interactions formed between the target molecule and the COF shell, as well as Lewis acid-base interactions occurring at the metal sites provided by the MOF core, played an important role in the occurrence of the adsorption process.^[61]

For some UiO-MOF@COF core-shell composites, the homogeneous distribution of heteroatoms (N) in COF shells makes them ideal platforms for anchoring other species such as Pd, which enhances the metal-carrier interactions and thus prevents aggregation and leaching of the loaded metal nanoclusters during the reaction. For instance, Zhu and co-workers prepared MOF@COP@Pd heterogeneous catalysts (Figure 3d). In this case, UiO-66- NH_2 was chosen as the core, and the reverse two-solvent method was adopted to confine the Pd nanoclusters in the composite.^[62] Specifically, the pre-synthesized UiO-66- NH_2 @COP was homogeneously dispersed with $Pd (AcO)_2$ and CH_2Cl_2 , and then a high concentration of $NaBH_4$ was added. The introduction of Pd nanoclusters hardly changed the structural morphology of the complexes. It could act as an active site to activate H_2 to H atoms, dissociate them, and react with 4-nitrophenol (4-NP) adsorbed on the surface of the material to obtain the product 4-aminophenol (4-AP). The obtained catalysts loaded with Pd nanoclusters exhibited good crystallinity, strong stability, and excellent hierarchical porous structures. The special structure enabled the components to show a strong synergistic effect, which led to excellent catalytic performance and good recovery.

2.1.3. Other Types of MOF@COF

In order to design more MOF@COF core-shell hybrids with excellent morphology and function, the selection of MOFs must be expanded. In addition to the common MIL- and UiO-based MOFs combined with COFs, researchers have successively experimented with other types of MOFs and synthesized a series of COF-based core-shell compounds with structural and performance advantages. Zhang's group prepared MOF-808@COF hybrid materials, where MOF-808, a typical MOF without $-NH_2$ groups, was chosen as the core.^[63] First, MOF-808 was modified with p-amino benzoic acid (PABA), thus introducing the amino group. Subsequently, the amino group introduced on MOF reacts with the aldehyde group in COF monomers to form a covalent connection. The UV-vis diffuse reflectance spectra (DRS) of the UiO-66@TpPa-1-COF hybrids showed a reflectance band edge similar to that of TpPa-1-COF compared to the two reflectance band edges of the physically mixed UiO-66/TpPa-1-COF sample, indicating the successful formation of covalent bonds (Figure 3e). This MOF@COF assembly strategy could be used to fabricate MOF-COF composites with ideal morphology and properties. The photocatalytic mechanism will be discussed in detail in the application section. Gao et al. developed a novel PCN-222-Co@TpPa-1 composite by strong π - π stacking between the PCN-222-Co core and COF shell, which led to a unique core-shell structure, strong interactions, and a considerable specific

surface area. The obtained composites were rich in Lewis acid sites and Brønsted base active sites, making it possible to catalyze the deacetylation–Knoevenagel reaction.^[64] This method did not introduce amines, but also consequently resulted in uneven loading of the COF shell, which can be overcome by polyvinylpyrrolidone (PVP) surface modification. Liu et al. presented a core–shell catalytic platform by combining ZIF-67 and TP-BPY, which was embedded with Co nanoparticles and atomic Co-N₄.^[65] The transmission electron microscopy (TEM) image (Figure 3f) showed that the loading of COF resulted in uniform dispersion of nanoparticles and still retained the rhombic morphology. The introduction of the COF shell could efficiently protect ZIF-67 from aggregation and collapse and improve the thermal stability of the composite, making it possible to be a precursor for the preparation of COF@ZIF800 by pyrolysis. Zhang et al. first obtained ZIF-67 particles by chemical etching of ZIF-67 dodecahedra, which created favorable conditions for the formation of COF shell, and then converted to MOF-GC core by pyrolysis. Subsequently, the COF monomers were covalently attached to the MOF-GC core by Schiff base reaction, forming a core–shell heterogeneous structure, and finally, the composite was pyrolyzed to obtain GC@COF-NC with excellent electrical conductivity.^[66] There was a confining effect between COF and GC, which ensured that the core and shell would not separate during the pyrolysis and facilitated the formation of homogeneous microporous or mesoporous structures. In addition, the pyrolysis temperature affects the electron mobility since it can influence the degree of graphitization. In this study, the optimal pyrolysis temperature was 800 °C, when the catalyst had the best nitrogen content (4.61 at%) and graphite N ratio (36.34%). Moreover, Zhou et al. prepared a novel Ce-MOF@MCA nanocomposite with Ce-MOF as the core, where MCA was composed of melamine and cyanuric acid. The MCA synthesized in this study was a porous nanosphere formed by nanosheets with abundant pores aggregating with each other, while the Ce-MOF had a neat rod-like structure and interacted with each other to form large bundles. TEM images (Figure 3g) showed that the MCA shell did not change the irregular rod-like morphology of the hybrid during the synthesis process. The prepared nanohybrids not only maintained their original chemical structures and characteristics, but also exhibited interpenetrating morphology.^[67]

2.1.4. COF@MOF

With the continuous development of MOF@COF composites, researchers have gradually expanded their ideas to COF@MOF. Similarly, COFs can be used as cores with a MOF shell loaded on top, resulting in COF@MOF nanomaterials. However, in addition to covalent linkage, COF@MOF can also be prepared by coordination bonding and noncovalent linkage, which are determined by the matching size of the MOF and COF unit cells.^[68] Feng et al. proposed a modular approach for synthesizing COF@MOF.^[69] Specifically, an integrated system was separated into small individual modules, and the complex target structure was synthesized bottom-up through interchangeable modules. Due to the excellent stability of COF-303 and the mild synthesis conditions of zinc-based MOF-5, both were selected as the modular platform and shell, respectively. The PXRD patterns

were analyzed, and it was found that the crystal structures of COF-303 and MOF-5 were preserved intact during the synthesis process. In addition, the authors further synthesized other COF@MOF crystalline materials including COF-303@PCN-160, further illustrating the versatility of the modular synthesis strategy. This combination strategy not only facilitated the development of multicomponent frameworks, but also provided a possible way to construct stable, accurate, and high-performance COF@MOF core–shell materials. In order to obtain an excellent electrocatalyst, Huang's group reported a COF@ZIF-67 hybrid and used it as a precursor to obtain H-NSC@Co/NSC composites with core–shell structure by direct pyrolysis.^[70] Imidazole-functionalized COF (COF-SM) was selected as the core and ZIF-67 crystals were loaded on its surface by epitaxial growth. During the pyrolysis process, the strong force between COF and MOF resulted in the formation of an internal cavity, which was favorable for the charge diffusion kinetics and high accessibility of the active sites. In contrast, the shell Co/NSC embedded with Co gave the compound a stronger catalytic activity and effectively enhanced the potential for application in electrocatalysis.

2.2. Carbon Nanomaterials@COF

COFs with lightweight elements, robust chemical/thermal stability, and abundant long-range ordered nanopores might pose as efficient polymer electrocatalysts, however, their inherent low conductivity and the lack of metal sites hinder further applications.^[71–73] To address this issue, the combination of COFs with conductive substances to form a core–shell structure is an effective solution. The strong interaction between COF nanoshells and conductive carbon nanomaterials not only stabilizes the overall nanostructure but also effectively accelerates the electron transfer process.^[74] In particular, carbon nanomaterials can be used not only as electron transport channels but also as supports for other functional materials owing to their superior electron conductivity and outstanding stability.^[75] In this section, conducting carbon nanomaterials@COF composites with core–shell structure are summarized, and the carbonaceous core includes common carbon nanotubes (CNTs) as well as graphene.

2.2.1. Carbon Nanotubes@COF

CNTs are a kind of carbon material with excellent electrical conductivity commonly used in electrochemistry, and more importantly, the hybrid nanostructure is not only stabilized but also facilitated by electron transfer between CNTs and COFs due to π – π stacking effect.^[76–78] Therefore, researchers have paid attention to synthesizing COF/CNT composites. Liu et al. synthesized a core–shell catalyst with large mesopores and excellent oxygen reduction reaction (ORR) performance.^[79] Briefly, a COF shell rich in Co-Salophen was prepared on a CNT line using 1,3, 5-tricresol and diamminobenzidine via Schiff-base condensation reaction. The FTIR spectra of the composites revealed the disappearance of the stretching vibrations of the –CHO and –NH₂ groups and the formation of a new characteristic peak of the imine group at 1591 cm^{–1}, which indicated the successful loading of the biphenyl-based shell of COFs (Figure 4a). The introduction

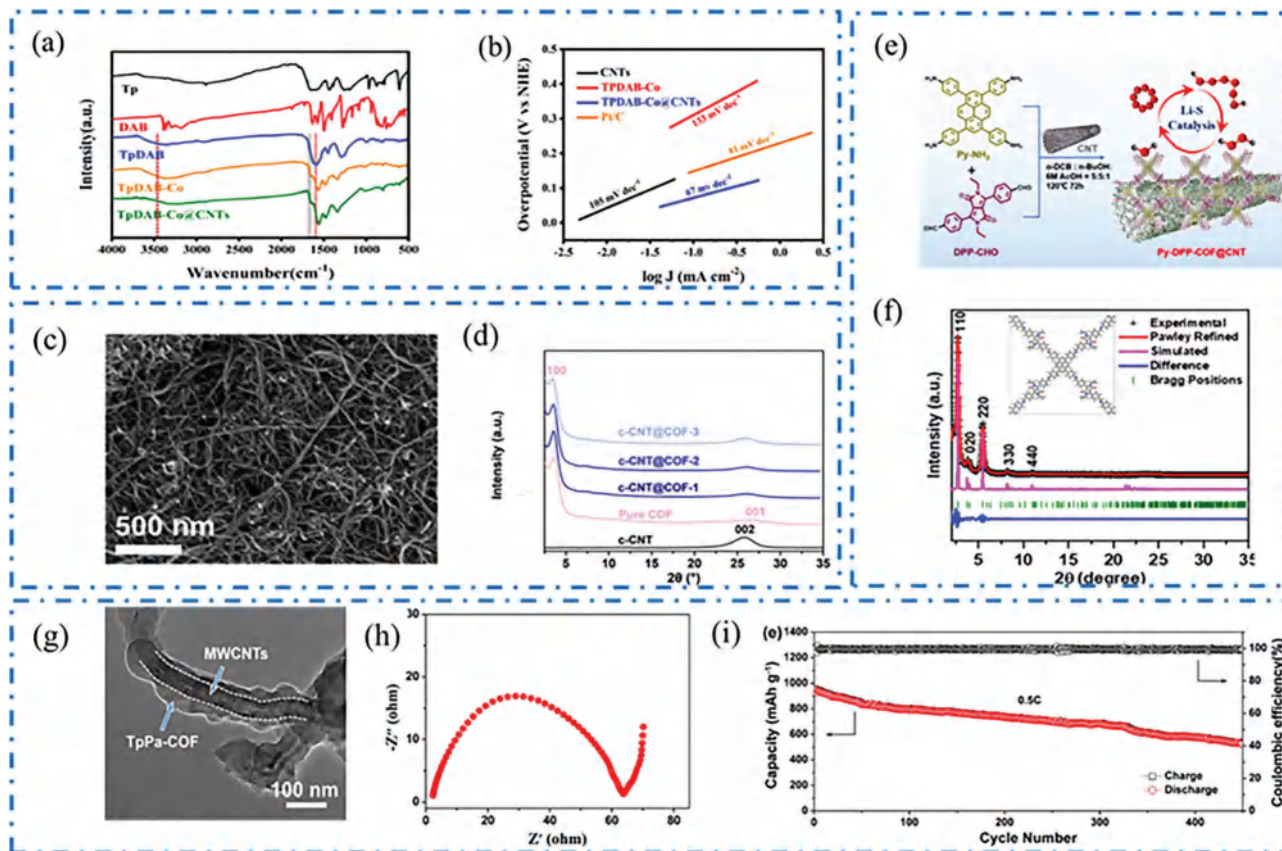


Figure 4. a) A comparison of the FTIR spectra of several materials. b) Tafel slopes of different catalysts. Reproduced with permission.^[79] Copyright 2020, Elsevier. c) SEM image of c-CNT@COF-3/CNT/CNF nanopaper. d) Powder X-ray diffraction patterns of the pure c-COF and CNT@COFs. Reproduced with permission.^[77] Copyright 2020, Elsevier. e) Schematic illustration of a method of preparing COF@CNTs and their application for Li-S catalysis. f) Experimental and simulated PXRD patterns of Py-DPP-COF. Reproduced with permission.^[80] Copyright 2021, American Chemical Society. g) TEM images of TpPa-COF@MWCNTs. h) The electrochemical impedance spectroscopy of S/TpPa-COF@MWCNTs. i) The cyclic performance and Coulombic efficiency at 0.5 C. Reproduced with permission.^[81] Copyright 2017 Elsevier B.V.

of CNTs reduced the resistance of the composites from 143.5 to 79.4 Ω for pure COFs, which undoubtedly enhanced the overall electron transport capability. Compared with 81 mV dec^{-1} of Pt/C, the Tafel slope of TPDA-B-Co@CNTs was 67 mV dec^{-1} , which confirmed the possible higher ORR efficiency of the core-shell composites from the side (Figure 4b). When used in the ORR reaction, its half wave potential ($E_{1/2}$) was 0.89 V, and the power density reached up to 156 mW cm^{-2} . The mesoporous structure of the core-shell material and the excellent electron transfer capability ensured efficient electrocatalytic reactions. Kong and co-workers successfully prepared c-CNT@COFs with core-shell structure.^[77] Carboxyl-functionalized carbon nanotubes (c-CNTs) were used as the core where DAAQ-TTFP COF shells with oxidation activity grew. The combination of the two components transformed the composite as a whole into nanofiber form (Figure 4c). XRD showed that all samples had a clear peak at $2\theta \approx 3.6^\circ$, and the pure COFs had a wide and weak peak at $2\theta \approx 26.6^\circ$ due to the π - π superposition of 001 planes, which was consistent with previous studies indicating the successful integration of the COF on CNT (Figure 4d). Also in 2021, An's group, as shown in Figure 4e, constructed the core-shell CNT@COF by integrating Py-DPP-COF 3 onto the

CNT surface via in situ polymerization.^[80] Furthermore, the authors used PXRD analysis to determine the crystalline structure of Py-DPP-COF, which had five well-resolved peaks at 2.69° , 3.80° , 5.47° , 8.21° , and 10.96° . The results indicated that it was in excellent agreement with the AA-eclipsed stacking model in a C2/m space group (Figure 4f). Besides these CNT@COF heterostructures, Zhang et al. developed a novel MWCNTs@COF (TpPa) nanocomposite via solvothermal method, where the π - π interaction between the two building blocks was used to facilitate the stacked growth of COFs on MWCNTs.^[81] The S/TpPa-COF@MWCNTs were subsequently obtained by heating the composites with the sulfur source at 155 $^\circ\text{C}$ under an argon atmosphere for 12 h. A distinct core-shell structure was found in the TEM images, indicating that the composites were successfully synthesized (Figure 4g). The loading of the COF shell provided rich and orderly microporous channels, which effectively suppressed the volume expansion of sulfur during the reaction; the selection of WMCNTs as the conductive core ensured that the composites had excellent electrical conductivity, as evidenced by the small semicircular diameter of the core-shell composites in the high and medium frequency regions (Figure 4h). When used as the cathode of a lithium-sulfur battery,

it provided an excellent initial discharge capacity at 0.05 C (1242.2 mAh g⁻¹) with excellent stability and an ultralow capacity decay rate of only 0.099% after each cycle (Figure 4i).

2.2.2. Graphene@COF

As a class of carbon nanomaterials, graphene typically has properties including high intrinsic electron mobility, outstanding electrical conductivity, and good chemical stability. Therefore, it can also be used as a conductive agent to combine with COF materials to form core-shell structures.^[82] Xiao's group prepared graphene@COF and explored its application in Li-CO₂ batteries.^[83] Specifically, graphene@COF hybrids were synthesized via in situ growth of imine COF9 with carbon dioxide (CO₂) capture capability on graphene via Schiff base reaction. Compared with pure COF or pure graphene, the composites exhibited excellent CO₂ absorption capacity, which might be related to the increased density of exposed micropores during the growth of COFs from graphene templates while confining CO₂ within the nanopore size to prevent its excessive diffusion, and did not significantly reduce the electronic conductivity of graphene. Using it as a cathode successfully improved the reversibility and rechargeability properties of the Li-CO₂ battery. It should be noted that the stability of Li-CO₂ battery was highly dependent on the consumption of Li⁺. In contrast to pure graphene cathodes, which constantly consumed Li, the small sized Li₂CO₃ particles formed within the micro-pores of the graphene@COF during the discharge process and decomposed to Li⁺ and CO₂ in the charge process, indicating that the consumption and regeneration of Li were reversible. Sun et al. obtained smooth COF@G modified separators by filtration of COF and graphene suspensions using polypropylene (PP) membranes. The selection of 5,10,15,20-tetrakis(4-aminophenyl)porphyrin (TAPP) and 4,4',4'',4'''-(ethene-1,1,2,2-tetrayl)tetrabenzaldehyde (ETTB) as COF monomers could suppress exciton energy dissipation and form an N-containing framework with abundant lithium sites, ensuring the deposition and catalytic efficiency of polysulfides, while the introduction of graphene significantly enhanced the electrical conductivity of the material, and the square resistance of COF@G was only 33 Ω square⁻¹, much smaller than the square resistance of over 20 000 Ω square⁻¹ of pure COF, ultimately forming a unique electron transfer chemistry.^[84]

2.3. Metal Nanoparticles@COF

Many metal nanoparticles (MNPs) have a wide range of applications in sensing,^[85,86] catalysis,^[47,87] medical,^[88,89] and devices.^[90] Although reducing the particle size to the nanoscale effectively enhances the reaction activity, unfortunately, they are thermodynamically unstable and usually show a tendency to aggregate with each other in order to reduce the surface energy. Therefore, controlling the dispersion of MNPs in solution is a key factor to ensure efficient and stable reactions.^[91] Among the many treatments, MNPs@COF core-shell compounds, obtained by combining different types of metal nanoparticles and COFs, have attracted the interest of researchers due to their unique advantages. For example, the programmable topology of COFs not only provides size selectivity but also carries a large number of active sites,

which can effectively enhance reactivity while avoiding the aggregation of MNPs. For a better understanding of MNPs@COF, the composites can be mainly divided into two categories according to their composition and functionalization. The first category is the primitive MNPs@COF, which includes only the MNPs core and the COF shell, and no other components. The second category is functionalized MNPs@COF, consisting of three or more components, which includes MNPs@COF and newly introduced components (precious metals, functional groups, etc.).

2.3.1. Primitive MNPs@COF

The composition of the primitive MNPs@COF is relatively simple, containing only MNPs and COFs. Currently, MNPs bound to COFs can be classified as magnetic and nonmagnetic according to whether they are magnetic or not. The most representative magnetic metal nanoparticles are magnetite (Fe₃O₄), maghemite (γ-Fe₂O₃), and relatively few nickel and cobalt compounds.^[49,92] The nonmagnetic MNPs are represented by CdS and TiO₂.

You's group prepared Fe₃O₄ NPs by a solvothermal method, and then the COF monomers, melamine (MA) and terephthalic acid (TPA), were used to synthesize the shell by Schiff base reaction to obtain magnetic covalent organic frameworks (Fe₃O₄@COF) modified by Fe₃O₄ nanoparticles (Figure 5a).^[93] As shown in Figure 5b, the isotherms of the composites were type IV with typical mesoporous properties, and both the specific surface area and pore volume were higher than those of pure NPs, indicating that the structural characteristics of the composites were favorable to the adsorption behavior. To understand the adsorption mechanism, the authors performed thermodynamic calculations, which showed negative values of ΔG⁰ and ΔH⁰, indicating that the adsorption behavior was a spontaneous and exothermic process and that physical adsorption dominated. The possible restriction of contaminant molecular motion after adsorption was demonstrated by ΔS⁰, and π-π interactions and hydrogen bonding were the main forces (Figure 5c). When used as an adsorbent, it showed excellent adsorption efficiency for bisphenol A (BPA: 140 mg g⁻¹) and bisphenol AF (BPAF: 290.4 mg g⁻¹). Deng et al. presented a core-shell Fe₃O₄@COF nanostructure by combining Fe₃O₄ NPs and COFs as a novel magnetic solid phase extraction (MSPE) adsorbent for four kinds of endocrine-disrupting phenols (Figure 5d). The FTIR spectra are shown in Figure 5e. Due to the benzene backbone and C=N bond introduced by the loading of the COF shell, the hybrids had new characteristic peaks at 1450–1600 and 1610 cm⁻¹, and the benzene ring and C=N bond can generate π-π interactions and hydrogen bonds with the target molecule to enhance the adsorption efficiency, respectively. The presence of carboxyl groups was evidenced by the absorption bands at 3421, 1640, and 1388 cm⁻¹, while the absorption band at 585 cm⁻¹ was attributed to Fe—O—Fe vibrations. TEM spectra showed that the composites exhibited a distinct core-shell structure, indicating the successful binding of COFs to MNPs with a shell thickness of about 25 nm (Figure 5f).^[44] Tan and co-workers had successfully constructed NiFe₂O₄@COF with a core-shell structure at room temperature.^[94] Like the previously mentioned Fe₃O₄, NiFe₂O₄@COF exhibited a typical type IV isotherm with mesoporous characteristics. However, since the specific surface area of NiFe₂O₄ was 32.7 m² g⁻¹, which was much higher than

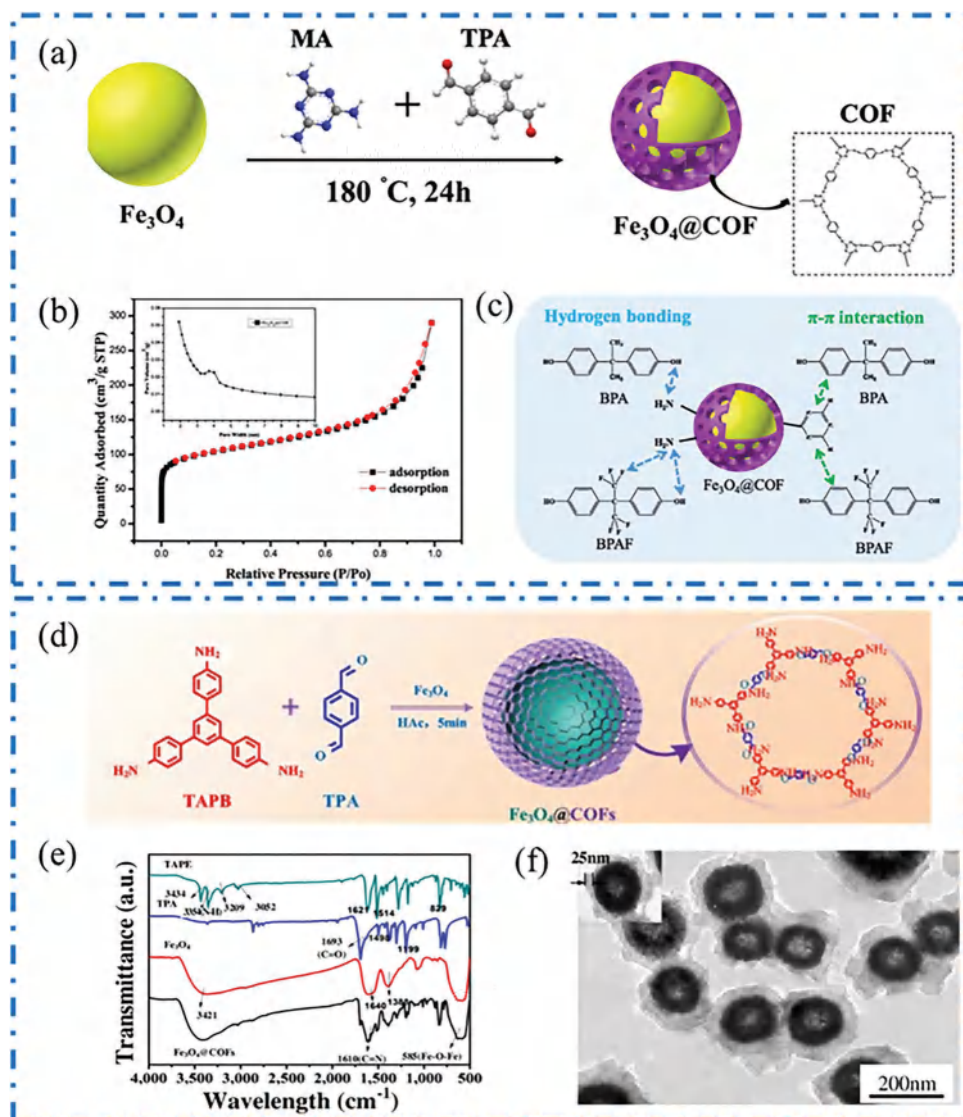


Figure 5. a) Schematic diagram of synthesized of $\text{Fe}_3\text{O}_4@\text{COF}$. b) N_2 adsorption–desorption isotherms and pore size distribution of $\text{Fe}_3\text{O}_4@\text{COF}$. c) Adsorption mechanism of BPA and BPAF on $\text{Fe}_3\text{O}_4@\text{COF}$. Reproduced with permission.^[93] Copyright 2020, Elsevier B.V. d) Preparation process of $\text{Fe}_3\text{O}_4@\text{COF}$. e) FTIR spectra of several materials. f) TEM images of Fe_3O_4 at 25 000 \times magnification. Reproduced with permission.^[44] Copyright 2019, Springer-Verlag GmbH Austria.

that of bare Fe_3O_4 of $9.6 \text{ m}^2 \text{ g}^{-1}$, $\text{NiFe}_2\text{O}_4@\text{COF}$ ($169.7 \text{ m}^2 \text{ g}^{-1}$) possessed better structural features than $\text{Fe}_3\text{O}_4@\text{COF}$ ($39.8 \text{ m}^2 \text{ g}^{-1}$) under the same synthesized conditions, which was a prerequisite for the excellent adsorption performance of the hybrids. When used as an extractant, it exhibited the highest average extraction efficiency of 90.01% for the six endocrine disruptors (EDS). The primitive magnetic MNPs@COF synthesized in recent years are shown in Table 1.

2.3.2. Functionalized MNPs@COF

Functionalized MNPs@COF are multifunctional composite materials consisting of three parts: the MNPs core, the COF shell, and functional components added as needed for the expected ap-

plication and required performance. The unique properties of both NPs and COFs make them suited to surface modification and functionalization to prepare functional materials according to requirements. Therefore, functionalized MNPs@COF composites can be classified into three categories depending on the location of surface modification and functionalization. The first category is that functionalized MNPs are encapsulated by the COF shell. The second is that the surface modified COF shell is wrapped with NPs. The third is where both the shell and the core are functionalized.

Functionalization of MNPs: MNPs are known to be less stable and have a tendency to aggregate with each other in solution due to their higher specific surface energy. Several effective strategies have been developed to prevent NPs aggregation, such as coating other materials,^[95,96] fixed in various

Table 1. Monomer and applications of primitive MNPs@COF (NA: not applicable).

Primitive MNPs@COF	COF components	Amount [mmol]	Objects	BET area [m ² g ⁻¹]	Pore volume [cm ³ g ⁻¹]	Pore diameter [nm]	COF shell thickness [nm]	Aspects	Ref.
TiO ₂ @COF	PDA; PAPB	0.03; 0.02	Benzyl alcohol (BA)	316.7	NA	NA	2–50	Catalytic	[47]
Fe ₃ O ₄ @COF	Dha Tab	0.048; 0.072	Parabens	267.5	NA	NA	35	Adsorption	[177]
Fe ₃ O ₄ @COF	MA; TPA	2.0; 3.0	Bisphenols	335.23	0.34	4.0	NA	Adsorption	[93]
Fe ₃ O ₄ @COF	TP; DA	0.30; 0.45	Plant growth regulators (PCR)	180.2	0.31	3.5	75	Adsorption	[178]
Fe ₃ O ₄ @COF	TP; BD	0.30; 0.45	Benzimidazole (BZD)	103.15	0.25	NA	NA	Adsorption	[112]
Fe ₃ O ₄ @TpPa-1	TP; Pa-1	0.30; 0.45	Cr (VI) Bisphenol A	485.2	0.34	2.0	10	Adsorption	[179]
Fe ₃ O ₄ @COFs	4,4'-biphenyldi-carboxaldehyde and TAP	0.15; 0.05	Sulfonamides (SAs)	30.6	0.187	2.0–5.0	10 ± 2	Adsorption	[180]
γ-Fe ₂ O ₃ @CTF-1	1,4-dicyanobenzene	0.016	Arsenic and mercury	1049	0.46	NA	NA	Adsorption	[92]
Fe ₃ O ₄ @BTA-DHBD	BTA; DHBD	0.30; 0.45	Bisphenols (BPs)	82.96	NA	2.82	30	Detection	[181]
Fe ₃ O ₄ @COF-DhaTph	Tph; Dha	0.0226; 0.0452	Cancer cells	200.5	NA	NA	70.75	Medical	[182]
NiFe ₂ O ₄ @COF	TPA; TAPB	0.30; 0.45	Triclosan (TCS)	169.7	0.276	3.9	NA	Extraction	[183]
Co ₃ O ₄ @TAPB-DMTP-	DMTP; TAPB	0.045; 0.030	Tertbutylhydroquinone (TBHQ)	1234	NA	2.5	NA	Detection	[85]
UCNPs@COFs	TFB; PDA	0.20; 0.30	Perfluorooctane sulfonate (PFOS)	NA	NA	1.6	5	Detection	[184]

porous support materials,^[93] or encapsulated in liposomes.^[97] These protective surface strategies not only enhance the stability and dispersion of NPs particles in water but also facilitate the introduction of COF shells, resulting in better performing composites.^[49] For example, Chen's group developed a novel Fe₃O₄@PEI@COF-LZU1 nanocomposite absorbent, where polyethyleneimine (PEI)-functionalized Fe₃O₄ NPs as the core (Figure 6a).^[98] Fe₃O₄ nanoparticles were first coated with PEI, the main purpose of which was to introduce amino groups to promote the formation of COF shells, and a tight covalent bond was formed between PEI and the shell. In addition, the aromatic ring and imine group on the outer shell of COFs could produce strong π - π stacking and hydrophobic interaction with the analyte, when used for the detection of polycyclic aromatic hydrocarbons (PAHs) by MSPE, which demonstrated a very low detection limit (0.2–20 pg mL⁻¹) and maintained a high operating level (91.0%–96.2%) after six cycles (Figure 6b). Excess copper in the environment can be a serious health hazard. To achieve accurate monitoring of copper ion concentrations, Li and co-workers prepared an Fe₃O₄@MOF@COF nanocomposite. Fe₃O₄@MOF was first synthesized by a modified solvothermal method, and then an appropriate amount of organic monomers were added and a COF shell was grown on its surface.^[99] Wrapping the MOF shell around the Fe₃O₄ NPs facilitated the retention of magnetism and prevented aggregation, while the introduction of the COF shell brought in more oxygen- and nitrogen-containing organic groups, which overcome the poor adsorption capacity of MOF for the target ions, resulting in a composite with excellent adsorption capacity and selectivity for Cu²⁺.

Functionalization of COFs: As mesoporous organic polymers composed of different kinds of covalently linked building blocks, COFs are easy to be modified in a highly controllable way due to

the adjustable aperture, regular voids, and other properties. The addition of functional components to COFs combines the favorable features of both, which increases the application potential of the hybrid. So far, there are several effective strategies that can be used for the efficient modification of COFs.

The first strategy is to selectively graft a functional group through addition or substitution reactions. Common types of functional groups include nitro, hydroxyl, carboxyl, etc. This not only selectively changes the properties of the composite itself, such as hydrophobicity and electronegativity, but also increases the active site and enhances the reactivity and selectivity. For example, Bi et al. prepared core-shell Fe₃O₄@COF-S-SH in two steps.^[100] Initially, the researchers synthesized magnetic COF (Fe₃O₄@COF-V) at room temperature and then mixed it with 1,2-ethylenedithiol and stirred vigorously. The thiol-ene "click" reaction of the mixed system occurred at 80 °C, and then sulfur-functionalized Fe₃O₄@COF-SH was obtained. The introduction of thioether functional groups allowed the hybrids to have stable planes and abundant adsorption sites for efficient extraction of trace Hg from water samples. Adsorption experiments confirmed that the hybrids showed excellent adsorption capacity for various forms of mercury, including monomeric mercury (571 mg g⁻¹), methyl mercury (559 mg g⁻¹), and ethyl mercury (564 mg g⁻¹). Chen's group synthesized a core-shell composite (Fe₃O₄@COF-(NO₂)₂). The nitro functional group was introduced because the authors chose to replace the benzidine (BD) monomer with BD-(NO₂)₂ during the monomer polymerization process (Figure 6c).^[101] The octanol-water partition coefficient of neonicotinoid insecticides was relatively low, and the introduction of nitro functional groups precisely enhanced the hydrophilicity of the composites. As shown in Figure 6d, the water contact angle of the hybrids decreased from 132.3° to 28.6°

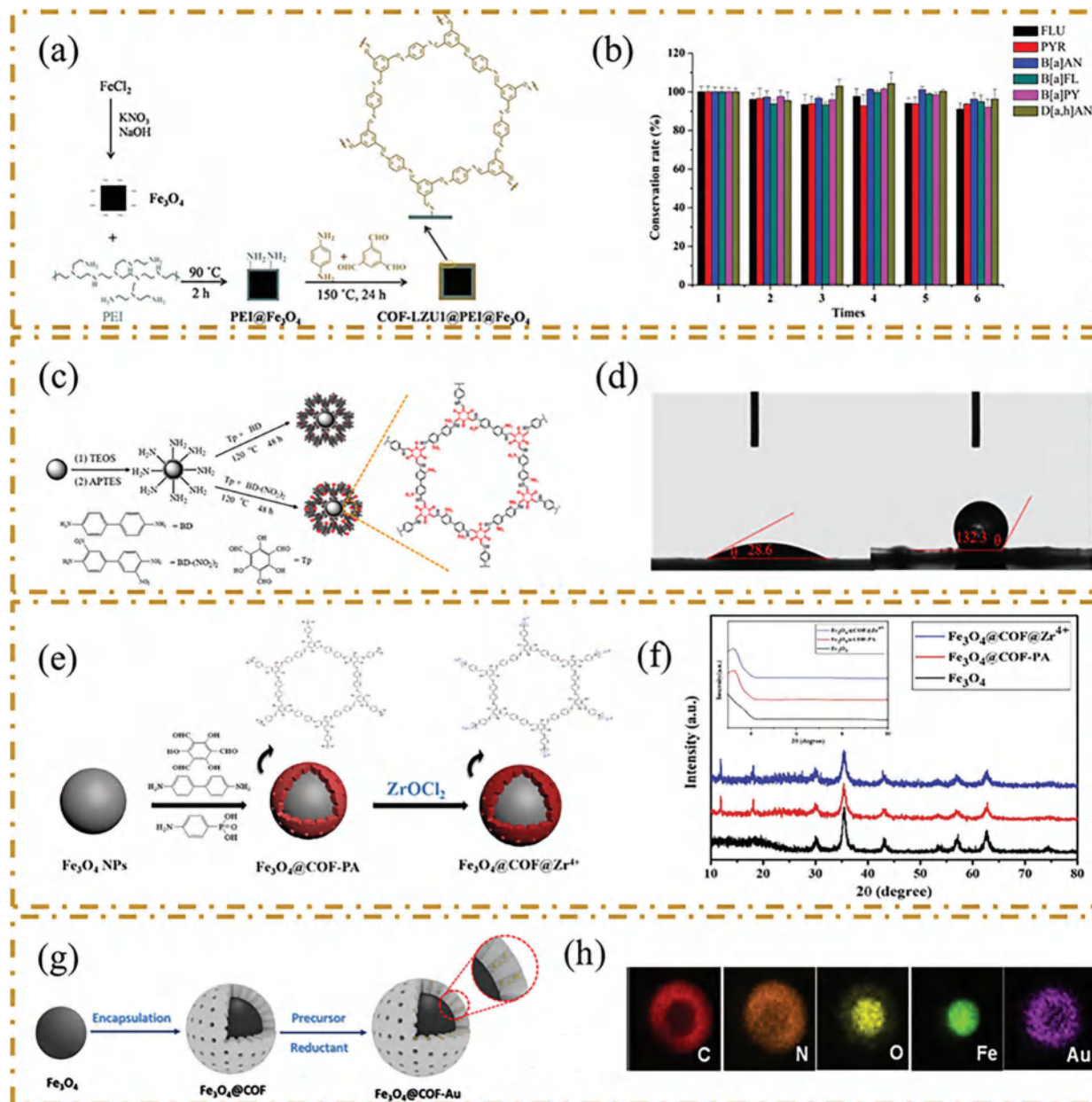


Figure 6. a) Schematic of preparation of COF-LZU1@PEI@Fe₃O₄. b) Reusability of COF-LZU1@PEI@Fe₃O₄. Reproduced with permission.^[98] Copyright 2017, Springer-Verlag GmbH Austria. c) Schematic illustration of the synthesized Fe₃O₄@COF-(NO₂)₂ microspheres. d) Water contact angle of Fe₃O₄@COF-(NO₂)₂ (left), and Fe₃O₄@COF (right). Reproduced with permission.^[101] Copyright 2020, Elsevier B.V. e) Schematic fabrication process of Fe₃O₄@COF@Zr⁴⁺ nanocomposites. f) XRD spectra of several materials. Reproduced with permission.^[103] Copyright 2020, Elsevier. g) Schematic diagram of the preparation procedure of Fe₃O₄@COF-Au NPs with core-shell structure. h) EDX maps of Fe₃O₄@COF-Au. Reproduced with permission.^[104] Copyright 2019, Elsevier B.V.

after the introduction of nitro groups. In addition, it would also form hydrogen bonding sites with the target molecules and thus possess excellent adsorption properties. The LOD was 0.02–0.05 ng mL⁻¹ when used as MSPE for the determination of contaminants in samples, and the recoveries remained at high levels (77.5%–110.2%) after seven cycles.

The second strategy is to modify COFs with metal elements, including metal ions or NPs. The introduced metals may form coordination bonds with the reactants to enhance the catalytic ef-

fect or participate in the adsorption process through electrostatic forces. And before implementing the metal modification strategy, the possible agglomeration phenomenon, the magnitude of the binding energy between the two and the possible changes in the structural properties should be considered.^[102] Li et al. as shown in Figure 6e, successfully synthesized the Zr⁴⁺-immobilized COF-based core-shell composites. Fe₃O₄@COF@Zr⁴⁺.^[103] At first, the magnetic nanoclusters were obtained by a solvothermal reaction. The core-shell structure of Fe₃O₄@COF-Au was

subsequently synthesized using a one-pot strategy. The required phosphate ions could be obtained directly through the coordination of Zr^{4+} phosphate, resulting in the surface of the COF shell being decorated with a large amount of Zr^{4+} ions. Due to the successful loading of the COF shell, new peaks of 3.31° and 11.92° appeared in the XRD patterns (Figure 6f), while the introduction of Zr^{4+} changed the zeta potential of the core-shell composites from -4.3 to $+3.7$ mV and did not change its crystallinity. In addition, some ultrafine noble metal nanoparticles with excellent catalytic properties, such as Au and Pd, can also be confined within the COFs to prevent aggregation, allowing the compound to integrate both catalytic and magnetic properties. For example, Zheng's group reported the preparation of $\text{Fe}_3\text{O}_4@\text{COF-Au}$ NPs nanocatalysts with excellent catalytic performance for 4-NP and methylene blue (MB) by encapsulating small-size noble metal Au NPs in COFs using the NaBH_4 post-reduction method (Figure 6g).^[104] The uniform color distribution of energy dispersive X-ray (EDX) spectroscopy (Figure 6h) indicated that the COF shell was successfully loaded with Fe_3O_4 NPs and the Au NPs were uniformly distributed inside the COF cavity. Through the same procedure, Pd and Pt ultrafine NPs could also be successfully anchored in the shell of $\text{Fe}_3\text{O}_4@\text{COF}$ by the same method, indicating that this method could be extended to the fabrication of $\text{Fe}_3\text{O}_4@\text{COF}$ core-shell hybrids containing other precious metal ultrafine NPs.

Functionalized MNPs@COF: Functionalized MNPs@COF is one in which both the core and the shell are modified. In general, their synthesis is not a single process; it combines both synthesis and modification steps and generally uses a multistep modification approach, making the preparation process more complicated than the original NPs@COF.

$\text{Fe}_3\text{O}_4@\text{COF-COOH}$ is a typical example.^[105] The Fe_3O_4 NPs were first wrapped with a layer of SiO_2 with the aim of enhancing the nanoparticle reaction stability and providing a sufficient pore volume for shell loading, followed by the introduction of carboxyl groups on the loaded COF shell, which can be involved in weak cation exchange interactions. Some halogen elements, including fluorine, could also be suitable for use in modifying NPs@COF, to obtain functionalized COF-based core-shell materials. Zhang et al. introduced fluorine-containing ligands into NPs@COF and synthesized magnetic adsorbents $\text{Fe}_3\text{O}_4@\text{TpPa-F}_4$.^[106] The Fe_3O_4 NPs were first modified, thereby obtaining $\text{Fe}_3\text{O}_4@\text{NH}_2$. Then $\text{Fe}_3\text{O}_4@\text{TpPa-F}_4$ was finally obtained by two steps, namely the synthesis of $\text{Fe}_3\text{O}_4@\text{TpPa}$ and the introduction of fluorine-containing ligands. The introduction of fluorinated COF-containing shells not only improved the stability and specific surface area of the complexes but, more importantly, increased the adsorption capacity and selectivity of the complexes for perfluorinated compounds (PFCs) due to strong fluorine-fluorine interactions, which led to a greater potential for applications in the treatment of related contaminants.

2.4. Other Materials@COF

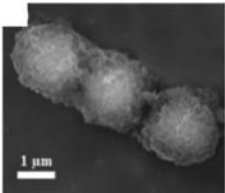
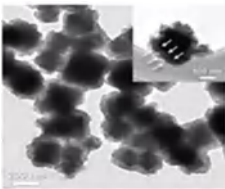
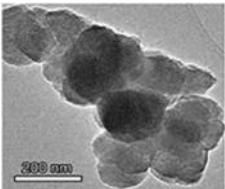
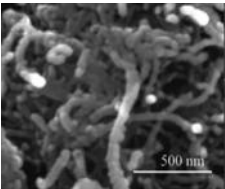

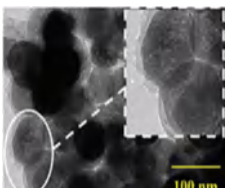
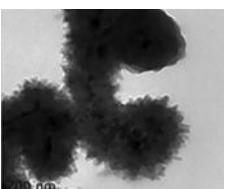
In addition to the usual MOFs, MNPs, and CNTs, researchers have also attempted to combine other materials with COFs to obtain core-shell composites. Recently, Gao et al. prepared $\text{MCNC}@\text{COF}@\text{Zr}^{4+}$ composites where highly magneti-

cally responsive magnetic colloidal nanoclusters (MCNC) as the core.^[107] The 2D COF shell was first loaded onto the inner core surface by aldimine condensation. The obtained $\text{MCNC}@\text{COF}$ was then reacted sequentially with succinic anhydride (SA) and pamidronic acid (PA). Finally, the $\text{MCNC}@\text{COF}@\text{Zr}^{4+}$ composites were synthesized via Zr^{4+} -phosphate coordination. Using phosphopeptides as subjects, the researchers found that the core-shell materials exhibited excellent adsorption capacity and selectivity in practical applications. Nanocrystals are nanoscale crystals with homogeneous dimensions, usually with good dispersion. To overcome the shortcomings of conventional synthesis methods that allow NCs to be confined by COF pores, Guntern et al. synthesized NCs@LZU1 hybrids by encapsulating nanocrystals (NCs) in COFs via the seed growth method. The material synthesized by this method could be precisely tuned to its thickness and retain crystallinity.^[108] It was worth mentioning that the synthesized complexes retained all the functions of NCs, providing a reference for the design of synergistic hybrids. There are relatively few reports on COF@COF materials because it is difficult to tune the morphological structure of the materials. Recently, Zhao et al. synthesized a COF@COF photocatalyst with S-scheme heterojunction for photocatalytic regeneration of nicotinamide adenine dinucleotide phosphate (NADPH) using two COFs of different Fermi energy levels.^[109] The inner core COF (HCOF) had a hollow structure that improved light collection efficiency through multiple scattering, while the pyridine structure of the COF shell (COFBpy) helped to immobilize the Rh-based co-catalyst. HCOF@Rh-COFBpy exhibited a more negative shift in surface potential under light, which proves that electrons were transferred from the inner COF core to the outer COF shell and finally combined with holes. And the photogenerated electrons generated on the COF shell were involved in the photoreduction reaction to obtain the reaction product 1,4-NADPH. The stepwise charge transfer path in the S-type heterojunction enhanced the charge separation efficiency, so the prepared heterojunction had high catalytic efficiency. Photocatalytic experiments showed that the turnover frequency of NADPH regeneration was almost three times higher than that of Rh-COFBpy ($2.6 \text{ mmol g}_{\text{Rh-COF}}^{-1} \text{ h}^{-1}$). After seven run cycles, 73% of the initial activity was still present.

3. Synthesis Method of COF-Based Core-Shell Composites

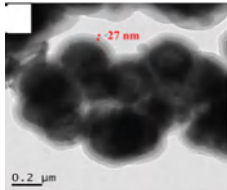
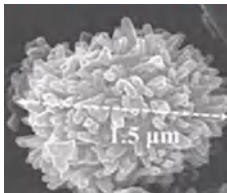
The unique properties of COF-based core-shell hybrids make them ideal for applications in the environmental and energy fields. However, one factor that limits its further dissemination is the relatively complex synthesis. Hence, suitable methods to prepare COF-based core-shell materials must be developed. The key to the preparation of core-shell nanomaterials is the tightness of the core-shell connection and the growth thickness of the shell.^[32] Based on this, researchers have developed several synthetic approaches, such as seed-mediated in situ growth, one-pot polymerization, coating agent-assisted methods, and coordination-induced interlinked hybrid methods. This section provides a systematic discussion of these classical synthetic methods. In particular, **Table 2** summarizes the morphology of some core-shell hybrids as well as the synthesis conditions to

Table 2. Preparation method of COF-based core-shell structure.

Composites	SEM/TEM images	Method	Conditions	Ref.
COF@MoS ₂		Seed-mediated in situ growth	120 °C for 72 h	[185]
dye/MOFs@COFs		Seed-mediated in situ growth	Room temperature for 3 d	[186]
aza-MOF@COF		Seed-mediated in situ growth	110 °C for 3 h	[187]
ZW-COF@CNT		One-pot polymerization	120 °C for 72 h	[188]
COF@CNT		One-pot polymerization	120 °C for 72 h	[148]
Fe ₃ O ₄ @TpTta		One-pot polymerization	120 °C for 72 h	[189]
CuO@TAPB-DMTP-COF		One-Pot polymerization	120 °C for 72 h	[190]

(Continued)

Table 2. (Continued).

Composites	SEM/TEM images	Method	Conditions	Ref.
Fe ₃ O ₄ @COF-COOH		Coating agent-assisted growth	120 °C for 72 h	[105]
COF/Mn-MOF		Coordination-induced interlinked hybrid	160 °C under microwave irradiation for 30 min	[117]

Reproduced with permission.^[185] Copyright 2022, Elsevier Ltd. Reproduced with permission.^[186] Copyright 2022, American Chemical Society. Reproduced with permission.^[187] Copyright 2020, Wiley-VCH GmbH. Reproduced with permission.^[188] Copyright 2022, Elsevier Inc. Reproduced with permission.^[148] Copyright 2022, the Royal Society of Chemistry. Reproduced with permission.^[189] Copyright 2023, American Chemical Society. Reproduced with permission.^[190] Copyright 2022, Elsevier B.V. Reproduced with permission.^[105] Copyright 2020, Elsevier B.V. Reproduced with permission.^[117] Copyright 2019, Wiley-VCH Verlag GmbH & Co.KGaA.

visualize the correspondence between the aforementioned methods and structures.

3.1. Seed-Mediated In Situ Growth Method

The seed-mediated in situ growth method is derived from the synthesis of imine-linked COFs by heterogeneous nucleation and growth.^[110] In general, this method consists of two steps. At first, seed particles are grown on the substrate surface using low concentrations of organic monomers. Prior to this, the substrate needs to be modified to introduce amino groups, which facilitate compatibility. And then, amino or aldehyde groups on the seed surface can guide the monomer to form a COF shell, resulting in a hyperbranched and cross-linked core-shell structure. A typical example was the NH₂-MIL-125@TAPB-PDA nano-photocatalyst.^[55] First, a small amount of terephthalaldehyde (PDA) was dissolved in the MOF suspension and stirred thoroughly for 1 h until well mixed, and then acetic acid (HAC) and 1,3,5-tris(4-aminophenyl) benzene (PAPB) were added, thus forming seed particles on the MOF surface. Next, the pre-synthesized intermediate products were mixed with monomeric PDA and PAPB solutions and heated with continuous stirring at 120 °C for 72 h. Finally, the yellow product obtained by centrifugation was dried under vacuum at 120 °C for 12 h, resulting in successful MOF@COF composites with core-shell structures (Figure 7a). This new approach provided a facile and effective means for synthesizing COF core-shell structures. Similarly, Yola et al. synthesized novel core-shell Ti-MOF@COF compounds by assembling COF shells on Ti-MOF core.^[111] First, PDA was dissolved in Ti-MOF solution with strong stirring for 1 h, then PAPB and HAC were mixed with the above suspension and stirred until homogeneous, by which time heterogeneous seed nuclei had formed on Ti-MOF. Then the monomer solutions PDA and PAPB were continued to be added to the final solution and heated at 100 °C for 60 h, and finally porous Ti-

MOF@COFs materials with core-shell structure were successfully obtained (Figure 7b). Interestingly, the composites could be bound to the target via π - π stacking, electrostatic, and hydrogen bonding, thus allowing their application in electrochemical sensors.

The seed-mediated in situ growth method is universally applicable and can be used to obtain core-shell composites by introducing seed particles on the surface of other core materials, including MNPs or carbon nanomaterials, in addition to MOFs. Li et al. synthesized Fe₃O₄@COF core-shell hybrid materials by seed-mediated in situ technology.^[112] The pre-synthesized Fe₃O₄ nanospheres were first modified with 3-aminopropyltriethoxysilane (APTES), which led to the amino-modified Fe₃O₄-NH₂. Then, the monomer Tp of COFs was grafted onto Fe₃O₄-NH₂, and a seed was formed on its surface, which can act as a bridge and facilitate the formation of the core-shell structure through the Schiff base reaction. Then the Tp and BD monomer solutions were added, mixed thoroughly with xylene/dioxane and stirred at 120 °C for 48 h. Since the core of the composite material was magnetic, it could be quickly separated from the sample matrix under circumstances of external magnetic field conditions; thus, filtration, centrifugation, or other complex procedures were not necessary. Due to the good crystallinity and stability, Chen et al. synthesized core-shell composites by growing TAPB-DMTP-COF shells in situ on the surface of Co₃O₄ (Figure 7c).^[85] Researchers found that if the COF shells were grown directly on CO₃O₄-NH₂, the binding of the two was not complete, which led to the aggregation of amorphous 2D COFs. In contrast, pre-grafting the COF monomers onto CO₃O₄-NH₂ improved the homogeneity of the shell's growth, which suggested that using a seed-mediated in situ growth approach was key to the manufacturing of uniformly crystallized COF shells.

Compared with the conventional method, the seed growth method introduces seeds into the preparation system, which accelerates the COF shell growth rate, easily obtaining satisfactory core-shell structure and relatively high crystallinity. However, it

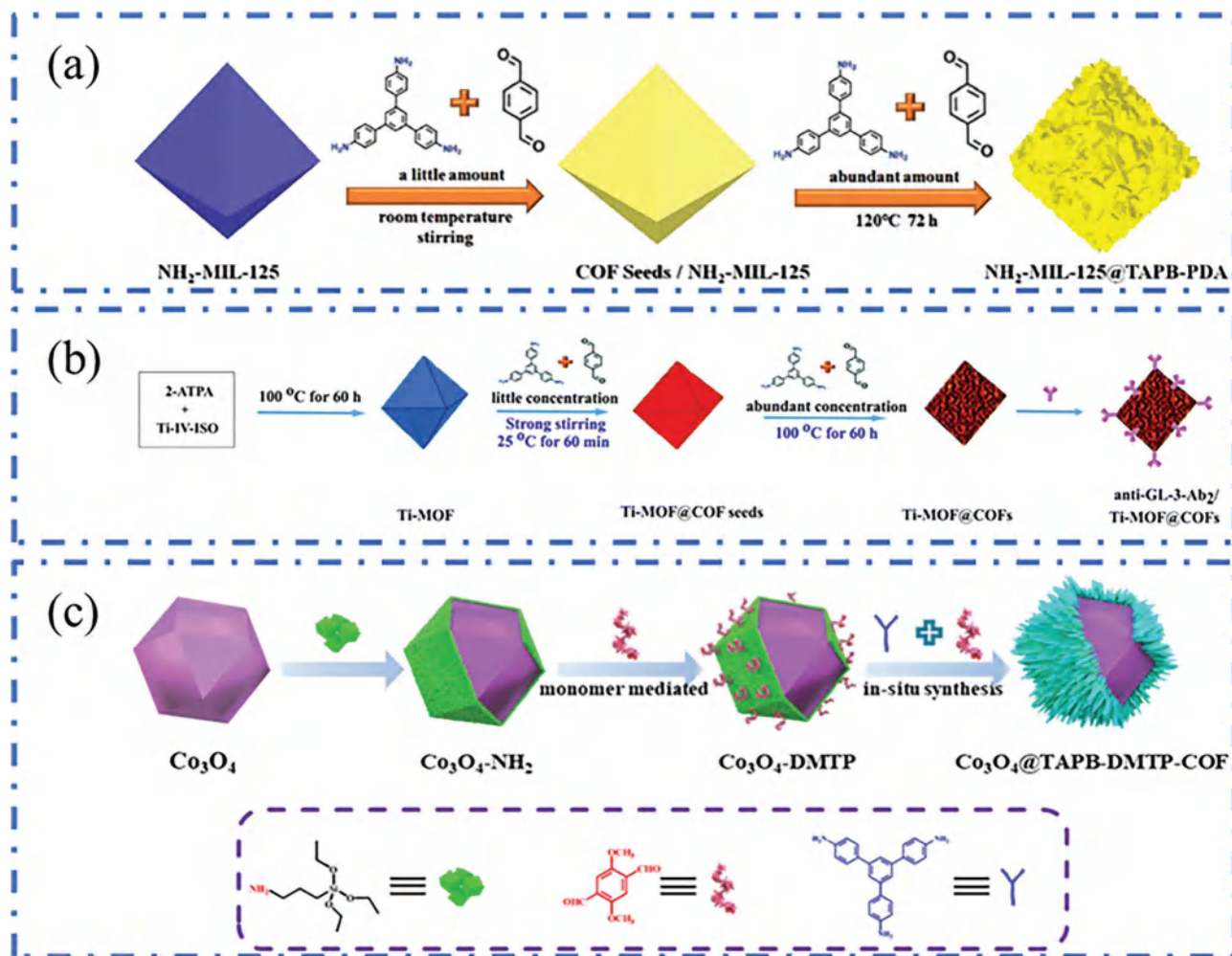


Figure 7. a) Schematic diagram of the preparation process of $\text{NH}_2\text{-MIL-125@TAPB-PDA}$ composites. Reproduced with permission.^[55] Copyright 2019, Elsevier B.V. and Science Press. b) Prepared core-shell Ti-MOF@COFs hybrid. Reproduced with permission.^[111] Copyright 2020, The Royal Society of Chemistry. c) Schematic illustration of the synthesis of $\text{Co}_3\text{O}_4\text{@TAPB-DMTP-COF}$ core-shell structure composite by in situ growth strategy. Reproduced with permission.^[85] Copyright 2021, Elsevier B.V.

is particularly important to mention that structural defects due to the aggregation of seed nuclei need to be avoided during the preparation process.

3.2. One-Pot Polymerization Method

The one-pot polymerization method refers to adding each component to the reaction system in one step, including the core material, COF monomers, and catalyst, and then synthesizing composites with homogeneous core-shell structure by polymerization reaction under specific conditions. The reaction components are usually well mixed by stirring or sonication before the reaction. Compared to other synthetic methods, one-pot polymerization synthesis has attracted the great interest of researchers because it shortens the reaction steps of the whole route without the separation of intermediates and improves the synthesis efficiency. Most Carbon Nanomaterials@COF composites can be synthesized by monomer polymerization. For example, Kong's

group synthesized core-shell CNT@COF material based on a one-pot condensation reaction (Figure 8a).^[113] In the present work, the desired reactants, including COF monomers, CNTs, FeCl_3 , and acetic acid, were mixed and stirred at room temperature. Pyrrole was then added, and the mixture was continued for another 12 h. The obtained COF@CNT hybrids were filtered and dried. It was worth mentioning that the synthesized COF@CNT nanocomposites could be used as precursors and annealed at 800°C to form CNT-twisted nitrogen-doped carbon nanospheres (N-C@CNTs) with good electrocatalytic properties. Similarly, to address the electrical insulation of COFs, Han et al. synthesized a SWCNTs@TpPa-COFs nanohybrid by a one-pot polymerization method (Figure 8b).^[74] SWCNTs as well as monomers Pa and Tp were first added to Pyrex tubes and then sonicated in a mixture of trimethylbenzene/1,4-dioxane/HAC for 30 min, degassed, and stored in an oven at 120°C for 3 d. After a series of filtration, washing, and drying, the red end product was obtained.

Recently, the encapsulation of nanoparticles in COFs has attracted extensive research by researchers. As mentioned in the

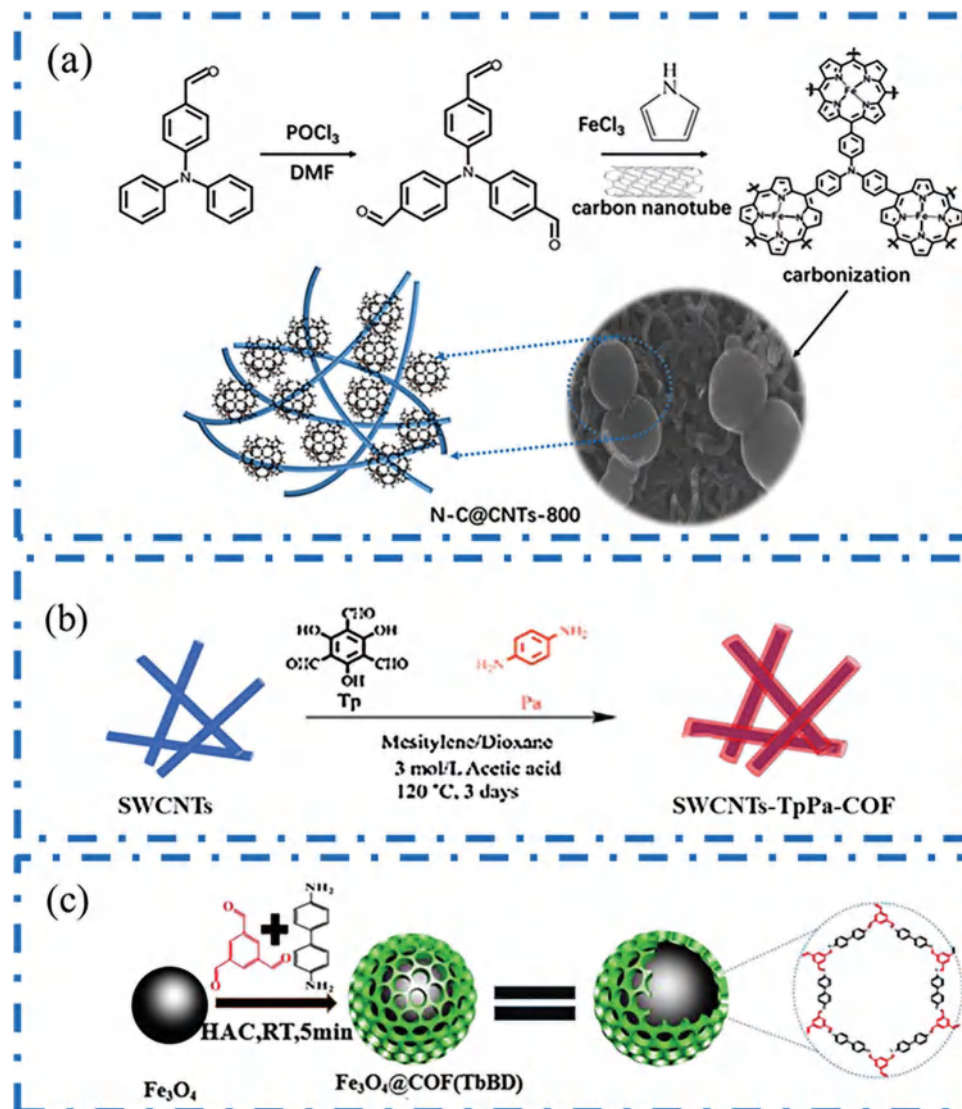


Figure 8. a) Schematic diagram of the synthesis of N-C@CNTs-800 carbon materials. Reproduced with permission.^[113] Copyright 2019, Springer-Verlag GmbH Germany. b) Schematic representation of the synthesis of SWCNTs-TpPa-COFs. Reproduced with permission.^[74] Copyright 2017, Elsevier B.V. c) Schematic representation of the fabrication process for Fe₃O₄@COF(TbBD) materials. Reproduced with permission.^[114] Copyright 2021, Springer Nature.

second part earlier, the synthesis of core-shell nanomaterials combines the advantages of COFs and NPs, can effectively prevent the aggregation of nanoparticles and facilitate surface modification. The preparation of MNPs@COF via a convenient and efficient one-pot polymerization method facilitates their large-scale application. For example, Zhao and co-workers developed Fe₃O₄@COF nanospheres.^[114] Specifically, Fe₃O₄ NPs previously prepared by a hydrothermal method were mixed with 1,3,5-trimethylbenzene (Tb) and benzidine (BD) with dimethyl sulfoxide (DMSO) and sonicated for 5 min, after which the catalyst HAC was added and the reaction was carried out at room temperature for 20 min. After that, the resulting product was washed and dried at 45 °C for 8 h (Figure 8c). Some surfactants, such as PVP, are often used during the construction of COF-based core-shell materials due to their ability to enhance

the interaction between the subject and the guest and effectively promote the heterogeneous nucleation of COFs.^[115] For example, Hou et al. synthesized CuFe₂O₄/Ag@COF by the one-pot polymerization method, in which CuFe₂O₄/Ag was used as the core.^[87] CuFe₂O₄/Ag nanoparticles were first mixed with amphiphilic PVP to assist in the formation of the COF shell due to its ability to stabilize nanoparticles in the reaction solution and to enhance the affinity between the polar groups of PVP and the organic linker. The synthesized composites had high catalytic performance and recoverability and high potential for application as reduction catalysts for 4-NP.

In general, the one-pot polymerization method can facilitate the construction of core-shell structured COFs with fewer reaction steps, simplifying the synthesis procedure and conforming to economic principles. However, this strategy requires stringent

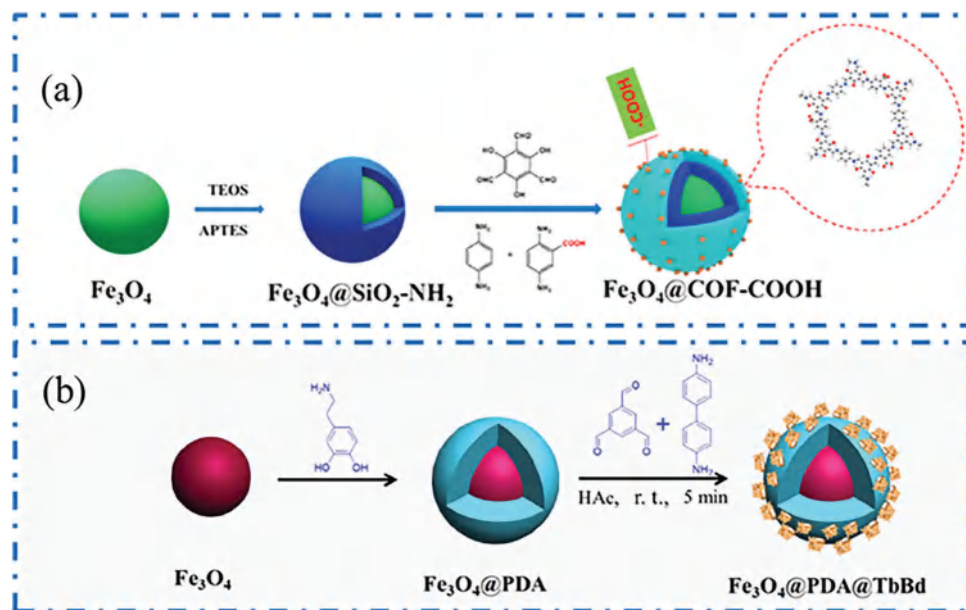


Figure 9. a) Synthetic strategy of $\text{Fe}_3\text{O}_4@\text{COF-COOH}$. Reproduced with permission.^[105] Copyright 2020, Elsevier B.V. b) Schematic illustrations of the preparation of $\text{Fe}_3\text{O}_4@\text{PDA@TbBd}$. Reproduced with permission.^[116] Copyright 2018, American Chemical Society.

reaction conditions to control the growth rate and morphology of the composite shells. Further exploration is needed if industrial production is to be carried out on a large scale.

3.3. Coating Agent-Assisted Growth Method

With their ability to deposit on a variety of organic and inorganic substrates and exhibit good environmental stability, excellent water dispersibility, and good biocompatibility, coating agents have attracted increasing interest from researchers by virtue of their versatile surface modification, and there have been several reports on the coating agent-assisted synthesis of COF-based core-shell materials. Commonly used coating agents today include tetraethyl orthosilicate (TEOS) and polydopamine (PDA).

Hu et al. synthesized a carboxyl-functionalized nanomaterial with core-shell structure by a coating agent-assisted method (Figure 9a).^[105] The Fe_3O_4 NPs obtained by a hydrothermal method were first coated with a layer of TEOS coating agent, and $\text{Fe}_3\text{O}_4@\text{SiO}_2$ was obtained by stirring at room temperature, followed by the introduction of amino groups to obtain $\text{Fe}_3\text{O}_4@\text{SiO}_2\text{-NH}_2$. $\text{Fe}_3\text{O}_4@\text{SiO}_2\text{-NH}_2$, TFP, acetic acid, and monomer solution were then mixed to obtain $\text{Fe}_3\text{O}_4@\text{COF-COOH}$ under specific conditions. The SiO_2 interlayer not only facilitated the loading of the COF shell, but also changed the hydrophobicity of the composite, and highly polar carboxylated COFs had a higher affinity for the analyte sulfonamide due to the principle of similar phase solubility. Yan and co-workers similarly prepared a $\text{Fe}_3\text{O}_4@\text{PDA@TbBd}$ hydrophilic nanosphere with core-shell structure by a coating agent-assisted method.^[116] First, polydopamine was coated on Fe_3O_4 NPs to create a PDA layer, and subsequently, nanospheres were attained by adding monomer solutions Tb, Bd, and DMSO and reacting under appropriate conditions (Figure 9b).

3.4. Coordination-Induced Interlinked Hybrid

As with the composites synthesized by previous synthetic methods, the binding between COFs and components is relatively simple, and interlinked hybridization at the molecular-level remains unexplored. Therefore, in order to fully utilize the advantages of COFs and other components to obtain optimal performance, Wang's group designed a COF/Mn-MOF hybrid structure by molecular linkage through ligand induction.^[117] Due to the strong coordination ability of the manganese ion, the Mn centers in Mn-MOF expanded from six-connected to seven-coordination and more connections with electron-rich N atoms in the COFs, which led to the formation of COF/Mn-MOF hybrids. In particular, the 2D layered COFs were dispersed and vertically stacked on the Mn-MOF core, with an overall spherical structure. It is worth mentioning that the interlinked structure of the COF/Mn-MOF composite led to a reassembled microstructure of COFs and MOFs, so that the composites had hierarchical porous features and more satisfying surface areas.

4. Effects of COF Shells on Structure and Performance of Composites

In line with the composition of the COF-based core-shell composites, the performance of materials is affected by the COF shell and the inner core. In general, the introduction of COF shells brings about structural changes and the resulting changes in magnetic, reusability, catalytic, and electrochemical properties that may arise.

4.1. Structure

The surface morphology and dimensions of the composites can be obtained by scanning electron microscopy (SEM) and TEM,

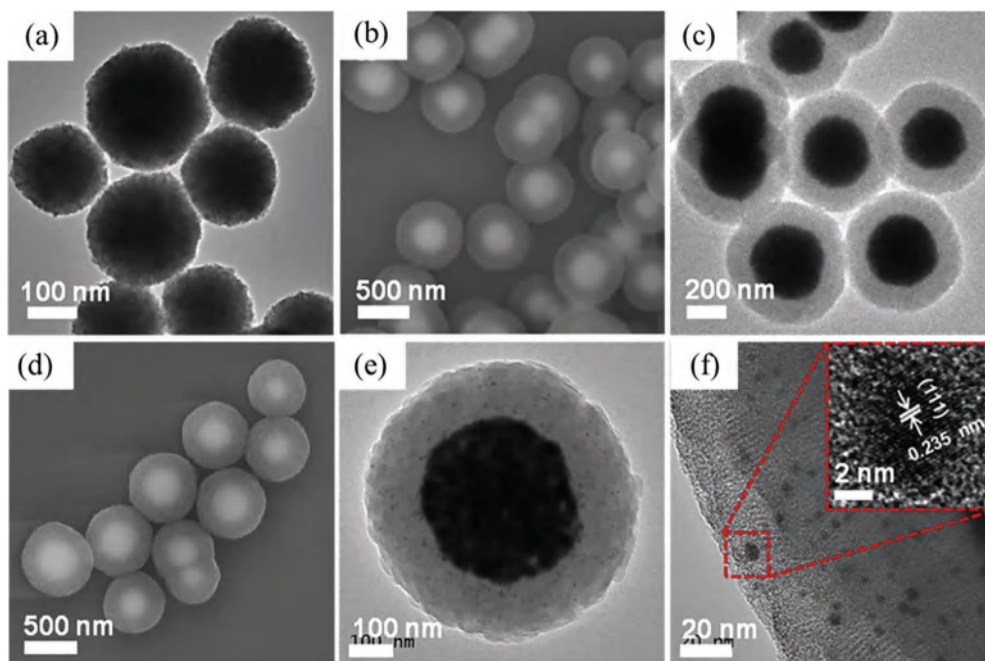


Figure 10. a) TEM image of Fe_3O_4 NPs. b) SEM and c) TEM images of $\text{Fe}_3\text{O}_4@\text{COF}$. d) SEM, e) TEM, and f) HRTEM images of $\text{Fe}_3\text{O}_4@\text{COF-Au}$. Reproduced with permission.^[104] Copyright 2019, Elsevier.

interestingly, the core-shell structure as well. The complexes usually have a rough appearance due to the encapsulation of the COF shell. For example, **Figure 10d–e** shows the TEM and SEM images of the synthesized $\text{Fe}_3\text{O}_4@\text{COF}$, respectively. From this, it was obtained that the edges of $\text{Fe}_3\text{O}_4@\text{COF}$ showed a smooth spherical shape and had a distinct core-shell structure, in which the total particle diameter was 650 nm while the shell thickness was 150 nm.^[104]

The various properties of the synthesized COF-based core-shell composites are influenced by the porous polymer COF shell and the special core-shell structure, which determines their potential for excellent application in a particular field. A key factor in determining the effectiveness of adsorption, catalytic activity, and other properties of porous materials is the specific surface area, and its determination is of great importance for scientific research as well as industrial production, which can generally be determined by the Bruno–Emmett–Teller (BET) apparatus.

In general, the surface area of COF-based core-shell hybrids lies between the shell and the core. Specifically, when the surface area of the selected core is larger than that of the individual COF, the surface area of the synthesized composite is between the core and the shell and decreases slightly with increasing of the COF shell thickness. When the specific surface area of the inner core is inferior to the pure COFs, then the loading of the shell facilitates an overall increase in the specific surface area of the material.^[34,118] If quasi-microscale pores are formed at the interface between the COF crystal and the core, or if the COFs distribution in the composite is more dispersed, the complex possesses a larger surface area and pore volume.^[117,119] Furthermore, doping or modification can sometimes change the specific surface area of the materials. For instance, the surface area of $\text{Fe}_3\text{O}_4@\text{COF}@\text{Zr}^{4+}$ was relatively low, which might be due

to the fact that Zr^{4+} blocks the pores to some extent.^[103] The adsorption–desorption isotherm of N_2 is often used to determine the pore structure of porous materials. In some reports, the N_2 adsorption–desorption isotherms of COF-based core-shell materials are usually type IV, indicating that the loading of the COF shell accumulated in the micropores of the core to form a mesoporous structure, which increases the accessibility of the active sites. For instance, the $\text{NH}_2\text{-MIL-125(Ti)}@\text{TpPa-1}$ hybrid had a type IV isotherm curve with a type H3 hysteresis loop because of the formation of mesopores through bulk stacking during synthesis (**Figure 11a**).^[120]

The thermal stability and thermal decomposition of the composite can be determined by thermogravimetric analysis (TGA). In general, COF-based core-shell composites inherit the high thermal stability of COFs and do not collapse easily during heat treatment. The MIL@NTU composite was a typical example (**Figure 11b**). $\text{NH}_2\text{-MIL-101 (Fe)}$ showed a significant weight loss at 200 °C, which meant that its structure started to disintegrate, whereas the MIL@NTU-*x* series hybrids had a higher thermal stability up to 400 °C.^[58]

Overall, the introduction of the COF shell gives the core-shell composite a large specific surface area, a rich pore structure, good thermal stability, and versatile chemical properties, making it a promising application for both environmental remediation and energy conversion.

4.2. Magnetism

If the encapsulated core is magnetic, the introduction of the COF shell tends to slightly reduce the overall magnetic properties of the composite, and the thicker the shell, the weaker the

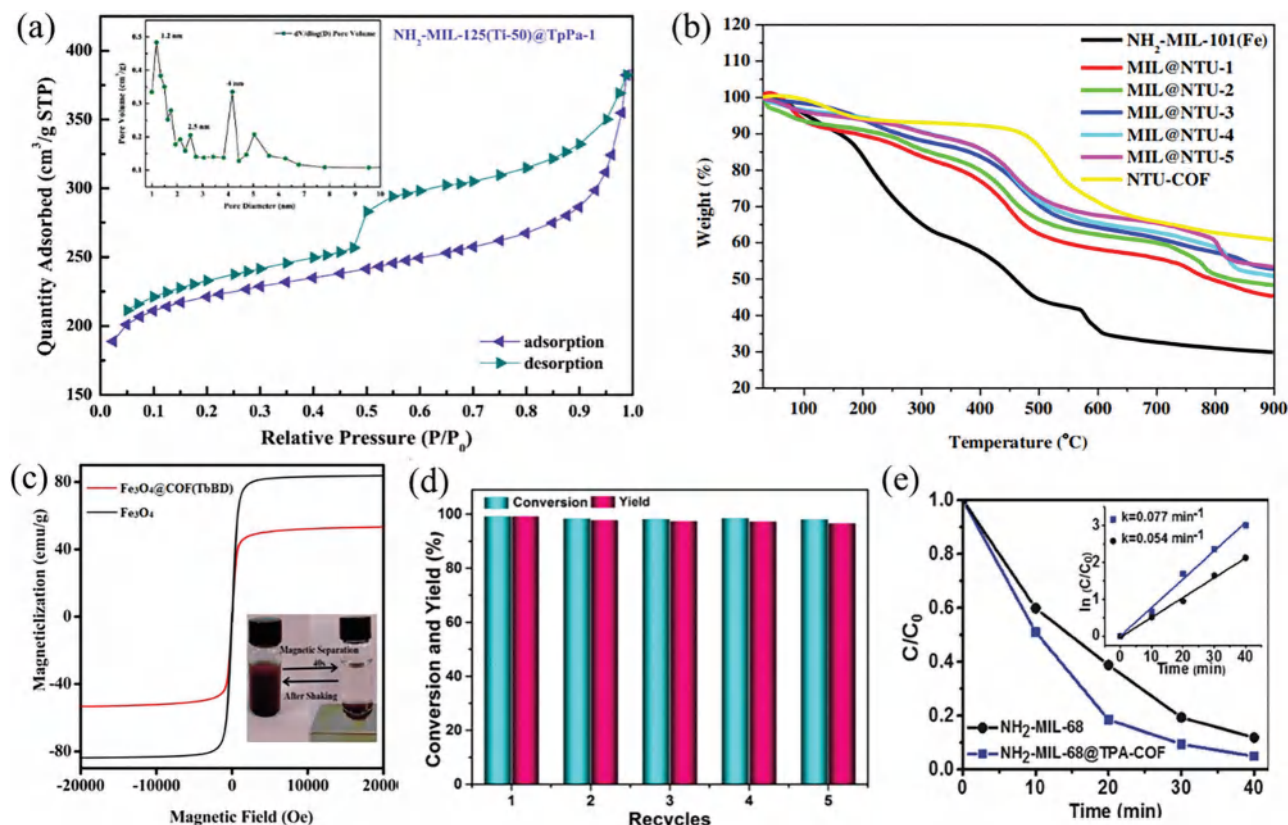


Figure 11. a) N_2 adsorption/desorption isotherms of the synthesized NH_2 -MIL-125(Ti-50)@TpPa-1. Reproduced with permission.^[120] Copyright 2021, American Chemical Society. b) TGA profiles of NH_2 -MIL-101(Fe), MIL@NTU-x, and MIL@NTU. Reproduced with permission.^[58] Copyright 2019, Wiley-VCH. c) Hysteresis loops (schematic illustration of the magnetic separation behavior of Fe_3O_4 @COF nanocomposites). Reproduced with permission.^[114] Copyright 2018, Elsevier B.V. d) Recycle capacity tests of PCN-222-Co@TpPa-1 for the cascade deacetalization–Knoevenagel reaction. Reproduced with permission.^[64] Copyright 2019, Royal Society of Chemistry. e) The efficiency of NH_2 -MIL-68 and NH_2 -MIL-68@TPA-COF photocatalytic degradation of Rh B. Reproduced with permission.^[133] Copyright 2017, Wiley-VCH.

saturation magnetization becomes.^[121] For example, Zhao's group developed magnetic nanospheres Fe_3O_4 @COF (TbBD) under ultrasonic conditions. According to the graphing of the magnetic hysteresis curves (Figure 11c), the saturation magnetization value of Fe_3O_4 @COF was 53.3 emu g^{-1} , which was slightly worse than that of pure Fe_3O_4 nanoparticles.^[114] Similarly, Li et al. studied and compared the hysteresis curves of Fe_3O_4 and Fe_3O_4 @COF (TpBD) materials and found that the saturation magnetic (Ms) value of core-shell hybrids was 61.1 emu g^{-1} , slightly lower than the 87.8 emu g^{-1} of Fe_3O_4 .^[122] Although the introduction of COF shell led to a slight loss of magnetism of the composites, the absence of significant hysteresis, residual, and coercivity on their hysteresis curves indicated that the synthesized materials were superparamagnetic and still had great magnetic responsiveness, and the Fe_3O_4 @COF compounds could be separated from samples by applying an external magnetic field, avoiding the traditional filtration step and saving experimental time. In addition, experimental results showed that the overall magnetic properties of the hybrids were related to the amount of MNPs and the thickness of the COF shell.^[123,124] Therefore, it is important to obtain core-shell materials with sufficient magnetic properties by adjusting the growth thickness of the shell and the dose of NPs.

4.3. Reusability

Reusability is quite a critical parameter for the commercial practicability of COF-based core-shell materials. Since monomers for the synthesis of COFs are usually more expensive, the synthesis of composites with good reusability is in line with economic and environmentally friendly principles. The encapsulation of the COF shell and the unique core-shell structure result in a composite material with unexpected stability and good recyclability. Researchers often perform reproducible cycle experiments to assess the reusability of materials, and the degree of performance loss during the reaction can be obtained from the experiments. For instance, the researchers investigated the reproducibility of core-shell composite as a multifunctional catalyst for the catalysis of the deacetalization–Knoevenagel reaction, and as shown in Figure 11d, the prepared PCN-222-Co@TpPa-1 material maintained high catalytic activity after five consecutive cycles.^[64] The reproducibility of the prepared Fe_3O_4 @COF (TpDA) material was investigated by Shi et al. The high adsorption capacity of the composites after five cycles demonstrated their high potential for applications in environmental protection.^[125] The reusability of some COF-based core-shell materials is shown in Table 3.

Table 3. Reusable times and postcycle processing efficiency of some COF-based core-shell materials.

Core-shell composites	Applications	Targets	Amount	Time	Reusable times	Treatment efficiency	Ref.
TiO ₂ @COF	Catalyst	BA	20 mg	30 h	5	86.5%	[47]
TiO ₂ @QH-COF	Catalyst	BA	16 mg	3 h	5	No significant loss	[144]
Fe ₃ O ₄ @COF-AuNP	Catalyst	Luminol-H ₂ O ₂ reaction	0.15 mg	NA	6	Over 90%	[191]
Fe ₃ O ₄ @COF	Adsorbent	Rh B	5 mg	20 min	10	80%	[192]
NH ₂ -Fe ₃ O ₄ @COF	Adsorbent	Benzoylurea insecticides	10 mg	10 min	9	80%	[193]
MOF-808@TpPa-1-COF	Catalyst	Hydrogen	10 mg	5 h	5	No significant loss	[63]
MIL@NTU-1	Catalyst	Styrene	10 mg	12 h	4	No significant loss	[58]
UiO-66@COF-V	Adsorbent	Phenoxy carboxylic acids	20 mg	15 min	10	95.30%–98.80%	[61]
Fe ₃ O ₄ @SiO ₂ @COF-V	Adsorbent	Polybrominated diphenyl ethers	20 mg	15 min	20	95.70%–98.08%	[194]
Fe ₃ O ₄ @COF-Apt	Enzyme reactor	Acetylcholinesterase	NA	NA	8	87.9%	[195]
Fe ₃ O ₄ @COF@2-FPBA	Adsorbent	Dopamine	10 mg	10 min	8	No significant loss	[196]
Fe ₃ O ₄ @TbBd	Adsorbent	Hydrophobic peptides	5 mg	10 min	30	Over 97.5%	[197]
Fe ₃ O ₄ @MOF@COF	Adsorbent	Azo dyes	NA	120 min	7	Over 80%	[159]
NiFe ₂ O ₄ @COF	Adsorbent	Endocrine disruptors	10 mg	NA	6	Over 90%	[94]
Fe ₃ O ₄ @COF-TpPa1	Adsorbent	BPA	40 mg	10 min	6	Over 84.8%	[198]

4.4. Photocatalysis

Catalytic technology is a hopeful solution for energy crisis and environmental pollution problems.^[32] By effectively integrating different types of substances and COFs, the obtained COF-based core-shell heterostructures exhibit good crystallographic, structural properties, and synergy of components, and thus various materials based on this have been used for multifunctional catalysts.^[126] Among them, photocatalysis and electrocatalysis are the main catalytic forms of COF-based core-shell composites for environmental and energy applications. Photocatalysis has received widespread attention because of the ability to capture ubiquitous solar energy and generate clean energy or degrade pollutants. During the catalytic process, photogenerated electrons (e⁻) and holes (h⁺) produced by semiconductor photocatalysts exposed to UV or visible light play an important role, and their severe recombination is an important factor limiting the wide application of photocatalysis.^[57,127,128] The specific applications correspond to the photocatalytic applications in Section 5. COFs combined with MOFs and NPs have good catalytic activity in photocatalytic H₂ evolution, environmental contaminant removal, and CO₂ reduction.

The possible reasons for enhancing photocatalytic properties through the introduction of COF shells are as follows: I) the remarkable core-shell structure together with the tight covalent connection between the core and the shell contribute significantly to the separation efficiency of photogenerated electrons and holes; II) the introduction of COF shells reinforces the structural advantage of the hybrids, which reduces the migration distance for the substrates; and III) COF shell reduces the bandgap and improves light absorption, and it is difficult for the nanoscale thickness of the shell to prevent the photoreaction of the core.^[129]

4.5. Electrochemistry

The specific applications of COF-based core-shell composites in electrochemistry correspond to Section 5. Applications of COF-based core-shell materials in electrochemistry include electrochemical sensors and capacitors. Despite the inherent poor conductivity of COFs, the core-shell composites formed by their combination with MOFs or CNTs exhibit good photocatalytic properties. For example, studies had demonstrated that UiO-66-NH₂@COF had excellent electrochemical sensing performance, exhibiting high sensitivity and great stability when used for electrochemical monitoring of ATP and CAP in samples, which further expanded its application prospects as a biosensor.^[36]

The excellent electrochemical performance of the COF-based core-shell composites may have several explanations, as follows: I) The COF-based core-shell materials are synthesized to form a high surface area and a special hollow structure, thus exposing more active sites and improving mass transport and ion diffusion properties; II) COFs have an extended π - π conjugated structure that enhances the adsorption capacity and affinity for pollutants through π - π stacking, hydrogen bonding, and electrostatic interactions, or a combination of them; and III) the introduction of conductive cores such as CNTs enhances the electron interaction between the COF shell and core and enhances the electron transfer, which enhances the electrochemical properties of the composites.^[43,130]

5. Applications

Figure 12 illustrates the applications of different types of COF-based core-shell materials. In short, the introduction of the COF shell and the special core-shell structure will bring

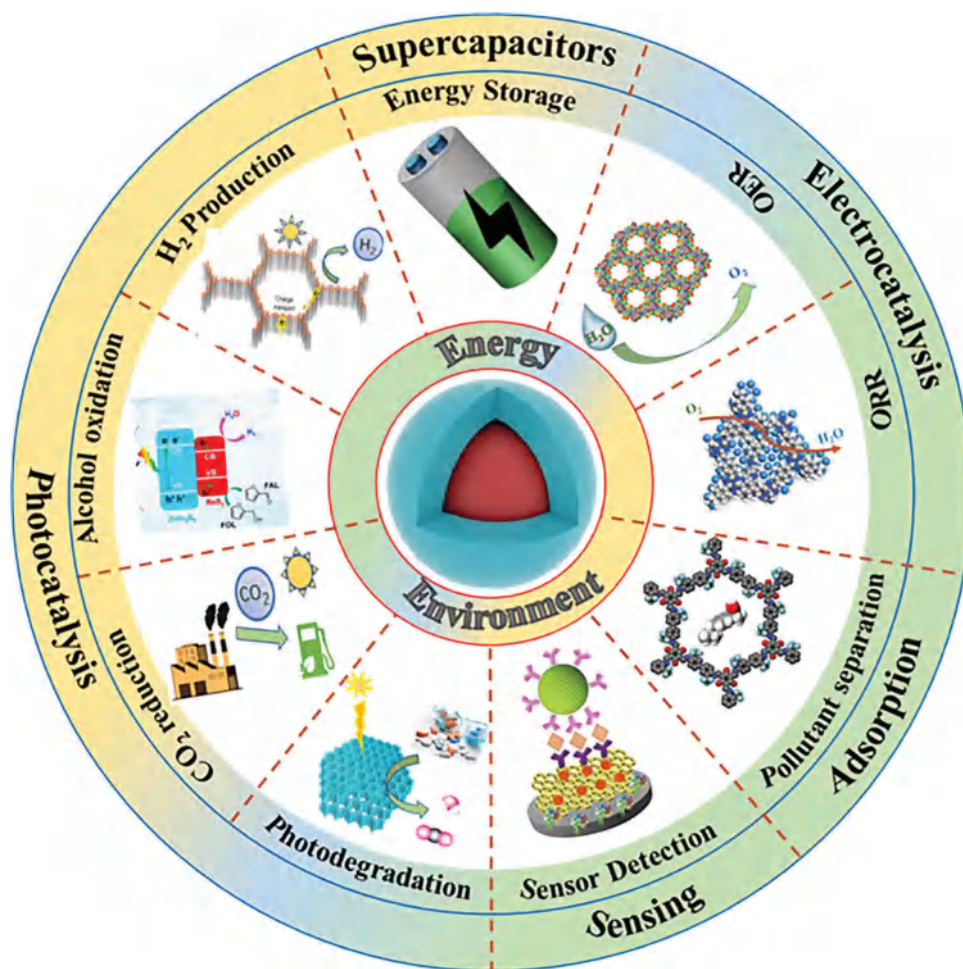


Figure 12. Application of different types of COF-based core-shell composites.

surprising performance improvements, thus extending the application range. Different types of materials have different application areas, and therefore different levels of importance are attached to various properties. For instance, MOF@COF focuses on catalytic performance and adsorption; MNPs@COF focuses on magnetism, adsorption, and reusability; and CNT@COF focuses on electrochemical properties.

5.1. Photocatalysis

5.1.1. Photocatalytic Degradation of Pollutants

The resources that people depend on for survival, such as water and soil, are being polluted via rapid advancement of human society. Since the 1970s, when Fujishima and Honda first used TiO_2 electrodes to achieve water separation under ultraviolet (UV) radiation, researchers have been interested in artificial photosynthesis.^[131] In general, the photocatalytic reaction process consists of the following three main links: First, a photocatalyst generates photoexcited electron-hole pairs after receiving light with energy higher than the energy bandgap. Second, the electrons on the photocatalyst VB are excited and thus

transferred to the CB, while the holes remain in the VB. Finally, these electrons and holes are involved in photocatalytic redox reactions, thus successfully converting solar energy into chemical energy and meeting the demand for energy forms.^[132] **Figure 13** summarizes the mechanism of some photocatalytic applications.

Peng et al. evaluated the photoactivity of $\text{NH}_2\text{-MIL-68@TPA-COF}$ using Rh B dyes as a target contaminant, which was widely regarded as a commonly used material for verifying the effects of photocatalytic degradation.^[133] The authors claimed that the reaction rate constant of the hybrid under visible light irradiation was 0.077 min^{-1} , which was almost 1.4-folds as high as the pure MOF and was significantly better than single component references (Figure 11e). It was attributed to the fact that hybrid materials possessed a larger surface area ($539 \text{ m}^2 \text{ g}^{-1}$) and a smaller E_g (2.21 eV). MOF@COF photocatalysts can also activate persulfate (PS) and utilize solar energy to degrade organic contaminants. Lv et al. explored the effect of a solar/MOFs@COFs/PS system on the degradation of the pollutant bisphenol A (BPA) and found that the degradation efficiency could reach up to 99%.^[133] The radical trapping experiments demonstrated that the introduction of PS facilitated the production of $\text{SO}_4^{\cdot-}$ which played a major role during the oxidation of bisphenol A.

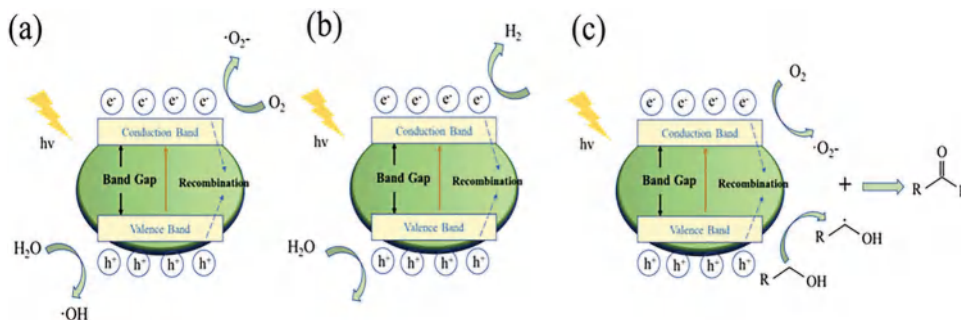


Figure 13. Schematic diagram of photocatalysis for a) pollutant degradation, b) hydrogen production, and c) alcohol oxidation.

5.1.2. Photocatalytic Hydrogen Evolution

Since the first industrial revolution, the use of fossil fuels has given a huge impetus to the development and progress of society; however, the resulting environmental pollution and energy shortages have become more frequent over the years.^[134] It is therefore imperative that alternative, clean energy sources are developed. Among the many possible options, hydrogen (H_2) is considered one of the most prospective alternatives to fossil energy due to the properties of easy storage, non-toxic, and high energy density.^[135] Photocatalysis has received widespread attention due to its ability to produce H_2 by directly converting ubiquitous solar energy into chemical energy.^[136] As a promising photocatalytic material, COFs themselves have a low H_2 precipitation capacity. To increase photocatalytic efficiency, the synthesis of COF-based core-shell photocatalysts has attracted a lot of attention.

We previously talked about the fact that Zhang's group developed a series of MOF@COF materials with different weight ratios, where MOF-808 and pPa-1-COF were selected as core and shell, respectively. (Figure 14a).^[63] The H_2 yield over the optimum sample (6/4) reached $11.88 \text{ mmol g}^{-1} \text{ h}^{-1}$, which was ≈ 5.6 times higher compared to the TpPa-1-COF (Figure 14b). MOF-808/TpPa-1-COF (6/4) showed the smallest semicircle radius and the strongest photocurrent response, indicating that the photogenerated carriers would migrate more efficiently through the covalent bonds of the hybrids with small barriers to charge transfer in the electric field, which confirmed the excellent photocatalytic performance of the catalyst from the side (Figure 14c,d). Based on the mentioned experimental data, a possible internal mechanism of photocatalytic H_2 production was proposed by the author, as shown in Figure 14e. Under visible light, the COF shell of the composite was excited to generate photogenerated electrons, which were transferred from the VB to the CB and then rapidly to the CB of the MOF-808. In particular, the covalent bond between the COF shell and the MOF core acted as a bridge, and the possibility that the electron-hole pairs recombine could be significantly reduced. Subsequently, the added Pt co-catalyst and the sacrificial agent sodium ascorbate (SA) successfully blocked the electrons recombined with holes in the MOF as well as trapped the holes left on the COFs, respectively. Sun and co-workers reported a unique palladium (Pd)-doped Pd/TiATA@LZU1 core-shell photocatalytic platform and investigated the feasibility of the hybrids for H_2 production from photocatalytic ammonia borane (AB) (Figure 14f).^[137] The authors claimed that when Pd/TiATA@LZU1 was in the dark and the

H_2 /AB molar ratio was 3.0, complete evolution of H_2 could be achieved in 55 min but only in 8 min in visible light. The result was due mainly to the synergy between the three components: the MOF core could provide electrons, the COF shell facilitated electron transfer, while the doped Pt acted as the active center. Specifically, the loading of the COF shell greatly inhibited the luminescence compared to MOF and Pd/MOF, which could act as a mediator to facilitate electron transfer from the MOF core to the Pd active sites and participate in the reduction reaction, while the electron-withdrawing aldehyde group on the shell could interact with the amino group on the MOF, resulting in a redshifted luminescence band. TiATA had a broad luminescence band at 434 nm due to the ATA ligand in the MOF core (Figure 14g). For core-shell photocatalysts, the appropriate shell thickness also affects the rate of H_2 production. For instance, Chen and co-workers constructed a NH_2 -UiO-66@TFPT-DETH heterogeneous framework and applied it to photocatalytic H_2 evolution.^[138] Due to the fact that an excessively thick shell prevented the bulk material from absorbing enough light and the high recombination rate of the photogenerated carriers triggered by the short exciton diffusion length and low mobility of the semiconductor. On the basis of this, U@TDE4 ($20 \pm 1 \text{ nm}$) achieved the highest H_2 evolution rate of $7178 \mu\text{mol g}^{-1} \text{ h}^{-1}$ among all samples, which was about a twofold increase compared to pure COF.

Several metals and their compounds have good photocatalytic properties, including suitable band positions and fast electron mobility, so the collaboration with COFs has attracted the attention of researchers. Wang et al. prepared a unique core-shell Cu/ZnS/COF photocatalyst (Figure 15a), which proved to have excellent catalytic efficiency for photocatalytic H_2 production.^[139] The study confirmed that the optimal H_2 evolution rate of Cu/ZnS/COF composites was $278.4 \mu\text{mol g}^{-1} \text{ h}^{-1}$ (Figure 15b), which was significantly superior to most previously reported photocatalysts. The authors provided a mechanism that effectively explained the enhanced photocatalytic performance of the synthesized core-shell hybrids, as shown in Figure 15c. At first, in the presence of visible light, COFs and ZnS were excited to produce photogenerated electron-hole pairs. However, because of the intrinsic difference in electronic potential energy between the two components, the CB electrons of ZnS moved toward the VB electrons of COFs, while the holes in the VB of COFs were transferred to the opposite direction. In addition, doping Cu at low Fermi energy levels allowed the formation of a space charge layer at the interface and a Schottky junction, which could effectively capture photoelectrons. Interestingly, the addition of sacrificial

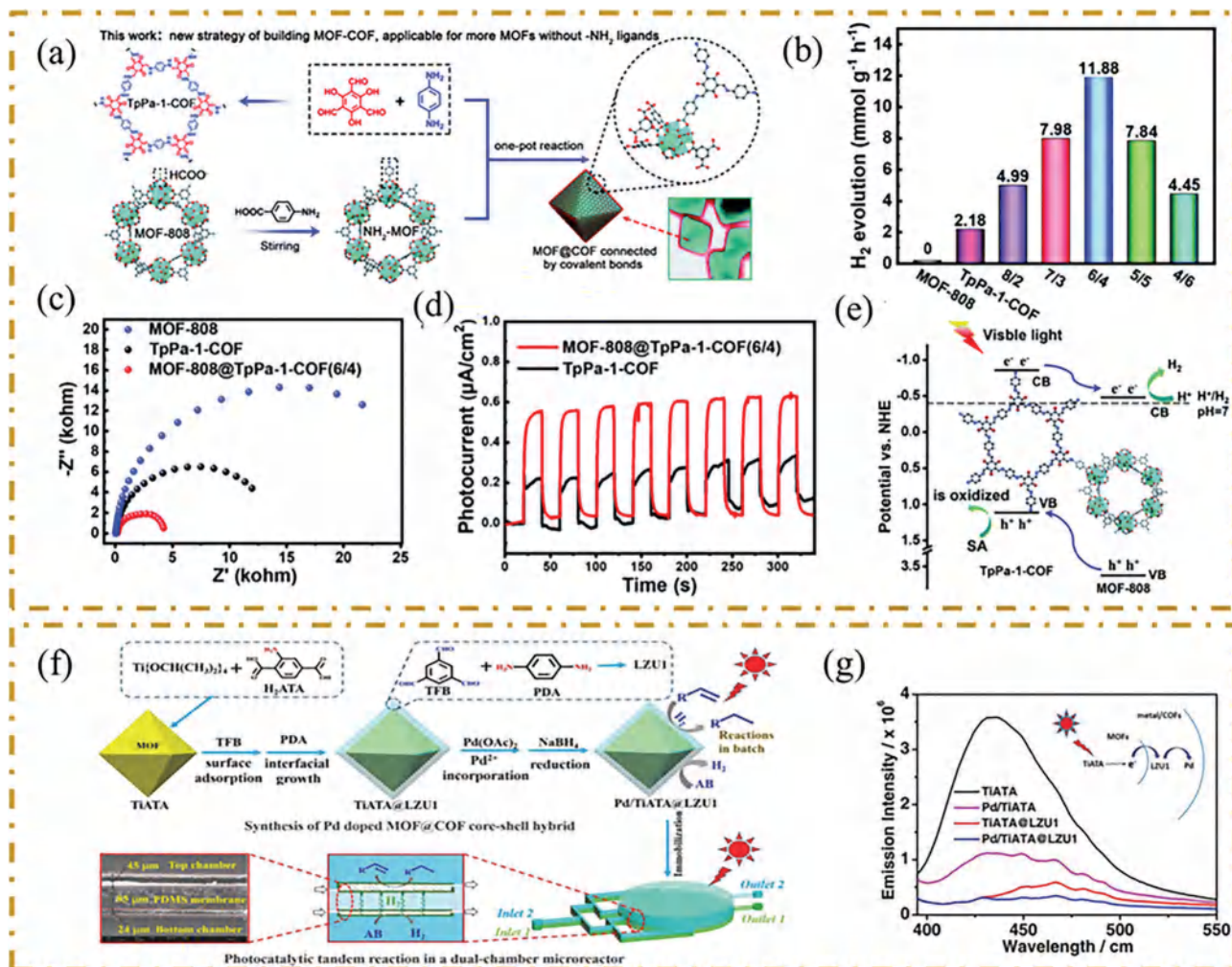


Figure 14. a) Schematic diagram of MOF@COF hybrid material constructed by new strategy. b) Photocatalytic H₂ evolutionary activity of various materials. c) EIS Nyquist plots of MOF-808, TpPa-1-COF, and MOF-808@TpPa-1-COF (6/4) composites. d) Transient photocurrent measurements. e) Photocatalytic mechanism diagram of MOF-808@TpPa-1-COF (6/4). Reproduced with permission.^[63] Copyright 2020, The Royal Society of Chemistry. f) Schematic diagram of the preparation of Pd/TiATA@LZU1 core-shell composites and their photocatalytic application in microreactors. g) Emission spectra of different catalysts excited at 380 nm. Reproduced with permission.^[137] Copyright 2018, Wiley-VCH.

formic acid (HCOOH) could consume holes to inhibit electron-hole recombination, thus favoring the whole photocatalytic H₂ evolution process.

5.1.3. Other Photocatalytic Applications

The development of COF-based core-shell composites has resulted in new trends in their use for other photocatalytic applications, such as the oxidation of alcohols and the reduction of CO₂. Selective oxidation catalysis plays an important role in today's human industrial production. First, it allows the production of key intermediates such as alcohols, epoxides, aldehydes, ketones, and organic acids in the chemical industry. Second, it helps establish new green and sustainable chemical processes.^[140] Among them, the photocatalytic selective oxidation of alcohols has attracted great interest because of its extensive application in numerous domains such as the pharmaceutical industry and the food indus-

try, as well as energy-saving and environmental protection.^[141,142] A typical alcohol photocatalytic oxidation process consists of five main steps: I) alcohols are adsorbed by the photocatalyst; II) in the presence of light, the photocatalyst is excited and electron-hole pairs are generated; III) charge separation and transfer to the surface of the photocatalyst; IV) the charge after migration is involved in redox reactions; and V) the desorption of the product.^[143] Therefore, light absorption capacity, band structure, crystallinity, and adsorption/desorption of alcohols/products are important criteria for selecting photocatalysts for efficient catalytic oxidation of alcohols.

There have been several reports of photocatalytic oxidation of alcohols using COF-based core-shell composites. However, sometimes the microscale spatial location of the COFs and inorganic semiconductors also changes the photocatalytic activity of heterojunctions significantly. For example, Yang's group synthesized QH-COF@TiO₂ (Figure 16a) and TiO₂@QH-COF (Figure 16b) and compared them for their photocatalytic

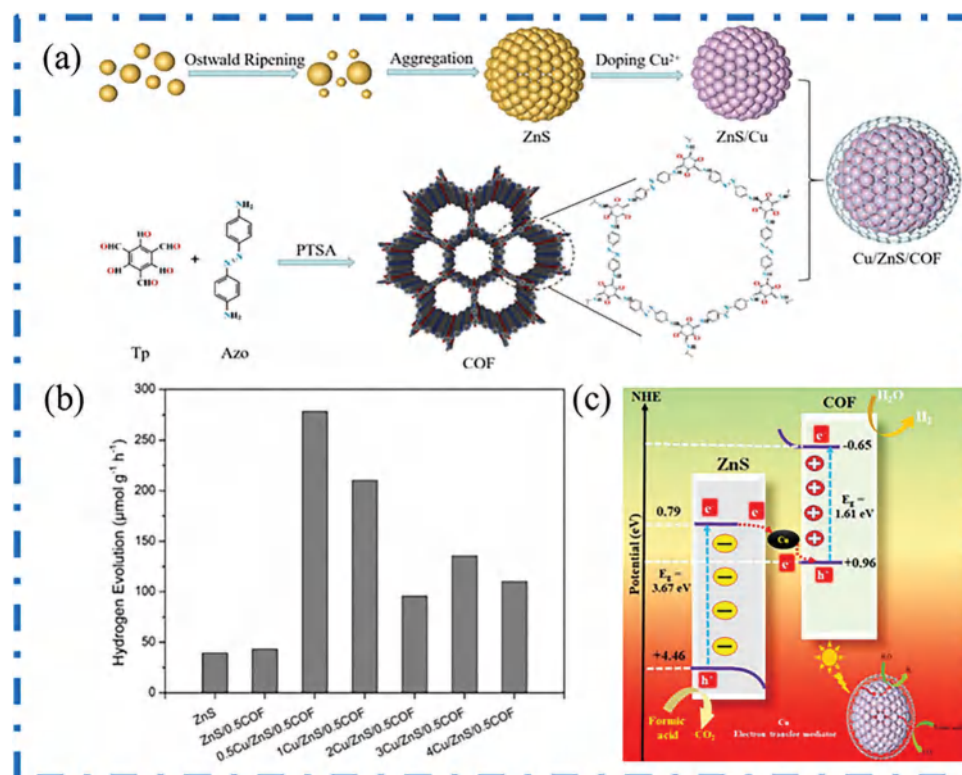


Figure 15. a) Schematic illustration of the preparation of Cu/ZnS/COF composites. b) Photocatalytic hydrogen evolution activities of as-synthesized photocatalysts. c) Mechanism of photocatalytic hydrogen evolution from Cu/ZnS/COF hybrids. Reproduced with permission.^[139] Copyright 2021, MDPI.

performance on BA and found that the reaction rate of the former was $1.19 \text{ mmol g}^{-1} \text{ h}^{-1}$, which was around a two-times increase compared to the latter.^[144] Although both samples possess similar light absorption properties as well as charge separation abilities, QH-COF@TiO₂ formed more superoxide radicals and higher electrical conductivity during the photocatalytic oxidation of BA, which were main reasons for its higher catalytic activity. Moreover, the stability of composite materials for the photocatalytic cross-dehydrogenative coupling (CDC) reaction was investigated and found to be stable for five cycles with no significant decrease in activity (Figure 16c).

Until now, the burning of traditional fossil fuels is still our main way of obtaining energy, which leads to a large amount of CO₂ emissions and causes serious harm to our environment, such as global warming, species extinction, etc.^[145] The reduction of CO₂ into usable fuels through photocatalysis contributes a possible solution for achieving carbon neutrality. Due to the unique advantages, the photocatalytic reduction of CO₂ by COF-based core-shell materials has been reported. As an example, CdS@COF nanowires were prepared for the photoreduction of CO₂ by Zou and co-workers (Figure 16d).^[129] The composites could well solve the problem of the poor electron transfer ability of the imine-linked COFs and thus have good photocatalytic properties. Due to the existence of N/Cd and Co/S interactions, there was local electron distribution at the core-shell interface, and their interactions could form an interfacial cascade channel to promote the transfer of photogenerated electrons from the imine bond in the COF shell to the cobalt sites on the core to

participate in the reduction reaction, where CdS could be used as a channel to improve the transfer efficiency, and the sacrificial agent 1,3-dimethyl-1,3-dihydro-2-phenyl-2H-benzimidazole (BIH) added during the reaction could quench the holes and reduce the recombination probability (Figure 16e,f). The test results indicated that the optimal CO yield was 4057 μmol g^{-1} within 8 h, which was apparently better than that of pure CdS as well as COFs.

5.2. Electrocatalysis

In the face of environmental and energy crisis, electrochemical energy conversion technology has attracted more and more attention due to its environmental friendliness and efficiency.^[146] However, its commercialization depends heavily on the intensive exploration of high-performance and low-cost electrocatalysts for cathodic oxygen reduction reactions.^[48] Although COFs themselves are not very conductive, they can be used to construct ideal platforms with precisely controllable structures by selecting suitable building blocks and connection patterns, which can then cooperate with other components to obtain electrocatalysts with excellent performance.^[147] For COF-based core-shell materials, the shell of COFs not only effectively protects the core from aggregation, but also its abundant cavities expose more active sites and accelerate mass transfer.^[73,148]

Recently, researchers have synthesized a series of COF-based core-shell materials by growing COFs on conductive materials.

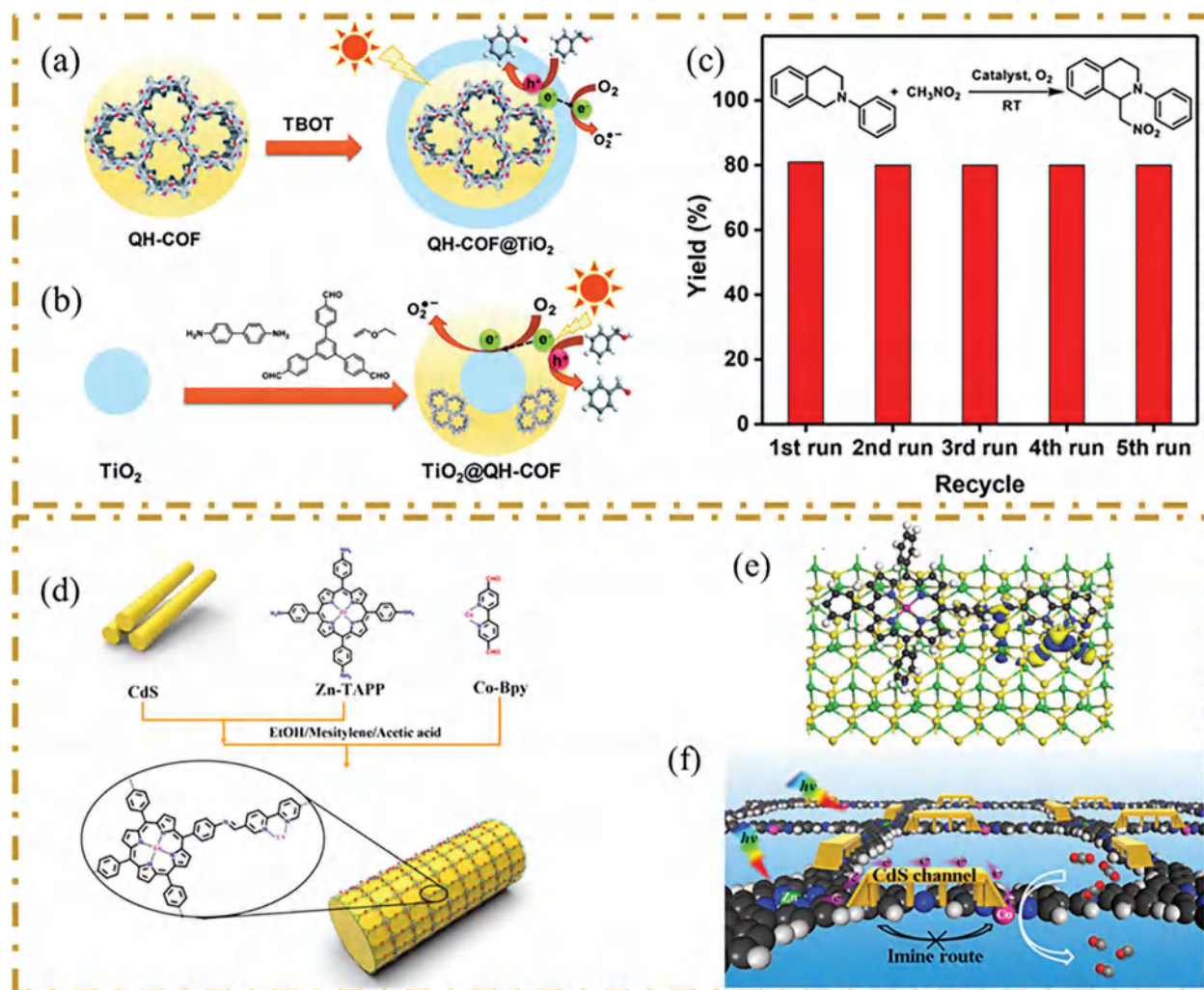


Figure 16. Schematic diagram of the construction of a) COF@TiO₂ and b) TiO₂@COF core-shell hybrids. c) Reusability of QH-COF@TiO₂ (10%) in photocatalytic CDC reaction. Reproduced with permission.^[144] Copyright 2020, The Royal Society of Chemistry. d) Schematic diagram of the synthesis of CdS@COF core-shell material. e) Differential charge density of CdS@COF. f) Photoelectron transfer mechanism on COF and CdS@COF. Reproduced with permission.^[129] Copyright 2022, American Chemical Society.

Since most MOFs are composed of common transition metals and organic ligands, especially their porous channels, which can bind to accessible active sites, MOFs are the most common conductive cores. Guo et al. synthesized MOF@COF-derived catalysts by immobilizing Zn atoms on hollow carbon and Pt/Zn bimetallic clusters/nanoparticles.^[149] The synergy of MOFs and COFs conferred a catalyst that included a high surface area and an abundance of active sites. In particular, the introduction of Pt²⁺ ions promoted the formation of hollow structures, which facilitated mass transport. The resultant Pt-COF@MOF800 displayed remarkable ORR activity with an $E_{1/2}$ of 0.85 V, which was slightly higher than the 0.81 V of Pt/C (Figure 17a). Furthermore, the Tafel slope of the core-shell composites was much lower than all other materials, indicating their better kinetic behavior (Figure 17b). To demonstrate the mass activity of Pt-COF@MOF800, the corresponding mass current densities were tested under acidic and basic conditions. The results of Pt-COF@MOF800 were 57.62 and 119.93 A g⁻¹ at 0.9 V, respectively, which were much higher than Pt/C. Miao et al. first pyrolyzed

MOF@COF to form MOF800-COF and then introduced iron phthalocyanine (FePc) by immersion to obtain the COF@MOF800-Fe composite.^[37] The COF@MOF800-Fe had higher activity and stability in ORR because of the formation of a biphasic atomic Zn-N₄ and Fe-N₄O catalyst. In which, COF@MOF800-Fe delivered $E_{1/2}$ of 0.89 V, with a limited current density (J_{lim}) of 6.2 mA cm⁻², which was slightly superior to the Pt/C electrode at 0.84 V with a J_{lim} of 5.3 mA cm⁻², respectively, indicating that COF@MOF800-Fe had better ORR activity. This result indicated excellent synergy between the Zn and Fe sites.

Some carbon substrates, such as CNTs, are also used in conjunction with COFs to form core-shell structures together for electrocatalysis because of the ability to effectively overcome the electrically insulating nature of COFs.^[80,150] Gan et al. successfully prepared COF@CNT core-shell hybrids for electrocatalytic oxygen evolution reaction (OER) and investigated the relationship between fine-tuning of active sites and catalytic performance (Figure 17c).^[151] First, a typical class of COF-covered COF-366-Co@CNT was synthesized by imine condensation, and then the

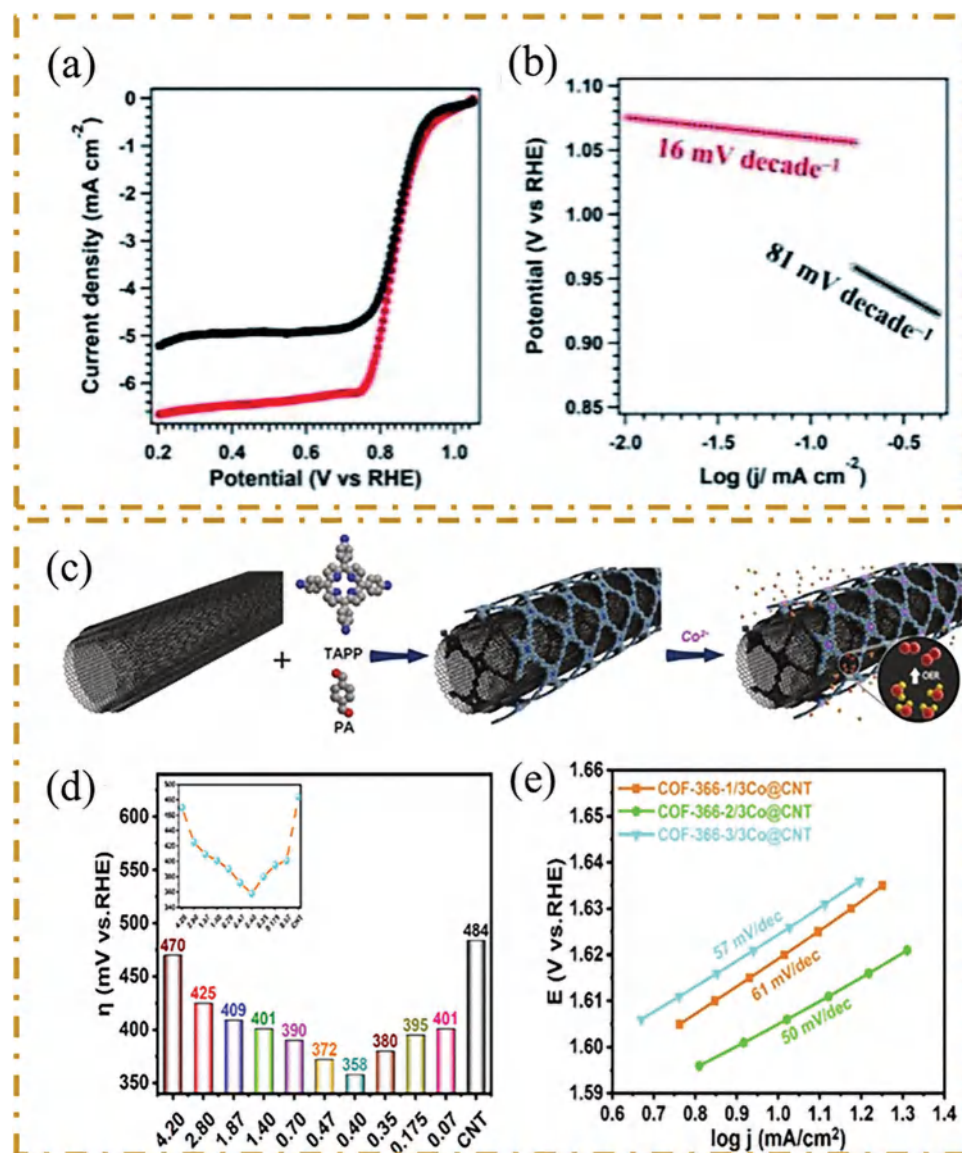


Figure 17. a) LSV curve and b) Tafel slope for Pt-COF@MOF800. Reproduced with permission.^[149] Copyright 2021, The Royal Society of Chemistry. c) Schematic diagram of the preparation of COF-366-Co@CNT composite; d) the overpotential at current density of 10 mA cm⁻². e) The corresponding Tafel plots of COF-366-xCo@CNT-0.35. Reproduced with permission.^[151] Copyright 2020, Elsevier.

cooperation of the introduced Co²⁺ with porphyrins not only facilitated the successful accumulation of the COF shell but also served as active centers. The overpotentials of the composites at 10 mA cm⁻² showed an increasing and then decreasing trend with decreasing COF monomer content (Figure 17d). The synthesized COF-366-Co@CNT-0.35 was selected as the subject to assess the impact of the number of active sites on the overall properties by changing the concentration of Co²⁺ ions (1/3, 2/3). The results indicated that the samples loaded with 2/3 saturated Co²⁺ exhibited the best OER electrocatalytic performance (Figure 17e), which was also confirmed by the variation of the turn-over frequency (TOF) values. Specifically, the TOF remained constant when the content of Co²⁺ was 1/3 and 2/3 saturated, while the TOF values decreased when saturation was reached due to the competition for the effective active site inhibiting the OER activ-

ity. And the low performance of the sample containing 1/3 saturated Co²⁺ was attributed to the low quantity of active sites. Interestingly, a proper COF shell thickness could effectively ensure charge transfer and a reasonable active site distribution, which improved the electrocatalytic efficiency.

5.3. Adsorption

Recently, large quantities of effluents containing antibiotics, dyes, heavy metals, and other pollutants have entered the water environment through various routes, seriously threatening the ecological environment and human survival. Industrial wastewater, sewage plants, agricultural runoff, and other human activities are its main sources.^[152] It is thus vital not only to prevent

environmental pollution at source but also to remediate the already polluted environment. Compared to other conventional water treatment techniques, adsorption has received most of the attention of researchers due to its simple operation process, mild conditions, and low cost.^[153–155] One of the keys to adsorption technology is the synthesis of adsorbents with excellent properties. Studies have suggested that UiO@TapbTp, a hybrid material with COFs (TapbTp) as the shell and MOFs (UiO-66-NH₂) as the core, could effectively adsorb nonsteroidal anti-inflammatory drugs (NSAIDs) from complex samples.^[156] To overcome the drawbacks of high consumption and inconvenient separation of powdered adsorbents, a corncob@MOF@COF adsorbent was prepared by Zhang et al.^[157] First, the carboxyl group was introduced into the corn cob by a hydrothermal-esterification process, which facilitated the in situ growth of MOF, while the COF shell was loaded by a Schiff base reaction between the monomers. Due to π - π stacking, hydrogen bonding, as well as SO₂-Zr-O coordination, the obtained corncob@UiO-66-NH₂@TpBD composites possessed a high adsorption capacity for sulphonamides (SAs) in aqueous media with a detection limit of 0.10 $\mu\text{g L}^{-1}$ when combined with ultraperformance liquid chromatography (UPLC). In addition, the adsorbent exhibited excellent reusability with no significant degradation over 20 cycles of adsorption-desorption. High adsorption performance and good recoverability made it show an extremely high practical application value.

On the one hand, magnetic nanoparticles have inherent advantages as adsorbents due to their superparamagnetic and can be rapidly separated from the sample under applied magnetic field conditions. On the other hand, COFs possess excellent features, including high thermal stability, high surface area, as well as regular porosity. Therefore, NPs@COF composites with core-shell structure combine the advantages of both components and have high application potential in the field of adsorption.^[158] In general, NPs@COF adsorbents interact with the target contaminants primarily through hydrogen bonding, π - π stacking, hydrophobic interactions, ion exchange, or ligand reactions.^[103,121,159,160] For example, Wei et al. investigated the mechanism by which the synthesized Fe₃O₄@TpND composites adsorb BPA from aqueous solutions.^[161] The authors found that Fe₃O₄ NPs did not really participate in the adsorption process (Figure 18a), but were responsible for post-regeneration and cost reduction. Static DFT calculations were performed for the purpose of elucidating the interfacial interaction of the target contaminant with the COF shell, and it was found that BPA molecules were preferentially trapped by the phenolic group of TpND through hydrogen bonding and then confined within the porous framework of the COF shell, gradually aggregated into clusters. (Figure 18b–d). The good adsorption performance (139.05 mg g⁻¹) and excellent reusability (2.2% decrease after five cycles) provided a promising guide for the application of COF-based core-shell materials in adsorption.

5.4. Sensing

Electrochemical sensor detection of pollutants is one of the commonly used analytical methods due to its short analysis time, low power consumption, high sensitivity, and adaptability for in situ measurement.^[162] COF-based core-shell hybrid materials can be applied in electrochemical sensors due to the follow-

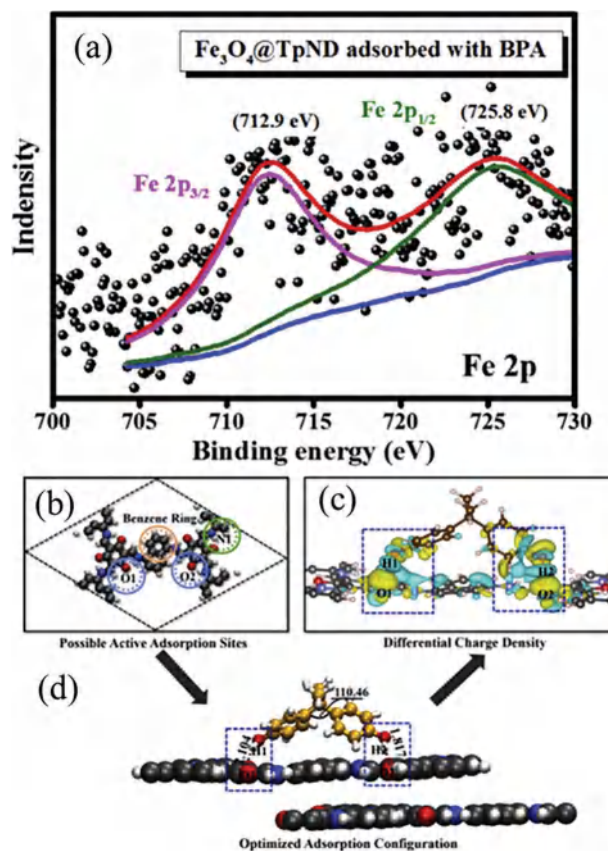


Figure 18. a) Fe 2p spectrum of Fe₃O₄@TpND after adsorption of BPA. b) The potential adsorbing sites of TpND, c) the optimum adsorption configuration, and d) the differential charge density of BPA on the surface of COF. Reproduced with permission.^[161] Copyright 2020, Elsevier B.V.

ing reasons: I) the COF shell has excellent structural advantages, which allow probe molecules to be embedded in COFs pores; II) COFs have excellent enrichment ability and can stably enrich the targets through π - π stacking, electrostatic interactions, or hydrophobic interactions; III) compared to pure COF, a core with excellent electrochemical conductivity and high charge carrier mobility is introduced in the core-shell composite, which facilitates signal amplification; IV) the unique core-shell structure facilitates the prevention of core aggregation and promotes the formation of heterogeneous structures with layered pores; and V) enhanced electrocatalytic activity by synergistic catalysis of individual components of binary nanocomposites with core-shell structure.^[42,163–165] Therefore, over the past few years, there has been a conscious effort to integrate functional components with COF shells to obtain composite materials with core-shell structures for electrochemical sensors.

The researchers found that when COFs are applied to fluorescence detection, intramolecular rotation occurs, causing aggregation-caused quenching (ACQ), which reduces the emission efficiency. To address this challenge, Yin's group synthesized UiO@COF1 and UiO@COF2 composites that could be used to recognize PO₄³⁻ and adenosine triphosphate (ATP), respectively (Figure 19a).^[166] To be specific, the UiO-66-NH₂ crystal was chosen as the MOF core due to the high affinity

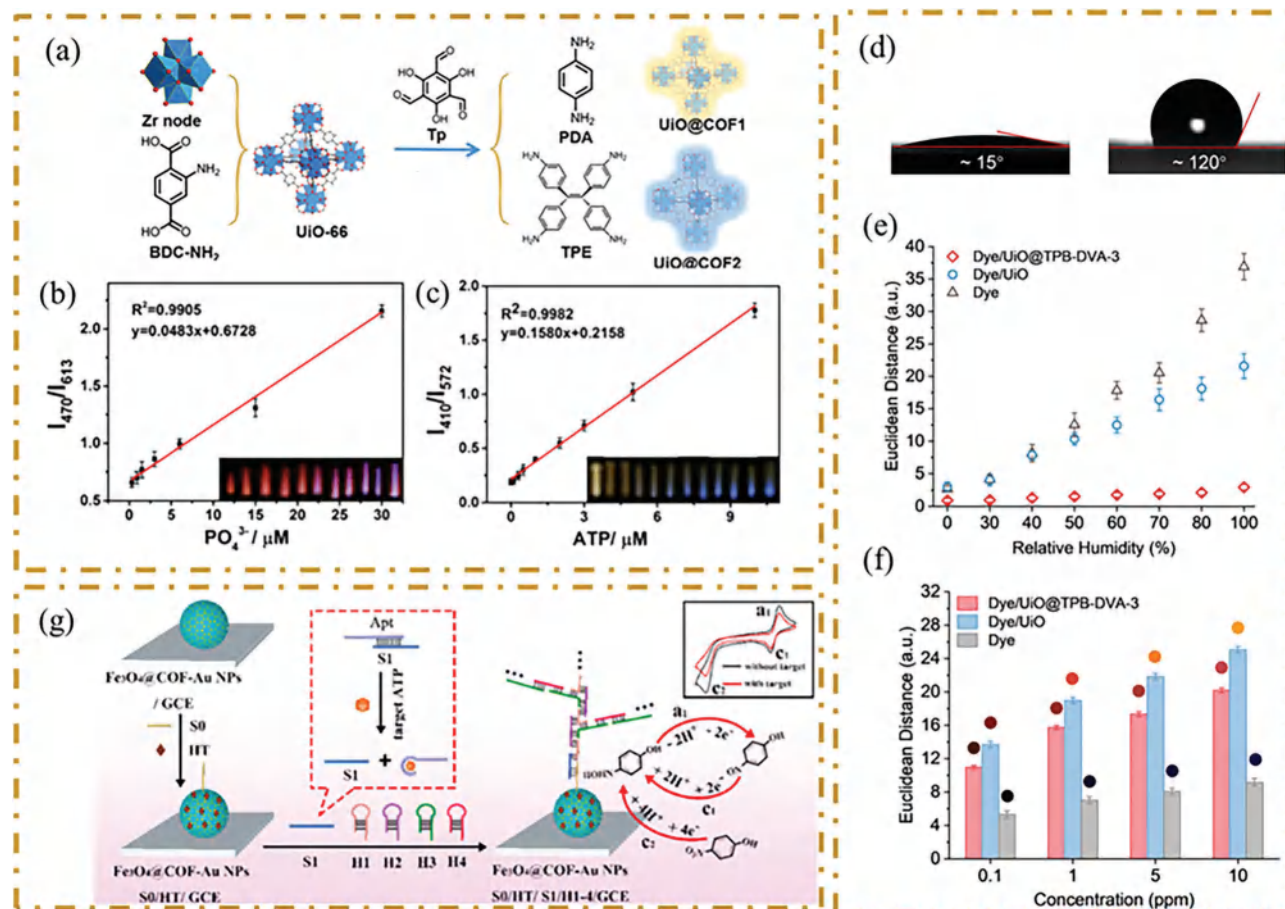


Figure 19. a) The synthesis process of UiO@COF1 and UiO@COF2. b,c) The relationship between luminosity ratio and PO_4^{3-} and ATP concentration. Reproduced with permission.^[166] Copyright 2020, American Chemical Society. d) Water contact angle, e) ED value, and f) color difference profile to 1-octen-3-ol with different concentrations of dye, dye/UiO, and dye/UiO@TPB-DVA-3. Reproduced with permission.^[168] Copyright 2022, American Chemical Society. g) Construction and principle of electrochemical sensors. Reproduced with permission.^[169] Copyright 2021, Elsevier B.V.

exhibited by the Zr^{4+} ion for the phosphate group, while the COF monomer was chosen (COF1: Tp, PDA; COF2: Tp, TPE (tetraamino-tetraphenylethylene)) due to the presence of hydroxyl and alkyl groups that could limit intramolecular rotation and ACQ and contribute to the formation of the excited-state intramolecular proton transfer (ESIPT) structure. In addition, the thin COF shell reduced thermal relaxation, all of which contributed to the improvement of fluorescence properties. UiO@COF1 was available as a probe for detecting PO_4^{3-} ions due to its strong emission and large Stokes shift with an LOD of 0.067×10^{-6} M and an R^2 of 0.9905 (Figure 19b). And when the UiO@COF2 probe was used to monitor ATP, there was a good linear relationship between the intensity ratio at 410/572 nm and the ATP concentration with an R^2 of 0.9982, and the LOD was 0.038×10^{-6} M (Figure 19c). The preparation of this MOF@COF core-shell composite improved multi-emission and enhanced affinity, thus expanding the application in sensing. The introduction of COF enclosures could also reduce the effect of humidity on detection results by adjusting the hydrophobicity of the material. For example, volatile organic compounds (VOCs) are typically toxic, teratogenic, or carcinogenic, so timely monitoring of VOCs in the atmosphere is essential to ensuring the health of

human life.^[167] However, in practice, the monitoring of VOCs is always subject to humidity disturbances, resulting in inaccurate results. To address this issue, Wang's group synthesized a hybrid dye/MOFs@COFs material with significantly improved performance and used it for the practical monitoring of VOCs.^[168] Specifically, first, the dye was uniformly distributed in the apertures on the MOFs, which ensured a much better sensitivity of the sensor; second, the composite material after loading with the TPB-DVA-COF shell exhibited excellent hydrophobic properties with a water contact angle of 120° , much higher than the 15° of dye@UiO (Figure 19d). The moisture resistance was further judged by the Euclidean distance (ED). As shown in Figure 19e, the ED values of the composite ensemble material were almost negligible in the range of 0–100% relative humidity (RH), so the composite material showed good resistance to various humidity levels, even at 100% RH with no significant humidity response. In addition, the ED values and the visualized color difference plots (Figure 19f) indicated that the sensitivity of dye/UiO@TPB-DVA-3 to VOCs molecules was enhanced. The dye/MOFs@COFs hybrids offered in this study provided a new idea for constructing VOCs sensors with good moisture resistance and sensitivity.

As a promising catalyst, the cooperation of metal nanoparticles with COFs has also received favorable attention from researchers in electrochemical sensors.^[85] For example, Li et al. synthesized an $\text{Fe}_3\text{O}_4@\text{COF-Au}$ electrocatalyst and used it as a nanocarrier for single-stranded DNA to construct an electrochemical biosensor for the sensitive detection of ATP.^[169] Specifically, the electrocatalytic reduction of 4-NP occurred under normal conditions, while ssDNA S1 modified on the surface of the glassy carbon electrode (GCE) was released in the presence of ATP, forming a kind of dendritic DNA strand, which hindered the reduction process of 4-NP (Figure 19g). The role of Au NPs was primarily to improve the sensitivity and electronic conductivity of the sensor, while the porous structure of the COF shell facilitated the uniform dispersion of NPs and created a stable microenvironment. The sensor had a low detection limit of 1.6 pM, and the recovery ranged from 98.60% to 103.8%, which showed a good practical application. Wang et al. reported a novel $\text{Fe}_3\text{O}_4@\text{AT-COF}$ nanocomposite that could be used for the electrochemical detection of *p*-nitrophenol (PNP) and *o*-nitrophenol (ONP).^[170] The catalysts were synthesized at room temperature, and the surface morphology of the composites could be changed by varying the concentration of catalyst HAC. In this research, the optimal volume of HAC (36%) was 2.0 mL when the hybrids possessed the best core-shell structure, which facilitated rapid electron transfer and amplification of electrical signals. And the main role of Fe_3O_4 NPs was to enhance the synergistic effect of the core and shell on the target molecules and to reduce the energy barrier for adsorption. The electrochemical results showed detection limits of 0.2361×10^{-6} M and 0.6568×10^{-6} M, respectively, with a wider linear detection range as well as satisfactory recoveries in real samples.

5.5. Supercapacitors

Energy is vital to human development, and in the face of the growing energy crisis, there is a growing demand for higher capacity, environmentally friendly, faster charging, and low-cost energy storage devices.^[171,172] Supercapacitors, due to their advantages over secondary batteries, have attracted the interest of many researchers.^[115] The key to improving the properties of capacitors is the synthesis of redox-active substances with outstanding structural characteristics and superior electrical conductivity. Although COFs have the potential to be used in supercapacitor applications, the random orientation of COF particles or strong $\pi-\pi$ interactions make it difficult for the electrolyte solution to penetrate, leading to low utilization of active sites. To explore the potential of COF-based core-shell materials in energy storage, a number of approaches have been explored.

The first approach is to prepare the composites into nanofilms. As we mentioned earlier, Kong et al. successfully synthesized core-shell c-CNT@COF nanofibers by growing DAAQ-TFP COFs on carboxylated carbon nanotubes (c-CNTs) (Figure 20a).^[77] Specifically, the COF shells were first grown by sequentially attaching organic monomers on the surface of the carboxyl-functionalized CNTs, and the synergistic interaction between the components promoted the electrochemical properties of the nanocomposites. In particular, the special fiber structure facilitated the formation of nanopaper. Flexible hybrid capacitors were constructed using c-CNT@COF-3 nanopaper with

a higher interfacial area as a candidate. The electrochemical analysis indicated that it possessed a specific capacitance of 418.7 F g^{-1} at a current density of 0.2 A g^{-1} , significantly superior to the individual CNT and c-CNT-COF (Figure 20b–g). The superior cycling performance and flexibility were attributed to the excellent stability of the composites as well as the interwoven fibrous network, respectively. Samori's group, on the other hand, chose to infiltrate redox-active 7,7,8,8-tetracyanoquinodimethane (TCNQ) into the pores of the scaffold of MOF@COF hybrids to obtain a novel MOF@COF-TCNQ composite.^[173] The homogeneous porous structure promoted ion transport and the introduction of TCNQ enhanced the quantum capacitance of the material. Due to the structural advantages and extra pseudocapacitance, the composites exhibited excellent supercapacitor performance with a specific area capacitance of 78.36 mF cm^{-2} accompanied by a stack capacitance of 4.46 F cm^{-3} , and a retention rate of 86.4% after 2000 cycles. **Table 4** summarizes the applications of COF-based core-shell composites in supercapacitors.

6. Summary and Future Outlook

Despite the short history of the evolution, COF-based core-shell materials have also attracted increasing attention from researchers due to the combination of COF materials with other building blocks to achieve a superposition of advantages and even to obtain unexpected properties and some progresses have been made as a result. This paper systematically summarizes recent advances in emerging COF-based core-shell composites, including their general classification, synthetic strategies, structures and their applications in photocatalytic, electrocatalysts, adsorption, sensing and supercapacitors. Although COF-based core-shell materials have made great breakthroughs in recent years, there are a number of challenges that need to be overcome before industrial production and application. It can be considered from the following aspects:

- (I) Expanding the range of applications. In terms of applications, the superiorities of COF-based core-shell composites have been demonstrated in only a few catalysis, adsorption, and sensing-related examples. In contrast, in some emerging fields, such as drug delivery and cancer therapy, the investigation has just started and needs to be further developed and improved. COF-based core-shell hybrid photocatalysts possess excellent structural properties, including large pores and specific surface areas, and smaller bandgaps, which enhance the transport and separation of photogenerated charges and holes. Interestingly, we found that most of the research in the field of photocatalysis has been done experimentally, but the photocatalytic efficiency of simulated sunlight in composite materials is often different from that of actual sunlight. In addition, considering the impacts on the ecology and health, the toxicology of the composite needs to be studied to prevent secondary contamination.
- (II) Diverse structure and composition. So far, most of the research in this area has been conducted using COFs as the shell. The preparation and application of core-shell compounds with COFs as a core need to be further explored. Furthermore, the structure of the synthesized core-shell

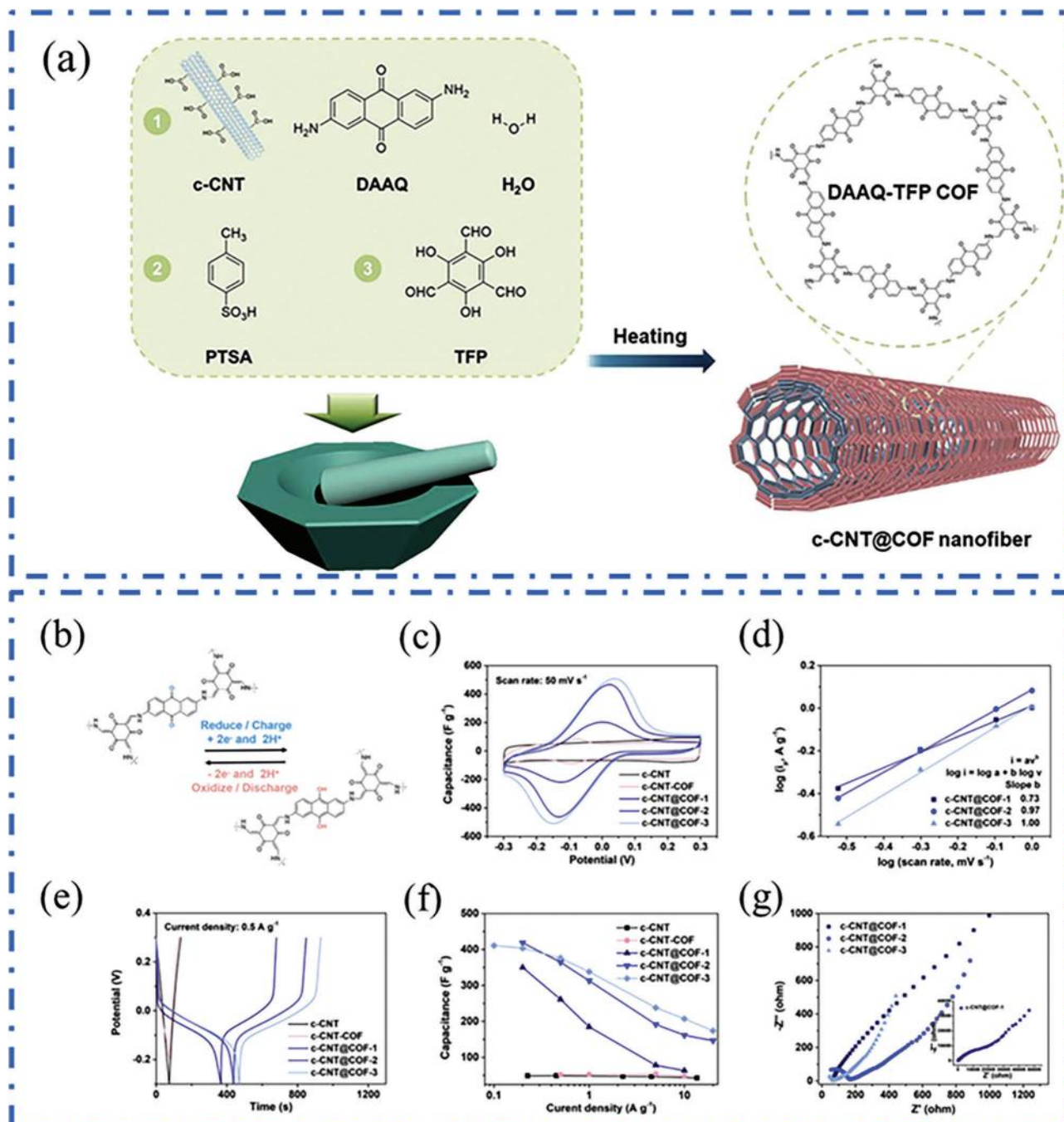


Figure 20. a) Schematic diagram of the preparation of c-CNT@COF, b) the reversible quinone to hydroquinone transformation in DAAQ-TFP COF showing its redox (charge/discharge) mechanism; c) cyclic voltammetry curves, e) galvanostatic charge–discharge (GCD) curves, and f) gravimetric capacitance comparisons of the c-CNT, c-CNT@COFs, and c-CNT-COF electrodes; d) plots of log(*i*_p) versus log(*v*) and g) electrochemical impedance spectra of the c-CNT@COFs electrodes. Reproduced with permission.^[77] Copyright 2020, Elsevier.

materials could be further expanded to include hollow or yolk–shell structures. In addition to MOFs, NPs, and CNTs as core materials, the selection of core materials can be expanded according to practical applications. Hence, it is necessary that further exploration of COF-based core–shell composites be intensified to diversify the composition and

structure of the composites to meet the requirements of different fields.

- (III) Exploring the role between components. COF-based core–shell hybrids possess increased specific surface areas and excellent chemical stability; however, the synthesis of structurally tunable composites remains challenging.

Table 4. A summary of COF-based core-shell composites for supercapacitors.

Sample	Electrolyte	SSA ^{a)} [m ² g ⁻¹]	Pore size [nm]	SR ^{b)} [mV s ⁻¹]/ CD ^{c)} [A g ⁻¹]	SC ^{d)} [mF g ⁻¹]	R _s ^{e)} [Ω]	Ref.
MOF@COF-TCNQ	1 M H ₂ SO ₄	265	0.9	0.2	78.36	NA	[173]
za-MOF@COF	1 M (C ₂ H ₅) ₄ NBF ₄	365	0.7	0.2	20.35	4.84	[187]
c-CNT@COF-3	0.5 M H ₂ SO ₄	576.7	NA	0.2	418.7 F g ⁻¹	NA	[77]
SWCNTs@TpPa-COFs	1 M H ₂ SO ₄	235.5	1.1–5	0.5	153 F g ⁻¹	4.9	[74]
COF@CNT-0.5	1 M H ₂ SO ₄	398	1	0.5	357 F g ⁻¹	4.8	[40]
N-C@CNTs-800	0.1 M KOH and 0.1 M HClO ₄	560	0.43	5	250 F g ⁻¹	NA	[113]

^{a)} Specific surface area; ^{b)} Scan rate; ^{c)} Current density; ^{d)} Specific capacitance; ^{e)} Equivalent series resistance.

Understanding of the synthesis mechanism of COF-based core-shell hybrids and interactions between different units will guide the synthesis. As the structure-function relationships of complexes become more complex, therefore, exploring the relationship between various factors, including porosity, shell thickness, and hydrophobicity, and the performance of the composite is instructive for the design of better COF-based core-shell materials. Moreover, complex experiments are often required, so we can apply computational simulations to reduce the workload and help explain specific mechanisms in complex applications.

- (IV) Optimizing preparation costs and methods. The monomers used to construct COFs are very expensive, resulting in the synthesis of COF-based core-shell hybrids at a high cost, which is not conducive to large-scale commercial applications. In addition, researchers often introduce functional groups, metals, and other functional components to make hybrids with a specific function, which undoubtedly increases the cost of synthesis. Some preparation methods are relatively cumbersome, difficult to control, and still in the laboratory stage. Therefore, the development of an easier and more efficient production process and optimizing various preparation parameters are essential for future mass production.

Acknowledgements

The study was financially supported by the National Natural Science Foundation of China (51979103, 52100181, and 51909085), the China Postdoctoral Science Foundation (2021T140192 and 2021M690054), and the Funds of Hunan Science and Technology Innovation Project (2022JJ10011 and 2020RC5012).

Conflict of Interest

The authors declare no conflict of interest.

Keywords

core-shell structures, covalent-organic frameworks, energy conversion, environmental remediation, synthetic strategy

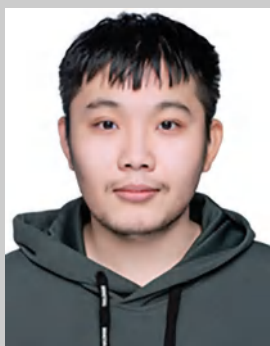
Received: May 5, 2023
Revised: July 13, 2023
Published online:

- Z. G. Zou, J. H. Ye, K. Sayama, H. Arakawa, *Nature* **2001**, 414, 625.
- C. H. Zhao, B. B. Shao, M. Yan, Z. F. Liu, Q. H. Liang, Q. Y. He, T. Wu, Y. Liu, Y. Pan, J. Huang, J. J. Wang, J. Liang, L. Tang, *Chem. Eng. J.* **2021**, 416, 128829.
- Y. M. Hu, C. Y. Zhou, H. Wang, M. Chen, G. M. Zeng, Z. F. Liu, Y. Liu, W. J. Wang, T. Wu, B. B. Shao, Q. H. Liang, *Chem. Eng. J.* **2021**, 414, 128795.
- Y. Pan, X. J. Liu, W. Zhang, Z. F. Liu, G. M. Zeng, B. B. Shao, Q. H. Liang, Q. Y. He, X. Z. Yuan, D. L. Huang, M. Chen, *Appl. Catal., B* **2020**, 265, 118579.
- C. Y. Cheng, Q. H. Liang, M. Yan, Z. F. Liu, Q. Y. He, T. Wu, S. H. Luo, Y. Pan, C. H. Zhao, Y. Liu, *J. Hazard. Mater.* **2022**, 424, 127721.
- Y. Liu, H. Cheng, M. Cheng, Z. F. Liu, D. L. Huang, G. X. Zhang, B. B. Shao, Q. H. Liang, S. H. Luo, T. Wu, S. Xiao, *Chem. Eng. J.* **2021**, 417, 127914.
- I. Hadjipaschalis, A. Poulikkas, V. Efthimiou, *Renewable Sustainable Energy Rev.* **2009**, 13, 1513.
- Y. Pan, Z. Peng, Z. F. Liu, B. B. Shao, Q. H. Liang, Q. Y. He, T. Wu, X. S. Zhang, C. H. Zhao, Y. Liu, L. Ge, M. He, *J. Environ. Chem. Eng.* **2022**, 10, 107366.
- T. Wu, Q. Y. He, Z. F. Liu, B. B. Shao, Q. H. Liang, Y. Pan, J. Huang, Z. Peng, Y. Liu, C. H. Zhao, X. Z. Yuan, L. Tang, S. X. Gong, *J. Hazard. Mater.* **2022**, 424, 127177.
- T. Wu, X. J. Liu, Y. Liu, M. Cheng, Z. F. Liu, G. M. Zeng, B. B. Shao, Q. H. Liang, W. Zhang, Q. Y. He, W. Zhang, *Coord. Chem. Rev.* **2020**, 403, 213097.
- Y. P. Song, Q. Sun, B. Aguila, S. Q. Ma, *Adv. Sci.* **2019**, 6, 1801410.
- S. Y. Hu, Y. N. Sun, Z. W. Feng, F. O. Wang, Y. K. Lv, *Chemosphere* **2022**, 286, 131646.
- S. B. Alahakoon, C. M. Thompson, G. Occhialini, R. A. Smaldone, *ChemSusChem* **2017**, 10, 2116.
- H. Wang, H. Wang, Z. W. Wang, L. Tang, G. M. Zeng, P. Xu, M. Chen, T. Xiong, C. Y. Zhou, X. Y. Li, D. N. Huang, Y. Zhu, Z. X. Wang, J. W. Tang, *Chem. Soc. Rev.* **2020**, 49, 4135.
- C. S. Diercks, O. M. Yaghi, *Science* **2017**, 355, eaal1585.
- A. P. Cote, A. I. Benin, N. W. Ockwig, M. O'Keeffe, A. J. Matzger, O. M. Yaghi, *Science* **2005**, 310, 1166.
- J. S. Gan, X. B. Li, K. Rizwan, M. Adeel, M. Bilal, T. Rasheed, H. M. N. Iqbal, *Chemosphere* **2022**, 286, 131710.
- L. J. Zhu, Y. B. Zhang, *Molecules* **2017**, 22, 1149.

- [19] X. L. Zhang, G. L. Li, D. Wu, B. Zhang, N. Hu, H. L. Wang, J. H. Liu, Y. N. Wu, *Biosens. Bioelectron.* **2019**, *145*, 111699.
- [20] M. D. Zhang, D. H. Si, J. D. Yi, S. S. Zhao, Y. B. Huang, R. Cao, *Small* **2020**, *16*, 2005254.
- [21] D. K. Wang, H. Zeng, X. Xiong, M. F. Wu, M. R. Xia, M. L. Xie, J. P. Zou, S. L. Luo, *Sci. Bull.* **2020**, *65*, 113.
- [22] K. H. Xue, R. He, T. L. Yang, J. Wang, R. R. Sun, L. Wang, X. L. Yu, U. Omeoga, S. F. Pi, T. Yang, W. L. Wang, *Appl. Surf. Sci.* **2019**, *493*, 41.
- [23] Y. Fan, M. Chen, N. Xu, K. Wang, Q. Gao, J. Liang, Y. Liu, *Front. Chem.* **2022**, *10*, 942492.
- [24] H. J. Choi, W. L. Zhang, S. Kim, Y. Seo, *Materials* **2014**, *7*, 7460.
- [25] W. J. Lu, X. T. Guo, Y. Q. Luo, Q. Li, R. M. Zhu, H. Pang, *Chem. Eng. J.* **2019**, *355*, 208.
- [26] S. Das, J. Perez-Ramirez, J. L. Gong, N. Dewangan, K. Hidajat, B. C. Gates, S. Kawi, *Chem. Soc. Rev.* **2020**, *49*, 2937.
- [27] R. A. Ramli, W. A. Laftah, S. Hashim, *RSC Adv.* **2013**, *3*, 15543.
- [28] F. M. Galogahi, Y. Zhu, H. J. An, N. T. Nguyen, *J. Sci.: Adv. Mater. Devices* **2020**, *5*, 417.
- [29] M. B. Gawande, A. Goswami, T. Asefa, H. Z. Guo, A. V. Biradar, D. L. Peng, R. Zboril, R. S. Varma, *Chem. Soc. Rev.* **2015**, *44*, 7540.
- [30] L. J. Lauhon, M. S. Gudiksen, C. L. Wang, C. M. Lieber, *Nature* **2002**, *420*, 57.
- [31] H. P. Feng, L. Tang, G. M. Zeng, Y. Y. Zhou, Y. C. Deng, X. Y. Ren, B. Song, C. Liang, M. Y. Wei, J. F. Yu, *Adv. Colloid Interface Sci.* **2019**, *267*, 26.
- [32] D. H. He, C. Zhang, G. M. Zeng, Y. Yang, D. L. Huang, L. L. Wang, H. Wang, *Appl. Catal., B* **2019**, *258*, 117957.
- [33] Y. W. Peng, M. T. Zhao, B. Chen, Z. C. Zhang, Y. Huang, F. N. Dai, Z. C. Lai, X. Y. Cui, C. L. Tan, H. Zhang, *Adv. Mater.* **2018**, *30*, 1705454.
- [34] H. Yan, Y. H. Liu, Y. Yang, H. Y. Zhang, X. R. Liu, J. Z. Wei, L. L. Bai, Y. Wang, F. M. Zhang, *Chem. Eng. J.* **2022**, *431*, 133404.
- [35] X. Zhong, Y. X. Liu, W. X. Zeng, Y. L. Zhu, B. W. Hu, *Sep. Purif. Technol.* **2022**, *285*, 120405.
- [36] H. W. Zhang, Q. Q. Zhu, R. R. Yuan, H. M. He, *Sens. Actuators, B* **2021**, *329*, 129144.
- [37] Q. Y. Miao, S. Yang, Q. Xu, M. H. Liu, P. Wu, G. J. Liu, C. B. Yu, Z. Jiang, Y. H. Sun, G. F. Zeng, *Small Struct.* **2022**, *3*, 2270013.
- [38] P. Gao, R. Y. Wei, X. H. Liu, Y. Y. Chen, T. Wu, M. W. Shi, M. Z. Wang, N. Li, B. Tang, *Chem. Commun.* **2021**, *57*, 5646.
- [39] L. Zhang, Z. W. Liu, Q. Q. Deng, Y. J. Sang, K. Dong, J. S. Ren, X. G. Qu, *Angew. Chem., Int. Ed. Engl.* **2021**, *60*, 3469.
- [40] F. Liu, C. Wang, C. Liu, Z. Yu, M. Xu, Y. Chen, L. Wei, *Appl. Phys. Lett.* **2021**, *119*, 211905.
- [41] Y. D. Cheng, Y. P. Ying, L. Z. Zhai, G. L. Liu, J. Q. Dong, Y. X. Wang, M. P. Christopher, S. C. Long, Y. X. Wang, D. Zhao, *J. Membr. Sci.* **2019**, *573*, 97.
- [42] S. Zhang, K. Chen, L. Zhu, M. R. Xu, Y. P. Song, Z. H. Zhang, M. Du, *Dalton Trans.* **2021**, *50*, 14285.
- [43] X. K. Liu, M. Y. Hu, M. H. Wang, Y. P. Song, N. Zhou, L. H. He, Z. H. Zhang, *Biosens. Bioelectron.* **2019**, *123*, 59.
- [44] Z. H. Deng, X. Wang, X. L. Wang, C. L. Gao, L. Dong, M. L. Wang, R. S. Zhao, *Microchim. Acta* **2019**, *186*, 108.
- [45] J. H. Liu, D. Wu, Y. X. Yu, J. C. Liu, G. L. Li, Y. N. Wu, *J. Sci. Food Agric.* **2021**, *101*, 1666.
- [46] Z. P. Chen, C. Yu, J. B. Xi, S. Tang, T. Bao, J. Zhang, *Microchim. Acta* **2019**, *186*, 393.
- [47] G. L. Lu, X. B. Huang, Z. Y. Wu, Y. Li, L. W. Xing, H. Y. Gao, W. J. Dong, G. Wang, *Appl. Surf. Sci.* **2019**, *493*, 551.
- [48] S. H. Zhang, W. Xia, Q. Yang, Y. V. Kaneti, X. T. Xu, S. M. Alshehri, T. Ahamad, M. S. A. Hossain, J. Na, J. Tang, Y. Yamauchi, *Chem. Eng. J.* **2020**, *396*, 125154.
- [49] M. He, Q. Liang, L. Tang, Z. Liu, B. Shao, Q. He, T. Wu, S. Luo, Y. Pan, C. Zhao, C. Niu, Y. Hu, *Coord. Chem. Rev.* **2021**, *449*, 214219.
- [50] J. Guo, D. L. Jiang, *ACS Cent. Sci.* **2020**, *6*, 869.
- [51] X. Han, C. Yuan, B. Hou, L. J. Liu, H. Y. Li, Y. Liu, Y. Cui, *Chem. Soc. Rev.* **2020**, *49*, 6248.
- [52] M. C. Wang, M. Wang, H. H. Lin, M. Ballabio, H. X. Zhong, M. Bonn, S. Q. Zhou, T. Heine, E. Canovas, R. H. Dong, X. L. Feng, *J. Am. Chem. Soc.* **2020**, *142*, 21622.
- [53] C. Guo, F. Duan, S. Zhang, L. He, M. Wang, J. Chen, J. Zhang, Q. Jia, J.-P. Zou, *Appl. Catal., B* **2022**, *10*, 475.
- [54] Z. Chen, X. Li, C. Yang, K. Cheng, T. Tan, Y. Lv, Y. Liu, *Adv. Sci.* **2021**, *8*, 2101883.
- [55] G. L. Lu, X. B. Huang, Y. Li, G. X. Zhao, G. S. Pang, G. Wang, *J. Energy Chem.* **2020**, *43*, 8.
- [56] F. Li, D. Wang, Q.-J. Xing, G. Zhou, S.-S. Liu, Y. Li, L.-L. Zheng, P. Ye, J.-P. Zou, *Appl. Catal., B* **2019**, *243*, 621.
- [57] M.-Y. Zhang, J.-K. Li, R. Wang, S.-N. Zhao, S.-Q. Zang, T. C. W. Mak, *Adv. Sci.* **2021**, *8*, 2101884.
- [58] M. K. Cai, Y. L. Li, Q. L. Liu, Z. A. Xue, H. P. Wang, Y. N. Fan, K. L. Zhu, Z. F. Ke, C. Y. Su, G. Q. Li, *Adv. Sci.* **2019**, *6*, 1802365.
- [59] X. H. Liu, S. H. Zhang, G. L. Feng, Z. G. Wu, D. Wang, M. D. Albaqami, B. H. Zhong, Y. X. Chen, X. D. Guo, X. T. Xu, Y. Yamauchi, *Chem. Mater.* **2021**, *33*, 1657.
- [60] A. H. Vahabi, F. Norouzi, E. Sheibani, M. Rahimi-Nasrabadi, *Coord. Chem. Rev.* **2021**, *445*, 214050.
- [61] Q. B. Fu, B. B. Sun, J. Fan, M. L. Wang, X. Sun, G. I. N. Waterhouse, P. Wu, S. Y. Ai, *Food Chem.* **2022**, *371*, 131090.
- [62] Y. Zhu, W. D. Wang, X. Sun, M. Fan, X. Hu, Z. Dong, *ACS Appl. Mater. Interfaces* **2020**, *12*, 7285.
- [63] H. Y. Zhang, Y. Yang, C. C. Li, H. L. Tang, F. M. Zhang, G. L. Zhang, H. Yan, *J. Mater. Chem. A* **2021**, *9*, 16743.
- [64] M. L. Gao, M. H. Qi, L. Liu, Z. B. Han, *Chem. Commun.* **2019**, *55*, 6377.
- [65] M. Liu, Q. Xu, Q. Miao, S. Yang, P. Wu, G. Liu, J. He, C. Yu, G. Zeng, *J. Mater. Chem. A* **2021**, *10*, 228.
- [66] S. H. Zhang, Q. Yang, X. T. Xu, X. H. Liu, Q. Li, J. R. Guo, N. L. Torad, S. M. Alshehri, T. Ahamad, M. S. A. Hossain, Y. V. Kaneti, Y. Yamauchi, *Nanoscale* **2020**, *12*, 15611.
- [67] N. Zhou, Y. Ma, B. Hu, L. He, S. Wang, Z. Zhang, S. Lu, *Biosens. Bioelectron.* **2019**, *127*, 92.
- [68] Y. Deng, Y. Wang, X. Xiao, B. J. Saucedo, Z. J. Zhu, M. S. Xie, X. R. Xu, K. Yao, Y. L. Zhai, Z. Zhang, J. Chen, *Small* **2022**, *18*, 2202928.
- [69] L. Feng, K. Y. Wang, X. L. Lv, T. H. Yan, J. R. Li, H. C. Zhou, *J. Am. Chem. Soc.* **2020**, *142*, 3069.
- [70] W. Li, J. Y. Wang, J. X. Chen, K. Chen, Z. H. Wen, A. S. Huang, *Small* **2022**, *18*, 2202018.
- [71] Y. J. Feng, L. S. Yang, J. F. Liu, B. E. Logan, *Environ. Sci.: Water Res. Technol.* **2016**, *2*, 800.
- [72] B. P. Chaplin, *Acc. Chem. Res.* **2019**, *52*, 596.
- [73] Z. Li, W. Zhao, C. Yin, L. Wei, W. Wu, Z. Hu, M. Wu, *ACS Appl. Mater. Interfaces* **2017**, *9*, 44519.
- [74] Y. Han, Q. Zhang, N. Hu, X. Zhang, Y. Mai, J. Liu, X. Hua, H. Wei, *Chin. Chem. Lett.* **2017**, *28*, 2269.
- [75] S. Binbin, X. Yuantao, L. Zhifeng, W. Ting, P. Yuan, Z. Xiansheng, H. Miao, G. Lin, L. Yue, L. Yang, Z. Weimin, T. Lin, *J. Cleaner Prod.* **2022**, *384*, 135518.
- [76] Q. Q. Zhu, H. K. Li, X. L. Sun, Z. Y. Han, J. C. Sun, H. M. He, *J. Mater. Chem. C* **2021**, *9*, 8043.
- [77] X. Y. Kong, S. Y. Zhou, M. Stromme, C. Xu, *Carbon* **2021**, *171*, 248.
- [78] L. Wu, T. Wu, Z. F. Liu, W. W. Tang, S. Xiao, B. B. Shao, Q. H. Liang, Q. Y. He, Y. Pan, C. H. Zhao, Y. Liu, S. H. Tong, *J. Hazard. Mater.* **2022**, *431*, 128536.
- [79] J. Liu, T. Cheng, L. Jiang, H. Zhang, Y. Shan, A. Kong, *Electrochim. Acta* **2020**, *363*, 137280.
- [80] J. Xu, W. Q. Tang, C. Yang, I. Manke, N. Chen, F. L. Lai, T. Xu, S. H. An, H. L. Liu, Z. L. Zhang, Y. J. Cao, N. Wang, S. L. Zhao, D. F. Niu, R. J. Chen, *ACS Energy Lett.* **2021**, *6*, 3053.

- [81] X. Zhang, Z. Wang, L. Yao, Y. Y. Mai, J. Q. Liu, X. L. Hua, H. Wei, *Mater. Lett.* **2018**, 213, 143.
- [82] M. F. Li, Y. G. Liu, G. M. Zeng, N. Liu, S. B. Liu, *Chemosphere* **2019**, 226, 360.
- [83] S. Huang, D. D. Chen, C. Meng, S. J. Wang, S. Ren, D. M. Han, M. Xiao, L. Y. Sun, Y. Z. Meng, *Small* **2019**, 15, 1904830.
- [84] K. Sun, C. Wang, Y. Dong, P. Q. Guo, P. Cheng, Y. J. Fu, D. Q. Liu, D. Y. He, S. Das, Y. Negishi, *ACS Appl. Mater. Interfaces* **2022**, 14, 4079.
- [85] Y. Chen, Y. Xie, X. Sun, Y. Wang, Y. Wang, *Sens. Actuators, B* **2021**, 331, 129438.
- [86] W. R. Zhang, J. L. Ma, F. X. Meng, Y. Jiang, L. X. Shen, T. R. Sun, Y. N. Qin, N. Zhu, M. W. Zhang, *J. Alloys Compd.* **2022**, 891, 161983.
- [87] C. Hou, D. Zhao, W. Chen, H. Li, S. Zhang, C. Liang, *Nanomaterials* **2020**, 10, 426.
- [88] K. Zhao, P. Gong, J. Huang, Y. Huang, D. Wang, J. Peng, D. Shen, X. Zheng, J. You, Z. Liu, *Microporous Mesoporous Mater.* **2021**, 311, 110713.
- [89] A. Sharma, A. K. Goyal, G. Rath, *J. Drug Targeting* **2018**, 26, 617.
- [90] Y. Kim, M. Kim, H. Jung, Y. J. Choi, C. J. Kang, T. S. Yoon, H. H. Lee, *BioChip J.* **2014**, 8, 275.
- [91] Y. Liu, Z. F. Liu, D. L. Huang, M. Cheng, G. M. Zeng, C. Lai, C. Zhang, C. Y. Zhou, W. J. Wang, D. N. Jiang, H. Wang, B. B. Shao, *Coord. Chem. Rev.* **2019**, 388, 63.
- [92] K. Leus, K. Folens, N. R. Nicomel, J. P. H. Perez, M. Filippousi, M. Meledina, M. M. Durtu, S. Turner, G. Van Tendeloo, Y. Garcia, G. Du Laing, P. Van Der Voort, *J. Hazard. Mater.* **2018**, 353, 312.
- [93] L. You, K. Xu, G. Ding, X. Shi, J. Li, S. Wang, J. Wang, *J. Mol. Liq.* **2020**, 320, 114456.
- [94] C. Tan, J. Li, W. Liu, Q. Zhao, X. Wang, Y. Li, *Chem. Eng. J.* **2020**, 396, 125191.
- [95] A. G. Leonel, A. A. P. Mansur, H. S. Mansur, *Water Res.* **2021**, 190, 116693.
- [96] Z. P. Chen, Z. L. He, X. G. Luo, F. S. Wu, S. Tang, J. Zhang, *Food Anal. Methods* **2020**, 13, 1346.
- [97] F. Kong, X. Zhang, H. Zhang, X. Qu, D. Chen, M. Servos, E. Makila, J. Salonen, H. A. Santos, M. Hai, D. A. Weitz, *Adv. Funct. Mater.* **2015**, 25, 3330.
- [98] R. Wang, Z. L. Chen, *Microchim. Acta* **2017**, 184, 3867.
- [99] W. T. Li, W. Shi, Z. J. Hu, T. Yang, M. L. Chen, B. Zhao, J. H. Wang, *Appl. Surf. Sci.* **2020**, 530, 147254.
- [100] R. Bi, F. Li, J. Chao, H. Dong, X. Zhang, Z. Wang, B. Li, N. Zhao, *J. Chromatogr. A* **2021**, 1635, 461712.
- [101] J. Lu, R. Wang, J. Luan, Y. Li, X. He, L. Chen, Y. Zhang, *J. Chromatogr. A* **2020**, 1618, 460898.
- [102] J. Huang, X. Liu, W. Zhang, Z. Liu, H. Zhong, B. Shao, Q. Liang, Y. Liu, W. Zhang, Q. He, *Chem. Eng. J.* **2020**, 404, 127136.
- [103] G. L. Li, A. Wen, J. H. Liu, D. Wu, Y. N. Wu, *Food Chem.* **2021**, 337, 127974.
- [104] Y. L. Xu, X. F. Shi, R. Hua, R. Zhang, Y. J. Yao, B. Zhao, T. Liu, J. Z. Zheng, G. Lu, *Appl. Catal., B* **2020**, 260, 118142.
- [105] K. Hu, J. Cheng, W. Zhang, T. Pang, X. Wu, Z. Zhang, Y. Huang, W. Zhao, S. Zhang, *Anal. Chim. Acta* **2020**, 1140, 132.
- [106] M. Y. Zhang, J. Li, C. Zhang, Z. F. Wu, Y. X. Yang, J. G. Li, F. F. Fu, Z. Lin, *J. Chromatogr. A* **2020**, 1615, 460773.
- [107] C. Gao, J. Bai, Y. He, Q. Zheng, W. Ma, Z. Lei, M. Zhang, J. Wu, F. Fu, Z. Lin, *ACS Appl. Mater. Interfaces* **2019**, 11, 13735.
- [108] Y. T. Guntern, J. Vavra, V. V. Karve, S. B. Varandili, O. S. Lecina, C. Gadiyar, R. Buonsanti, *Chem. Mater.* **2021**, 33, 2646.
- [109] Z. Hao, W. Lirong, L. Guanhua, L. Yunting, Z. Suoqing, W. Lihui, Z. Xiaobing, Z. Liya, G. Jing, S. Jiafu, J. Yanjun, *ACS Catal.* **2023**, 13, 6619.
- [110] Y. C. Yuan, B. Sun, A. M. Cao, D. Wang, L. J. Wan, *Chem. Commun.* **2018**, 54, 5976.
- [111] M. L. Yola, N. Atar, *Nanoscale* **2020**, 12, 19824.
- [112] S. M. Li, Q. Liang, S. A. H. Ahmed, J. Zhang, *Food Anal. Methods* **2020**, 13, 1111.
- [113] R. Li, L. Xing, A. Chen, X. Zhang, A. Kong, Y. Shan, *Ionics* **2020**, 26, 927.
- [114] Y. L. Zhao, Z. B. Zhu, J. H. Liu, J. C. Liu, G. L. Li, *Food Anal. Methods* **2021**, 14, 2375.
- [115] C. Liu, J. Wang, J. Wan, C. Yu, *Coord. Chem. Rev.* **2021**, 432, 213743.
- [116] Y. H. Yan, Y. J. Lu, B. C. Wang, Y. Q. Gao, L. L. Zhao, H. Z. Liang, D. P. Wu, *ACS Appl. Mater. Interfaces* **2018**, 10, 26539.
- [117] W. W. Sun, X. X. Tang, Q. S. Yang, Y. Xu, F. Wu, S. Y. Guo, Y. F. Zhang, M. H. Wu, Y. Wang, *Adv. Mater.* **2019**, 31, 1903176.
- [118] L. Chen, Y. T. He, Z. X. Lei, C. L. Gao, Q. Xie, P. Tong, Z. Lin, *Talanta* **2018**, 181, 296.
- [119] L. Garzon-Tovar, J. Perez-Carvajal, A. Yazdi, J. Hernandez-Munoz, P. Tarazona, I. Imaz, F. Zamora, D. Maspoch, *Angew. Chem., Int. Ed. Engl.* **2019**, 58, 9512.
- [120] X. Zhong, Y. X. Liu, W. Liang, Y. L. Zhu, B. W. Hu, *ACS Appl. Mater. Interfaces* **2021**, 13, 13883.
- [121] W. J. Huang, H. M. Xu, X. S. Liu, L. L. Wang, S. T. Li, L. P. Ji, Z. Qu, N. Q. Yan, *J. Environ. Sci.* **2022**, 115, <http://doi.org/10.1016/j.jes.2021.07.017>.
- [122] N. Li, D. Wu, J. C. Liu, N. Hu, X. X. Shi, C. J. Dai, Z. W. Sun, Y. R. Suo, G. L. Li, Y. N. Wu, *Microchem. J.* **2018**, 143, 350.
- [123] J. L. Ge, J. D. Xiao, L. L. Liu, L. G. Qiu, X. Jiang, *J. Porous Mater.* **2016**, 23, 791.
- [124] J. Cao, B. Wang, D. Han, S. Yang, J. Yang, M. Wei, L. Fan, Q. Liu, T. Wang, *CrystEngComm* **2013**, 15, 6971.
- [125] X. X. Shi, N. Li, D. Wu, N. Hu, J. Sun, X. X. Zhou, Y. R. Suo, G. L. Li, Y. N. Wu, *Anal. Methods* **2018**, 10, 5014.
- [126] W. Q. Zhou, Y. Liu, W. L. Teo, B. Chen, F. C. Jin, L. Y. Zhang, Y. F. Zeng, Y. L. Zhao, *Cell Rep. Phys. Sci.* **2020**, 1, 10027.
- [127] B. B. Shao, Z. F. Liu, L. Tang, Q. H. Liang, Q. Y. He, T. Wu, Y. Pan, M. Cheng, Y. Liu, X. F. Tan, J. Tang, H. Wang, H. P. Feng, S. H. Tong, *Chemosphere* **2022**, 291, 133001.
- [128] Q. H. Liang, X. J. Liu, B. B. Shao, L. Tang, Z. F. Liu, W. Zhang, S. X. Gong, Y. Liu, Q. Y. He, T. Wu, Y. Pan, S. H. Tong, *Chem. Eng. J.* **2021**, 426, 130831.
- [129] L. Zou, R. J. Sa, H. Zhong, H. W. Lv, X. C. Wang, R. H. Wang, *ACS Catal.* **2022**, 12, 3550.
- [130] Q. Ai, Q. Y. Fang, J. Liang, X. Y. Xu, T. S. Zhai, G. H. Gao, H. Guo, G. F. Han, L. J. Ci, J. Lou, *Nano Energy* **2020**, 72, 104657.
- [131] A. Fujishima, K. Honda, *Nature* **1972**, 238, 37.
- [132] X. B. Liu, H. Q. Zhuang, *Int. J. Energy Res.* **2021**, 45, 1480.
- [133] S. W. Lv, J. M. Liu, C. Y. Li, N. Zhao, Z. H. Wang, S. Wang, *Chemosphere* **2020**, 243, 125378.
- [134] Q. Lei, S. Yang, D. Ding, J. Tan, J. Liu, R. Chen, *J. Mater. Chem. A* **2021**, 9, 2491.
- [135] N. Fajrina, M. Tahir, *Int. J. Hydrogen Energy* **2019**, 44, 540.
- [136] X. S. Zhang, S. H. Tong, D. L. Huang, Z. F. Liu, B. B. Shao, Q. H. Liang, T. Wu, Y. Pan, J. Huang, Y. Liu, M. Cheng, M. Chen, *Coord. Chem. Rev.* **2021**, 448, 214177.
- [137] D. Sun, S. Jang, S. J. Yim, L. Ye, D. P. Kim, *Adv. Funct. Mater.* **2018**, 28, 1707110.
- [138] Y. Chen, D. Yang, S. B. Shi, W. Dai, H. J. Ren, K. An, Z. Y. Zhou, Z. F. Zhao, W. J. Wang, Z. Y. Jiang, *J. Mater. Chem. A* **2020**, 8, 7724.
- [139] W. M. Wang, B. Li, H. J. Yang, Y. Z. Liu, L. Gurusamy, L. Karuppasamy, J. J. Wu, *Nanomaterials* **2021**, 11, 3380.
- [140] Z. Guo, B. Liu, Q. H. Zhang, W. P. Deng, Y. Wang, Y. H. Yang, *Chem. Soc. Rev.* **2014**, 43, 3480.
- [141] S. Higashimoto, N. Kitao, N. Yoshida, T. Sakura, M. Azuma, H. Ohue, Y. Sakata, *J. Catal.* **2009**, 266, 279.
- [142] H. Kasap, C. A. Caputo, B. C. M. Martindale, R. Godin, V. W. H. Lau, B. V. Lotsch, J. R. Durrant, E. Reisner, *J. Am. Chem. Soc.* **2016**, 138, 9183.

- [143] Z. Shen, Y. Hu, B. Li, Y. Zou, S. Li, G. W. Busser, X. Wang, G. Zhao, M. Muhler, *J. Energy Chem.* **2021**, 62, 338.
- [144] H. Li, H. R. Liu, C. Z. Li, J. L. Liu, J. Liu, Q. H. Yang, *J. Mater. Chem. A* **2020**, 8, 18745.
- [145] P. Prabhu, V. Jose, J.-M. Lee, *Adv. Funct. Mater.* **2020**, 30, 1910768.
- [146] Y. Yang, J. J. Fu, Y. Zhang, A. A. Ensafi, J. S. Hu, *J. Phys. Chem. C* **2021**, 125, 22397.
- [147] C.-Y. Lin, D. Zhang, Z. Zhao, Z. Xia, *Adv. Mater.* **2018**, 30, 1703646.
- [148] X. B. Yang, C. Lin, D. D. Han, G. J. Li, C. Huang, J. Liu, X. L. Wu, L. P. Zhai, L. W. Mi, *J. Mater. Chem. A* **2022**, 10, 3989.
- [149] Y. Guo, S. Yang, Q. Xu, P. Wu, Z. Jiang, G. Zeng, *J. Mater. Chem. A* **2021**, 9, 13625.
- [150] J. Tang, C. Su, Z. Shao, *Small Methods* **2021**, 5, 2100945.
- [151] Z. Gan, S. Lu, L. Qiu, H. Zhu, H. Gu, M. Du, *Chem. Eng. J.* **2021**, 415, 127850.
- [152] Z. Liu, M. He, L. Tang, B. Shao, Q. Liang, T. Wu, Y. Pan, X. Zhang, S. Luo, Q. He, L. Ge, *J. Colloid Interface Sci.* **2023**, 634, 255.
- [153] D. K. Yoo, B. N. Bhadra, S. H. Jhung, *J. Hazard. Mater.* **2021**, 403, 123655.
- [154] A. M. Awad, S. M. R. Shaikh, R. Jalab, M. H. Gulied, M. S. Nasser, A. Benamor, S. Adham, *Sep. Purif. Technol.* **2019**, 228, 115719.
- [155] Y. Yang, G. L. Li, D. Wu, A. Y. Wen, Y. N. Wu, X. X. Zhou, *Microchim. Acta* **2020**, 187, 278.
- [156] R. J. Zheng, Y. C. Yang, C. Yang, Y. Xia, *Microchim. Acta* **2021**, 188, 179.
- [157] N. Zhang, T. Bao, Y. Gao, X. L. Xu, S. C. Wang, *Appl. Surf. Sci.* **2022**, 580, 152285.
- [158] J. L. Segura, M. J. Mancheno, F. Zamora, *Chem. Soc. Rev.* **2016**, 45, 5635.
- [159] Q. Z. Wang, Y. J. Zhao, Z. Shi, X. Y. Sun, T. Bu, C. Q. Zhang, Z. X. Mao, X. H. Li, L. Wang, *Chem. Eng. J.* **2021**, 420, 129955.
- [160] X.-S. Yang, L.-L. Wang, Y.-S. Liu, C.-X. Yang, J. Zhao, S.-L. Ji, Q.-W. Liu, Z.-H. Hu, F.-J. Liu, P. Wang, *Food Chem.* **2022**, 386, 132843.
- [161] D. L. Wei, J. C. Li, Z. S. Chen, L. J. Liang, J. P. Ma, M. Z. Wei, Y. J. Ai, X. K. Wang, *J. Mol. Liq.* **2020**, 301, 112431.
- [162] L. Cui, J. Wu, H. X. Ju, *Biosens. Bioelectron.* **2015**, 63, 276.
- [163] H. Liang, H. Xu, Y. Zhao, J. Zheng, H. Zhao, G. Li, C.-P. Li, *Biosens. Bioelectron.* **2019**, 144.
- [164] M. R. Xu, K. Chen, L. Zhu, S. Zhang, M. H. Wang, L. H. He, Z. H. Zhang, M. Du, *Langmuir* **2021**, 37, 13479.
- [165] D. Liang, X. Zhang, Y. Wang, T. Huo, M. Qian, Y. Xie, W. Li, Y. Yu, W. Shi, Q. Liu, J. Zhu, C. Luo, Z. Cao, R. Huang, *Bioact. Mater.* **2022**, 14, 145.
- [166] X.-Y. Wang, H.-Q. Yin, X.-B. Yin, *ACS Appl. Mater. Interfaces* **2020**, 12, 20973.
- [167] F. F. Yin, W. J. Yue, Y. Li, S. Gao, C. W. Zhang, H. Kan, H. S. Niu, W. X. Wang, Y. J. Guo, *Carbon* **2021**, 180, 274.
- [168] X. Wang, Y. Wang, H. Qi, Y. Chen, W. Guo, H. Yu, H. Chen, Y. Ying, *ACS Nano* **2022**, 16, 14297.
- [169] H. Li, B. B. Kou, Y. L. Yuan, Y. Q. Chai, R. Yuan, *Biosens. Bioelectron.* **2022**, 197, 113758.
- [170] Q. Z. Wang, R. Li, Y. J. Zhao, T. T. Zhe, T. Bu, Y. N. Liu, X. Y. Sun, H. F. Hu, M. Zhang, X. H. Zheng, L. Wang, *Talanta* **2020**, 219, 121255.
- [171] K. S. Poonam, A. Arora, S. K. Tripathi, *J. Energy Storage* **2019**, 21, 801.
- [172] N. N. Zhang, X. Xiao, H. Pang, *Nanoscale Horiz.* **2019**, 4, 99.
- [173] H. J. Peng, S. H. Huang, D. N. Tranca, F. Richard, W. Baaziz, X. D. Zhuang, P. Samori, A. Ciesielski, *ACS Nano* **2021**, 15, 18580.
- [174] G. Lin, C. Gao, Q. Zheng, Z. Lei, H. Geng, Z. Lin, H. Yang, Z. Cai, *Chem. Commun.* **2017**, 3649.
- [175] S. Di, M. Zhang, C. Shi, S. Zhu, *Environ. Pollut.* **2023**, 326, 121475.
- [176] H. Guo, Y. Li, Y. Li, X. He, L. Chen, Y. Zhang, *ACS Appl. Mater. Interfaces* **2023**, 15, 14777.
- [177] X. S. Yang, J. Zhao, L. L. Wang, Y. S. Liu, Q. W. Liu, X. Y. Peng, P. Wang, *Microchim. Acta* **2022**, 189, 340.
- [178] N. Li, D. Wu, X. T. Li, X. X. Zhou, G. S. Fan, G. L. Li, Y. N. Wu, *Food Chem.* **2020**, 306, 125455.
- [179] X. Zhong, Z. Lu, W. Liang, B. Hu, *J. Hazard. Mater.* **2020**, 393, 122353.
- [180] J. Zhang, Z. P. Chen, S. Tang, X. G. Luo, J. B. Xi, Z. L. He, J. X. Yu, F. S. Wu, *Anal. Chim. Acta* **2019**, 1089, 66.
- [181] Q. Q. Sun, C. H. Gao, W. D. Ma, Y. T. He, J. Wu, K. L. Luo, D. Ouyang, Z. Lin, Z. W. Cai, *Microchim. Acta* **2020**, 187, 370.
- [182] J. Feng, W. X. Ren, J. L. Gao, F. Li, F. Kong, B. J. Yao, Y. B. Dong, *ACS Appl. Mater. Interfaces* **2021**, 13, 17243.
- [183] Y. Y. Li, G. Z. Dong, J. Y. Li, J. X. Xiang, J. R. Yuan, H. L. Wang, X. D. Wang, *Ecotoxicol. Environ. Saf.* **2021**, 219, 112319.
- [184] J. Li, C. Y. Zhang, M. Y. Yin, Z. Zhang, Y. J. Chen, L. Deng, S. Wang, *ACS Omega* **2019**, 4, 15947.
- [185] M. Xia, Y. Liang, W. Q. Luo, D. Cai, P. Zhao, F. F. Chen, Y. P. Li, Z. Y. Sui, L. L. Shan, R. M. Fan, F. S. Pan, D. Wang, M. Li, Y. J. Shen, J. X. Xiao, X. L. Wu, Q. Chen, *Mater. Today Energy* **2022**, 29, 101135.
- [186] X. Wang, Y. X. Wang, H. Qi, Y. Chen, W. Guo, H. Y. Yu, H. Y. Chen, Y. B. Ying, *ACS Nano* **2022**, 16, 14297.
- [187] H. J. Peng, J. Raya, F. Richard, W. Baaziz, O. Ersen, A. Ciesielski, P. Samori, *Angew. Chem., Int. Ed. Engl.* **2020**, 59, 19602.
- [188] L. Han, Y. X. Li, Y. Q. Yang, S. Z. Sun, M. K. Li, J. B. Yue, C. Y. Chuah, J. D. Li, *J. Colloid Interface Sci.* **2022**, 628, 144.
- [189] W. Gao, Y. Jian, Y. Li, C. Y. Pan, G. P. Yu, J. T. Tang, *Ind. Eng. Chem. Res.* **2023**, 62, 1891.
- [190] H. C. Chu, X. Sun, X. Q. Zha, Y. Zhang, Y. Wang, *Colloids Surf., A* **2022**, 648, 129238.
- [191] Y. Y. Ma, Y. X. Zhao, X. T. Xu, S. J. Ding, Y. H. Li, *Talanta* **2021**, 235, 122798.
- [192] Q. L. Liu, Q. Xu, W. Sun, *J. Chromatogr. A* **2021**, 1657, 462566.
- [193] J. H. Xin, Y. R. Zhou, X. Wang, G. J. Xu, M. Xie, L. Liu, R. S. Zhao, Y. N. Wu, M. L. Wang, *Food Chem.* **2021**, 347, 129075.
- [194] Q. B. Fu, H. L. Jiang, L. Q. Qiao, X. Sun, M. L. Wang, R. S. Zhao, *J. Chromatogr. A* **2020**, 1630, 461534.
- [195] L. P. Zhao, G. Yang, L. S. Li, C. Zhu, Y. Ma, F. Qu, *Anal. Chim. Acta* **2020**, 1140, 228.
- [196] Y. P. Wang, S. P. Wu, D. Wu, J. W. Shen, Y. M. Wei, C. Z. Wang, *Anal. Chim. Acta* **2020**, 1093, 61.
- [197] C. H. Gao, G. Lin, Z. X. Lei, Q. Zheng, J. S. Lin, Z. A. Lin, *J. Mater. Chem. B* **2017**, 5, 7496.
- [198] F. Lu, J. Lin, C. Lin, G. Qi, X. Lin, Z. Xie, *Talanta* **2021**, 231, 122343.



Teng Li received his bachelor's degree from Northeastern Agricultural University. He is now a master's candidate at Hunan University under the supervision of Prof. Zhifeng Liu. His current research interests are to develop porous polymerization catalysts and their applications in the field of advanced oxidation processes.



Zhifeng Liu received his Ph.D. degree from Hunan University in 2012. He used to be a visiting scientist at the University of Northern British Columbia. He became an assistant professor in 2016, and now, he is a professor of College of Environmental Science and Engineering, Hunan University. His research interests include organic solid waste treatment and resource recovery, water pollution control, contaminated soil/wetland remediation, and innovative talent development.